WORKSHOP ON

WATER ON MARS

MECA

LPI Technical Report Number 85-03

LUNAR AND PLANETARY INSTITUTE   3303 NASA ROAD 1   HOUSTON, TEXAS 77058-4399

WORKSHOP ON

WATER ON MARS

Edited by
Stephen Clifford

Sponsored by
The Lunar and Planetary Institute

A Lunar and Planetary Institute/MECA workshop
Hosted by NASA/Ames Research Center
November 30–December 1, 1984

Lunar and Planetary Institute   3303 NASA Road 1   Houston, Texas 77058

LPI Technical Report 85-03

N86-13282 #

Contents

Program

SESSION I - CURRENT AND PAST BULK WATER CONTENT
Chairmen: Heinrich Wänke and Robert Pepin

H. Wänke and G. Dreibus
  Volatiles on Mars

H. Watkins and J. S. Lewis
  Loss of Volatiles from Mars as the Result of Energetic Impacts

M. J. Rutherford and M. R. Carroll
  The Influence of H_2O on Volcanic Degassing of Aerosol Forming Elements S, Cl, and F

SESSION II - PRESENT WATER CYCLE AND RELATED PROCESSES
Chairmen: Bruce Jakosky and Robert Haberle

B. M. Jakosky
  The Seasonal Cycle of Water on Mars: A Review

L. E. Roth, R. S. Saunders, and G. Schubert
  Radar and the Detection of Liquid Water on Mars

P. R. Christensen and R. W. Zurek
  Mars Water-Ice Clouds

H. M. Hart and B. M. Jakosky
  Stability and Composition of Condensate at the Viking Lander 2 Site on Mars

L. J. Martin and P. B. James
  The Possible Role of Water in the Recession of Mars' Polar Caps

S. W. Lee
  Influence of Atmospheric Dust Loading and Water Vapor Content on Settling Velocities of Martian Dust/Ice Grains: Preliminary Results

R. Kahn
  Observational Constraints on the Global-Scale Wind Systems of Mars

P. B. James
  Hydrologic Cycle on Mars: Effects of CO_2 Mass Flux on Global Water Distribution

R. M. Haberle and T. Herdtle
  Numerical Simulation of the Current Water Cycle on Mars

J. B. Pollack , R. M. Haberle, J. White, and K. Bilski
New GCM Simulations of Transport into the Polar Regions

D. O. Muhleman, R. T. Clancy, F. P. Schloerb, L. Riley, and W. G. Wilson
Mapping of the Water Vapor Distribution on Mars; A Microwave Spectrometer and Radiometer for MG/CO

Friday, November 30
4:30 p.m.

MG/CO PRESENTATION

F. D. Palluconi and A. L. Albee
The Mars Geoscience/Climatology Observer (MG/CO) Mission

Saturday, December 1
8:30 a.m.—12:00 p.m.

SESSION III—PAST WATER CYCLE(S) AND CLIMATE(S)
Chairmen: James Pollack and Fraser Fanale

A. P. Zent, F. P. Fanale, and J. R. Salvail
Short Term Water Cycles Within the Mars Regolith

F. P. Fanale, J. R. Salvail, A. P. Zent, and S. E. Postawko
Mars: Long Term Changes in the State and Distribution of H_2O

B. M. Jakosky and M. H. Carr
Mars at High Obliquity: Possible Precipitation of Ice at Low Latitudes

J. H. Yatteau and M. B. McElroy
Mars: Effect of Water Vapor Abundance on Atmospheric Oxidation State

H. G. Marshall, J. C. G. Walker, and W. R. Kuhn
Cloud Properties in Past Martian Climates

G. D. Clow
Radiation-dominated Snowmelt on Mars

P. H. Schultz, J. Rogers, and S. Haber
Erosion of Martian Impact Basins and the Changing Water Cycle

V. R. Baker
Problems in the Paleohydrologic and Hydroclimatologic Interpretation of Valley Networks

R. C. Kochel and A. D. Howard
Groundwater Sapping and Ancient Valley Networks on Mars

H. Moore
Sublimation Rates Required for Steady-state Glaciers, Mars

SESSION IV - WATER SOURCES AND SINKS TODAY AND IN THE PAST
Chairmen: Michael Carr and Stephen Clifford

R. B. Singer, P. D. Owensby, and R. N. Clark
Direct Detection of Minor Clay Mineralogy on Mars

J. Posey-Dowty, L. B. Tanenbaum, B. M. Moskowitz, D. A. Crerar, and R. B. Hargraves
Controls on Precipitation of Various Iron Oxides and Hydroxides: Relevance to Mars

J. L. Gooding
Water and Ice in the Martian Regolith: Dependence of Stabilities on Regolith Mineralogy

R. L. Huguenin
Mars: Mineralogical Constraints on Volatile Evolution

D. M. Anderson
The Present Water Cycle on Mars: Some Thermodynamic Considerations

R. S. Saunders, T. J. Parker, J. B. Stephens, E. G. Laue, and F. P. Fanale
Sediment—Water Deposition and Erosion in the Martian Polar Regions

E. A. Guinness, C. E. Leff, and R. E. Arvidson
On the Latitudinal Distribution of Debris in the Northern Hemisphere of Mars

S. W. Squyres and M. H. Carr
The Distribution of Ground Ice Features on Mars

S. S. Nedell and S. W. Squyres
Geology of Layered Deposits in the Valles Marineris

P. H. Schultz
Polar Wandering on Mars and the Distribution of Water-Ice Through Time

S. M. Clifford
Mars: Permeability Requirements for a Global Groundwater System Driven by Polar Basal Melting

POSTER PRESENTATIONS

R. Batson
No corresponding abstract

H. Masursky
No corresponding abstract

F. D. Palluconi and A. L. Albee
The Mars Geoscience/Climatology Observer (MG/CO) Mission

S. S. C. Wu
Mars Topographic Maps

ABSTRACTS SUBMITTED FOR PRINT ONLY

S. M. Clifford
  Mars: Groundwater Mound Development in Response to Polar Basal Melting

E. K. Gibson, Jr.
  Sources and Sinks of Present Day Water Within the Martian Regolith: Evidence from a Terrestrial Analog of Martian Weathering Processes—The Dry Valleys of Antarctica

B. K. Lucchitta
  Ground Water in the Equatorial Region of Mars: Evidence from Landslides

Summary of Technical Sessions and Discussions

Water on Mars: New Ideas, Results, and Questions

How much water resides in the martian crust? What forms does it take and how is it distributed? What role do the martian polar caps, atmosphere, and regolith play in the seasonal and climatic water cycles? These were just a few of the many questions considered by the eighty-three participants of the Water on Mars Workshop, held November 30th and December 1st, 1984, at the NASA/Ames Research Center, Moffett Field, California. The meeting, which was sponsored by the Lunar and Planetary Institute and hosted at NASA/Ames by Bob Haberle, is the first in a series of topical workshops that are planned as part of the MECA Study Project.

The opening session of the Workshop focused on one of the most debated areas of Mars volatiles research—the size of the planet's past and present bulk water content. Current estimates of the inventory of H_2O on Mars range from an equivalent layer of liquid 10–1000 meters deep averaged over the planet's surface. The most recent of these estimates, presented at the Workshop, is based on the now popular belief that the SNC class of meteorites represent actual samples of the martian crust. From a model of planetary accretion and degassing founded on this assumption, it was determined that the present inventory of H_2O on Mars is equivalent to a global layer no more than 50 meters deep.

During the discussion generated by this estimate, several investigators expressed reservations about an H_2O inventory as small as a few tens of meters, for it appears to directly contradict the seemingly abundant morphologic evidence that Mars is (or has been) water-rich. Others, however, argued that the interpretation of much of this morphologic evidence is at best equivocal and that the case for a "wet" Mars is far from established. The issue is further complicated by the possibility that various processes may have altered the volatile budget of the planet over the course of its geologic history. In past discussions, the most frequently cited of these processes have been cometary influx, exospheric escape, and chemical weathering. At the Workshop, a new candidate was discussed—the possibility that shock waves generated by energetic impacts may have blown off a significant fraction of the primitive martian atmosphere.

Interestingly, a device capable of resolving much of the controversy over the present water content of the martian crust was on display in the hallway just outside the Workshop meeting room. Penetrators have been proposed as an inexpensive means of creating a global seismometer network on Mars. Such a network, consisting of perhaps ten or more well-placed instruments, could readily determine whether the seismic propagation characteristics of the outer crust are indicative of a water-rich or water-poor planet.

The next session of the Workshop was devoted to a discussion of the seasonal water cycle. Atmospheric water vapor measurements, compiled by Earth-based telescopes and the Viking Orbiter Mars Atmospheric Water Detectors (MAWD), now span a period of over six martian years. Analysis of this data suggests that the seasonal cycle is governed by both the sublimation and condensation of H_2O at the poles and by its adsorption/desorption within the regolith. So far, efforts to simulate the seasonal vapor cycle have failed to reproduce the observed behavior. This result is not altogether surprising, since many aspects of the seasonal cycle are still poorly understood. For example, how much water is transported in the non-vapor state? What effects do the global dust storms have? Do net annual sources (or sinks) of atmospheric vapor exist within the regolith? Answers to these and similar questions will hopefully be forthcoming following the arrival of the Mars Observer mission in the fall of 1991; a primary objective of this mission is to determine the temporal and spatial distribution of H_2O, CO_2, and dust over a complete martian year.

Following the seasonal discussion, attention at the Workshop turned to the martian climate, where the topic that appeared to generate the most interest was the origin of the valley networks. The networks appear to have been formed by a variety of fluvial and non-fluvial processes; yet, their almost exclusive occurrence in the ancient, heavily cratered terrain suggests that, whatever processes were responsible for their formation, they ceased to operate early in martian history. The central question is: why?

One analysis suggests that the impact creating the Argyre basin may have played a critical role. The basis for this supposition is the observation that channel drainage densities appear to have undergone a dramatic decline in terrains that post-date the Argyre event. An alternative hypothesis proposes a climatic link with the formation of the Tharsis volcanic complex. In this scenario, the high obliquities that are thought to have characterized pre-Tharsis Mars may have periodically resulted in the sublimation of large quantities of ice from the poles and its preferential deposition as snow at equatorial latitudes. Sunlight, absorbed within the snowpack, may have then led to significant melting, thus providing the necessary liquid water to carve the channels.

Another aspect of the martian climate discussed at the Workshop was the long-term redistribution of H_2O within the regolith. Detailed studies of the thermodynamic stability of ground ice on Mars suggest that there should be a net transfer of regolith H_2O from the warmer equatorial latitudes to the colder poles. Indeed, examination of high resolution Viking Orbiter imagery has revealed that the distribution of certain terrain features, whose origins have been attributed to the presence of interstitial ice, appears restricted to the latitudes poleward of 30 degrees. The absence of these features at more equatorial latitudes supports the conclusion that much of the near-surface regolith in this region may be ice-free.

The final session of the Workshop was devoted to the question of H_2O sources and sinks. Theoretical arguments and recently acquired spectroscopic evidence suggest that water has played an important role in the mineralogical development of the present martian surface. So too, various investigators have shown that the mineralogy of the surface may exert a strong influence on the exchange and storage of regolith H_2O. Clays are of particular importance, for their relative abundance, particle size, and specific surface area will determine both the regolith's adsorptive capacity and diffusive properties. Interestingly, an examination of Viking Orbiter imagery now indicates that the thick mantles of clay-size eolian material that were once thought to blanket temperate and polar latitudes, are far less extensive than previously suggested. This discovery implies a sizable reduction in the estimated volatile storage potential of the polar regolith.

If further emphasis were needed, the questions raised during the closing talks of the Workshop highlighted the uncertainty that underlies much of our current knowledge of water on Mars. For example, did large ice-covered lakes once fill the bottoms of the great equatorial canyons? Have the permanent polar caps always been in their present geographic locations, or have changes in the planet's moment of inertia led to polar wandering? What role, if any, does groundwater play in the martian hydrologic cycle? For the time being, these and many of the other intriguing questions raised at the Workshop remain unanswered; however, the ideas and cooperative efforts stimulated by their open discussion will inevitably provide us with new insights, and thus new questions, regarding the nature of water on Mars.

Summaries of the major results of the Water on Mars Workshop were presented by Heinrich Wänke, Bruce Jakosky, Jim Pollack, and Mike Carr at a special session of the Fall Meeting of the American Geophysical Union, held in San Francisco on December 3rd. The high level of interest displayed by the participants at both the Ames Workshop and the special session at AGU bodes well for future MECA workshops.

ABSTRACTS

This Page Intentionally Left Blank

THE PRESENT WATER CYCLE ON MARS: SOME THERMODYNAMIC
CONSIDERATIONS; Duwayne M. Anderson, Texas A&M University

Water-ice phase changes now occurring on Mars include:
adsorption-desorption; vaporization-condensation; and melting-
solidification. Conventional thermodynamic formulations
generally are adequate to describe water phase equilibria in
the martian setting, but discussion is required to resolve
certain difficulties that have been identified. For example,
the Clausius-Clapeyron equation can be applied to standard
water vapor adsorption-desorption isotherms to determine
standard heats of adsorption-desorption, albeit with the usual
complications of non-reproducibility due to hysteresis in the
adsorption isotherms. Complication appears when the
adsorption- desorption process is studied at temperatures
below 0°C. The isotherms show the same hysteresis effects as
they do above 0°C; the desorption curves are very reproducible
and the two inflection points that allow the mono layer and
two mono molecular layer surface coverage to be distinguished
are clearly evident. However, a choice of a standard state
for the water is required to construct the isotherms below
0°C; either ice I or the metastable supercooled water (1).

If ice I is chosen, the adsorption-desorption curves
intersect the abcissa at a definite point at $p/p° = 1.0$, where
p is the partial pressure of water vapor and p° is the
saturation pressure of ice I at the temperature of interest.
This choice is convenient and useful because it relates
adsorption- desorption data to the water-ice phase composition
diagrams that have now been determined for a number of frozen
earth and soil materials (2,3). A typical, idealized diagram
is shown in Figure 1 for two different total water contents.
The generalized ice and unfrozen water fields are identified
and the relationship between the total water content, w_t',
and the ice-unfrozen water content at a fixed temperature is
illustrated. A similar illustration for w_t'' could be drawn
by analogy from the relationship $w_t = w_{ice} + w_u$. At
a given temperature, the unfrozen water content can be shown
to correspond to the adsorbed water content at $p/p° = 1.0$ on
the corresponding water adsorption-desorption isotherm.

The latent heat, $\Delta\bar{H}$, associated with the unfrozen water-
ice transition is variable, diminishing as the temperature is
lowered (2). The symbol employed is conventional in chemical
thermodynamics and denotes the change in partial molar
enthalpy associated with the change in phase. Similar
considerations and notations have been employed in derivations
of freezing point depression and heat capacity equations that
also are directly related to the phase composition diagram
shown in Figure 1 (4).

Thermodynamic data on terrestrial earth and soil
materials at temperatures down to about -5°C are available to

support some computations and qualitative, preliminary
conclusions extrapolated to the Mars environment. The data
are insufficient for use at lower temperatures, however.
Additional data are needed. Also needed is an agreed upon
thermodynamical nomenclature and notation as the foundation
for expanded discussion in systematic terms of the present
water cycle on Mars is prepared.

REFERENCES

1. Anderson D. M., Schwarz M. J., and Tice A. R. (1978) Water
    Vapor Adsorption by Sodium Montmorillonite at -5°C.
    Icarus 34: 638-644

2. Anderson, D. M. (1967) The Interface Between Ice and
    Silicate Surfaces. Journal Colloid and Interface
    Science 25: 174-191

3. Anderson, D. M. and Morganstern N. R. (1973) Physics
    Chemistry and Mecanics of Frozen Ground: A Review.
    Permafrost: The North American Contribution to the
    Second International Conference, National Academy of
    Science: pp. 257-288

4. Low P. F., Anderson D. M. and Hoekstra P. (1968) Some
    Thermodynamic Relationships for Soils at or Below the
    Freezing Point. Water Resources Research 4: 379-394
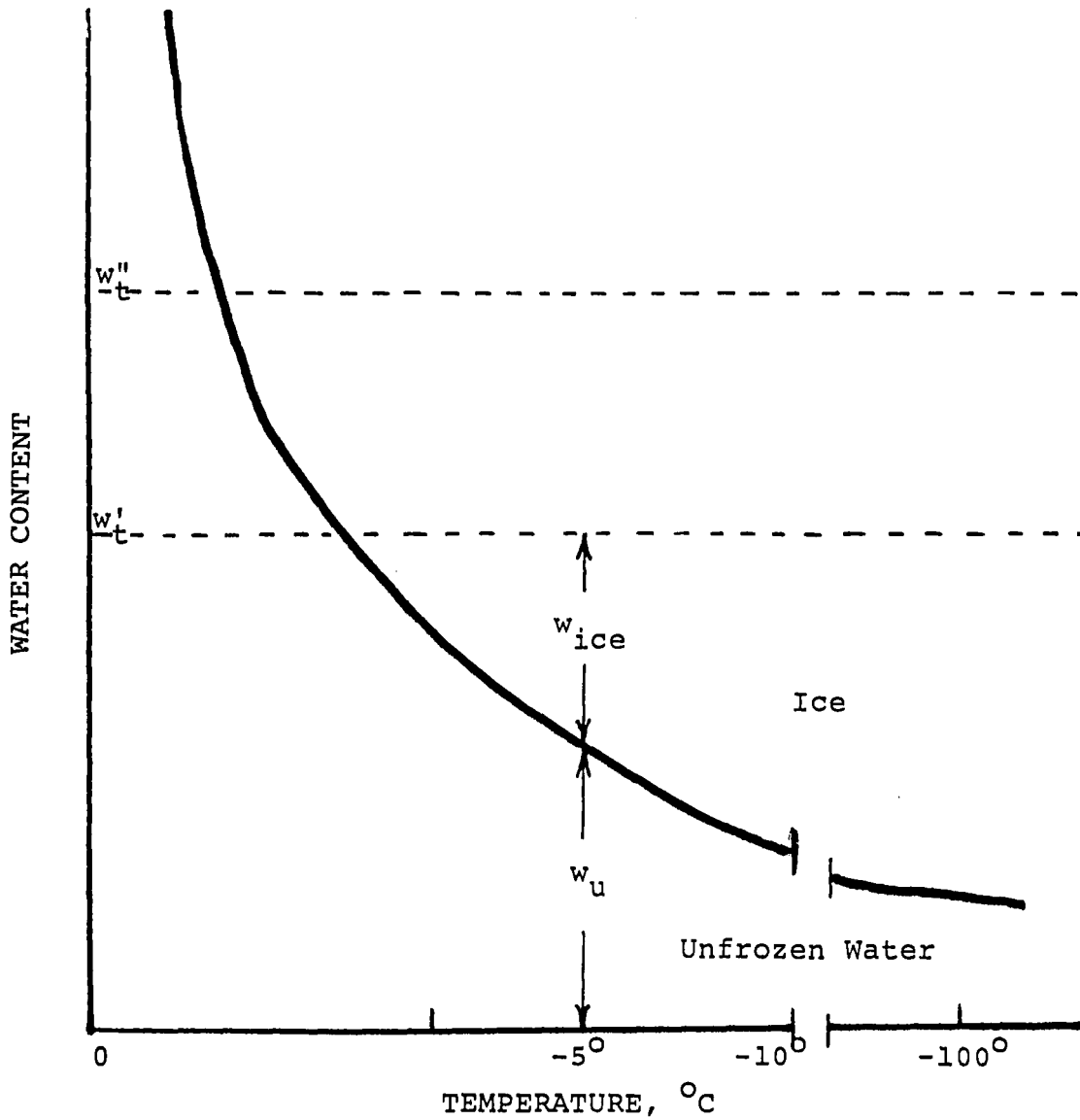
Figure 1. Generalized water-ice phase composition diagram

PROBLEMS IN THE PALEOHYDROLOGIC AND HYDROCLIMATOLOGIC INTERPRETATION OF VALLEY NETWORKS;   Victor R. Baker, Department of Geosciences, University of Arizona, Tucson, Arizona 85721.

The valley networks of the heavily cratered uplands on Mars are considered the most conclusive evidence for profoundly different hydroclimatic conditions in the first billion years of Mars history (1,2,3). It is clear that degraded networks formed during the heavy bombardment phase of cratering, ie. prior to 3.8 billion years ago. Younger networks, termed "pristine" for equatorial regions (4), formed at the very end of heavy bombardment and immediately thereafter. These younger valleys generally comprise segments of larger networks with degraded components. This suggests that valley formation was a prolonged process coeval with the heavy bombardment period and extending just beyond that period in martian history.

Numerous empirical relationships are available that relate various parameters of streamflow, such as mean annual discharge, to measurable properties of channel networks, including drainage area, drainage density, meander wavelength, channel width, and slope (5). Where streamflow is the major component of runoff, it should be directly related to the input of precipitation minus the loss of evaporation. The potential use for these relationships for hydroclimatologic assessment is limited by several considerations.

It is very difficult to measure network properties on Mars in a manner that is directly comparable to measurements on terrestrial networks. The complexities of heavily cratered terrain relationships make it exceedingly difficult to specify drainage divides. Surface drainage divides can be estimated in some instances (6,7). However, the lack of high-resolution topographic data precludes the definition of both surface divides and subsurface (ground water) divides in broad, undissected interfluves.

Drainage density is perhaps the most useful parameter that relates terrestrial network properties to climate (8). Although drainage densities can be specified for Martian networks (9), the results are not comparable to Earth because of difficulties in specifying drainage divides. Moreover, the most extensive networks are the most degraded, and therefore cannot be precisely measured.

The transformation of rainfall to runoff is highly dependent on the general mechanism of network formation. In the overland flow model (10) rainfall generates hillslope rills that evolve to a dendritic network by piracy and cross-grading. More likely in the development of a landscape is headward growth by abstraction (11). The role of sapping is also extremely important in the headward growth of terrestrial networks (12). The latter process produces morphological similarities to Martian networks (1,2).

The implication of sapping models for hydroclimate derives from the requirement of precipitation to recharge the groundwater system. Sapping also requires initiation, establishing a zone of low potential toward which a hydraulic gradient will drive ground-water flow. Such zones on Earth are established by regional fluvial incision.

Even when the genetic mechanism is known for the network, it is difficult to separate climatic controls on the network from structural or lithologic controls. For example, low drainage density and incomplete reduction of divides may result from immaturity of network development because of the short duration of favorable climate-related conditions (e.g. high water tables). Alternatively the very high permeability of

certain rock units (e.g. volcanic plains) may result in low hydraulic gradients and very slow headward retreat.

Most terrestrial studies of paleohydrology derive from studies of <u>channel</u> networks, but it is clear that on Mars the networks consist of relict <u>valleys</u>. Valley processes involve a considerable component of non-fluvial degradation in their origin. Valley incision drives this degradation, but that incision may involve relatively small discharges. For example, some geomorphologists hold that the most rapid process of terrestrial valley formation is the "Eisrinde effect", which occurs in regions of periglacial activity (13). The <u>Eisrinde</u> (ice rind) is the uppermost zone of permafrost which extends beneath braided meltwater channels in subpolar areas such as Svalbard (Spitzbergen). Seasonal melting and freezing beneath the stream bed concentrates mechanical weathering of bedrock at precisely the point where annual melt-season floods can remove the generated detritus. The result can be extremely rapid degradation, as much as 3000 mm/1000 yr. By contrast modern rates of terrestrial landscape degradation range from 50 to 500 mm/1000 yr (14).

If valleys can form on Mars by processes similar to the "Eisrinde effect", then the paleohydrologic implications of the valleys may not be as extreme as implied by models that use rainfall to generate overland flow or recharge aquifers. Nor is it necessary to justify long, continuous flow of surface water (15,16). Instead water can be transported in the frozen state. The phase changes necessary for freeze-thaw activity and/or surface streamflow might be generated by insolation changes associated with orbital parameters (17) or with geothermal effects, such as might be associated with impact (18) or with the volcanic emplacement of the intercrater plains. Thus, it may be appropriate to specify the most conservative deviation from modern hydrologic conditions on Mars that could account for the ancient epoch of valley formation.

Whatever the mechanism of stream incision on Mars, valley widening and modification was accomplished by a variety of non-fluvial processes. The relevant terrestrial analogs include morphogenetic change from an ancient climate favoring fluvial activity to a subsequent climate favoring mass wasting, eolian activity, and other hyperarid processes of divide reduction (19). Debris production and transport by frost-related processes was probably involved. Unfortunately the climatic conditions for the formation of whole landscapes, as opposed to certain diagnostic landforms, are not established.

References: (1) D. Pieri (1980) Science, 210, 895-897. (2) V.R. Baker (1982) The Channels of Mars, The Univ. of Texas Press. (3) M.H. Carr and G.D. Clow (1981) Icarus, 48, 91-117. (4) V.R. Baker and J.B. Partridge (19843) in Lunar and Planetary Science XV, Lunar and Planetary Inst., Houston, 25-26. (5) G.P. Williams (1984) in Developments and Applications of Geomorphology, Springer-Verlag, 343-367. (6) J.C. Boothroyd (1982) N.A.S.A. Tech. Memo. 85127, 209-212. (7) J.C. Boothroyd and J.A. Grant (1983) N.A.S.A. Tech. Memo. 86246, 182-184. (8) K.J. Gregory (1976) in Geomorphology and Climate, John Wiley, 289-315. (9) V.R. Baker and J.B. Partridge (1984) in Lunar and Planetary Science XV, Lunar and Planetary Inst., Houston, 23-24. (10) R.E. Horton (1945) Geological Soc. America Bull., 56, 275-370. (11) A.D. Abrahams (1984) Water Resources Research, 20, 161-188. (12) T. Dunne (1980) Progress in Physical Geography, 4, 211-239. (13) J. Budel (1982) Climatic Geomorphology, Princeton Univ. Press. (14) C.D. Ollier (1981) Tectonics and Landforms, Longman. (15) D. Wallace and C. Sagan (1979) Icarus, 39, 385-400. (16) M.H. Carr (1983) Icarus, 56, 476-495. (17) W.P. Ward (1974), Jour. Geophys. Res., 79, 3375-3386. (18) H.E. Newsom (1980) Icarus, 44, 207-216. (19) C.S. Breed, J.F. McCauley, and M.J. Grolier (1982) Jour. Geophys. Res., 87, 9929-9950.

MARS WATER-ICE CLOUDS; P.R. Christensen, Department of Geology, Arizona State University, Tempe, Arizona, 85287 and R.W. Zurek, Jet Propulsion Laboratory, California Institute of Technology

The distribution of water in the martian atmosphere plays an important role in the present meteorology of Mars. It also provides a key to understanding the past climate and climatic changes because direct observations of water and other volatiles provide a means for testing models of volatile transport between the regolith and atmosphere, for determining sources and sinks of volatiles, and for determining the time scales for volatile migration (e.g. 1,2,3).

Many recent studies have addressed the questions of atmospheric water vapor distribution and possible sources and sinks of water on the surface using earth-based observations of water vapor abundances and observations obtained by the Viking Mars Atmospheric Water Detector (MAWD) (e.g. 4,5,6,7, and many others). In addition to water vapor, however, condensed water in water-ice hazes and clouds plays an important role in the understanding of the processes controlling the distribution and history of water on Mars and must be included with water vapor in order to assess the total atmospheric water abundance. Furthermore, the presence of water-ice clouds provides direct evidence for the occurrence of saturation conditions within the atmosphere. Finally, the seasonal, diurnal, and spatial distribution of water clouds provides information about the variability of atmosphere water on these time scales and about the surface and atmospheric properties which influence cloud formation.

We have used Infrared Thermal Mapper (IRTM) mid-IR spectral observations to locate water-ice clouds using the infrared absorption properties of water-ice. The IRTM instrument obtained data in five thermal bands centered at 7, 9, 11, 15 and 20 μm, and one solar reflectance band between 0.3 and 3 μm (8). The thermal data are used to determine brightness temperatures, referenced to the band for which they were determined (i.e., T_7) that can be used to measure spectral variations in the martian surface and atmosphere due to non-uniform surface properties and atmospheric aerosols (9). In particular, the 11 μm band IRTM is located within a broad 10 to 18 μm absorption feature characteristic of water ice, and is therefore sensitive to the presence of water ice. The 20 μm band only partially overlaps this feature and the 7 and 9 μm bands are nearly transparent to water-ice. Thus, spectral observations can detect water-ice using differences between these brightness temperatures, provided there is sufficient contrast between the ground and atmospheric temperature (10).

Using this technique clouds and hazes have been detected and characterized on Mars through two years of observations. They are consistently observed in four northern hemisphere regions centered over Tharsis (-10°S to 50°N, 60° to 160°W), Arabia (0° to 20°N, 300° to 360°W), Elysium (20° to 40°N, 190° to 220°W), and along the boundary between the cratered uplands and the northern plains (-10°S to 10° N, 210° to 270°W). Clouds in those regions were observed at all seasons when the atmosphere had a low enough dust content to permit the spectral signature of water-ice to be observed; during the global dust storm period (L_s 200° to 300°) clouds are difficult to distinguish from dust.

During the northern spring and summer (L_s 0° to 180°) when the atmosphere is relatively free of dust, there is a distinct difference between the cloud abundance in the northern and southern hemispheres, with clouds and hazes being rare in the south. There are several possible explanations for this difference. First, clouds will be less likely to form in the south due to low, wintertime atmospheric temperatures and high atmospheric stability (11). A second possibility involves the importance of orographic control for cloud formation, resulting in more clouds centered over topographic highs that are preferentially located in the north. Finally, northern hemisphere clouds appear to occur preferentially over low thermal inertia regions which are primarily located in the northern hemisphere. If seasonal rather than surface, control is the dominant effect then the observed cloud pattern should reverse during southern spring and summer. However, clouds are difficult to detect during southern summer due to the presence of atmospheric dust. Clouds are much less commonly observed in both the north and the south during this season, but their presence within or beneath the dust haze cannot be ruled out on observational grounds.

A second important class of water-ice clouds are those observed along the boundary of the retreating north polar cap between L_s 340° and 65° (10). These clouds occur at all longitudes around the cap and are generally confined to within ±5° of the cap boundary. After L_s 65° polar water-ice clouds are no longer observed. Similar clouds are not observed along the southern cap during retreat, although observations are again impaired by the presence of atmospheric dust during this season.

The cloud opacities can be estimated using a δ-Eddington radiative transfer model (10) which incorporates Mie scattering and the electrical properties of water-ice. Assuming realistic, but non-unique, values for the ice particle size and cloud temperature, the derived opacities range from near-zero to 1.

In summary, IRTM observations provide a direct means of identifying water-ice clouds on Mars. These observations have sufficient spatial resolution, and spatial and temporal coverage to permit a detailed investigation of the important parameters governing their formation. They are consistently observed in four major northern hemisphere locations and along the edge of the retreating north polar cap. The IRTM data are currently being assembled into an "atlas" to permit further studies of their diurnal and seasonal behavior.

REFERENCES

(1) Leovy, C.B., 1973, Exchange of water vapor between the atmosphere and surface of Mars, Icarus, 18, 120-125.
(2) Fanale, F.P., J.R. Salvail, W.B. Banerdt, and R.S. Saunders, 1982, Mars: The regolith-atmosphere-cap system and climate change, Icarus, 50, 381-407.
(3) Pollack, J.B. and O.B. Toon, 1982, Quasi-periodic climate changes on Mars: A review, Icarus, 50, 259-287.
(4) Barker, E.S., R.A. Schorn, A. Woszczyk, R.G. Tull, and S.J. Little, 1970, Mars: Detection of atmospheric water vapor during the southern hemisphere spring and summer season, Science, 170, 1308-1310.

(5) Farmer, C.B., D.W. Davies, H.L. Holland, D.D. LaPorte, and P.E. Doms, 1977, Mars: water vapor observations from the Viking orbiters, J. Geophys. Res., 82, 4225-4248.

(6) Davies, D.W., 1981, The Mars water cycle, Icarus, 45, 398-414.

(7) Jakosky, B.M. and C.B. Farmer, 1982, The seasonal and global behavior of water vapor in the Mars atmosphere: Complete global results of the Viking atmospheric water detector experiment, J. Geophys. Res., 87, 2999-3019.

(8) Kieffer, H.H., T.Z. Martin, A.R. Peterfreund, B.M. Jakosky, E.D. Miner, and F.D. Palluconi, 1977, Thermal and albedo mapping of Mars during the Viking primary mission, J. Geophys. Res., 82, 4249-4292.

(9) Christensen, P.R., 1982, Martian dust mantling and surface composition: Interpretation of thermophysical properties, J. Geophys. Res., 87, 9985-9998.

(10) Christensen, P.R. and R.W. Zurek, 1984, Martian north polar hazes and surface ice: Results from the Viking Survey/Completion mission, J. Geophys. Res., 89, 4587-4596.

(11) Kahn, R., 1983, Some observational constraints on the global scale wind systems on Mars, J. Geophys. Res., 88, 10189-10209.

MARS: GROUNDWATER MOUND DEVELOPMENT IN RESPONSE TO POLAR BASAL
MELTING; S. M. Clifford, Lunar and Planetary Institute, 3303 NASA Rd 1,
Houston, TX 77058.

Given a planetary inventory of H_2O sufficient to saturate the pore volume
of the Martian cryosphere with ice, the deposition of dust and H_2O in the polar
regions will create a situation where the equilibrium depth to the melting
isotherm has been exceeded, thus basal melting will begin and continue until
such time as the equilibrium depth is reestablished (Figure 1). The subsequent
deep percolation of meltwater will result in the rise of the local water table
in the form of a groundwater mound. The gradient in hydraulic head created by
the presence of the mound will then drive the flow of groundwater away from the
poles. As discussed in the companion to this abstract (1), this equatorward
flow of groundwater may play in important role in the climatic cycling of H_2O
on Mars.

The development of a groundwater mound in response to basal melting at the
Martian poles is analogous to a situation that has frequently been addressed
on Earth: the artificial recharge of an aquifer beneath a circular spreading
basin (2,3,4). As a result, the problem of groundwater mound development on
Mars can be readily addressed on the basis of well-established terrestrial
hydrogeologic models.

The simplifying assumptions that must be made to obtain an analytical
expression for the growth of a groundwater mound beneath a recharging source
are: i) the aquifer is homogeneous, isotropic, infinite in areal extent, and
rests upon a horizontal and impermeable base; ii) the hydraulic properties of
the aquifer are invariant in both space and time; and iii) the constant
downward percolation of water proceeds at a rate which is sufficiently small
(compared to the aquifer permeability) that the influx is almost completely
refracted in the direction of the local slope of the water table when it
reaches the mound (2,3,4).

After Hantush (2), the governing equation for the growth of a groundwater
mound beneath a circular recharging area is:

$$\frac{\partial^2 z}{\partial r^2} + \frac{1}{r}\frac{\partial z}{\partial r} + \frac{2w\nu}{kg} = \frac{\varepsilon\nu}{\bar{h}kg}\frac{\partial z}{\partial t} \qquad (1)$$

where $Z = h^2 - h_i^2$, h is the height of the water table above the base of the
aquifer after an elapsed time t, h_i is the initial saturated thickness of the
aquifer, $\bar{h}$ is a constant of linearization which represents the weighted mean
depth of saturation [approximated by $\bar{h} = .5(h + h_i)$], r is the radial distance
from the center of the mound, w is the rate of recharge, k is the aquifer
permeability, g is the acceleration of gravity, ν is the groundwater viscosity,
and ε is the effective porosity. The boundary and initial conditions that
apply to Equation (1) are:

$$z(r,0) = 0$$

$$\partial z(0,t)/\partial r = 0$$

$$z(\infty,t) = 0$$

$$w = w \quad 0 < r < R_w$$

$$= 0 \quad r > R_w$$

These conditions correspond to four basic assumptions: i) that the water table
is initially horizontal, ii) the groundwater mound is symetric about its
vertical axis, iii) the effect of localized recharge on the shape of the water
table at large radial distances is negligible, and iv) the recharge is limited
to a circular region of radius R_w (2,3,4).

Equation (1) can be solved using Laplace and zero-ordered Hankel
transforms (2), thereby yielding the following expression for the maximum
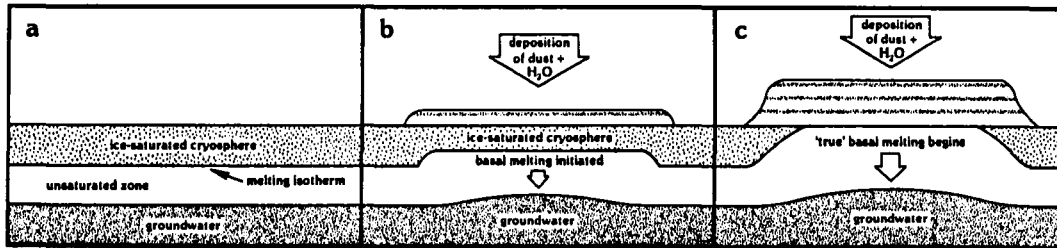
Figure 1. An idealized cross section of the Martian polar crust illustrating the possible time evolution of basal melting.

height, h_m, of the water table at a time t:

$$h_m^2 - h_i^2 = \frac{Q\nu}{2\pi kg}\left[W(u_o) + (1 - e^{-u}o)/u_o\right] \qquad (2)$$

where $Q = w \, \pi R_w^2$, $u_o = R_w^2 \nu \epsilon /4kght$, and where $W(u_o)$ is the well function for a nonleaky aquifer given by:

$$W(u_o) = \int_{u_o}^{\infty} \frac{e^{-u}o}{u_o} \, du_o \qquad (3)$$

In Table 1 groundwater mound heights are presented as a function of time based on aquifer hydraulic properties that might reasonably characterize the Martian crust. In these calculations the aquifer was assumed to have an initial thickness of 1 km, an effective porosity of 0.1, and a permeability of 10 md (10^{-14} m^2). The recharge area was taken to be equal in size to the Martian permanent north polar cap ($R_W = 500$ km); while the assumed recharge volume (Q) of .1 km^3 H_2O yr^{-1} is consistent with an average basal melting rate within this area of $\sim 10^{-4}$ m yr^{-1}. Given these conditions, we find that the resulting groundwater mound could grow to a height ($h_m - h_i$) of 1 km in $\sim 10^6$ years.

While the calculations presented in Table 1 assume an aquifer that is initially unconfined, they may be considered reasonable approximations for the case of an initially confined aquifer as well. Although it is clear that a groundwater mound, as such, cannot develop under conditions where the pore volume beneath the cryosphere is saturated with water, an increase in hydraulic head will nonetheless result in response to basal melting. The magnitude and time evolution of this increase will parallel that of the initially unconfined case illustrated in Figures 1 and 2.

Clearly, the growth of a polar groundwater mound raises the possibility that even an initially unconfined aquifer may eventually evolve to the point of confinement. In that event, any further increase in calculated mound height will again be realized as an effective increase in confined hydraulic head. Indeed, this interpretation is the appropriate one for the larger (≥ 1 km) mound height entries listed in Table 1. In this regard, the hydrostatic head represented by the last entry of 7250 m is the equivalent of the lithostatic pressure exerted by a 3 km-thick layer of ice-rich permafrost; as such, it probably reflects the maximum hydraulic head that could be achieved in a polar subpermafrost aquifer.

Eventually the polar groundwater mound may reach the height where the equatorward flow of groundwater will balance the vertical recharge that results from basal melting. When this steady-state condition is reached, any further growth of the mound will cease. Alternatively, if the permeability of the Martian crust is extremely low, the continued increase in confined hyraulic

Figure 2. Schematic illustrating the various relations
in groundwater mound development.

Table 1. Groundwater Mound Heights as a Function of Time.*

Time (yrs)	u_o	$W(u_o)$	Mound Height (m) $(h_m - h_i)$
1×10^6	5.212	9.43×10^{-4}	899
5×10^6	7.369	3.48×10^{-1}	2920
2.5×10^7	8.688	1.95	5370
1.25×10^8	1.159	3.93	7250

*Assumed values: porosity = 10%, permeability = 10^{-2} darcies, basal melting rate = .1 km^3/yr, basal melting radius = 500 km, initial aquifer thickness = 1 km.

head could eventually lead to the disruption of the overlying cap and catastrophic flooding within the polar terrains (5).

Basal melting and groundwater mound development may represent important stages in the regional and global redistribution of H_2O within the Martian crust. Further aspects of these processes, with particular emphasis on the permeability requirements necessary to support large-scale groundwater flow, are discussed elsewhere in these abstracts (1).

1) Clifford, S. M. (1984) Mars: Permeability requirements for a global groundwater system driven by polar basal melting. These abstracts.

2) Hantush, M. S. (1967) Growth and decay of groundwater-mounds in response to uniform percolation. Water Resources Research, 3, 227-234.

3) Marino, M. A. (1975) Artificial groundwater recharge, I. Circular recharging area. J. of Hydrology, 25, 201-208.

4) Schmidtke, K. D., McBean, E. A., and Sykes, J. F. (1982) Stochastic estimation of states in unconfined aquifers subject to artificial recharge. Water Resources Research, 18, 1519-1530.

5) Clifford, S. M. (1984) Polar basal melting on Mars, submitted to the J. Geophys. Res..

MARS: PERMEABILITY REQUIREMENTS FOR A GLOBAL GROUNDWATER SYSTEM
DRIVEN BY POLAR BASAL MELTING; S. M. Clifford, Lunar and Planetary Institute,
3303 NASA Rd 1, Houston, TX 77058.

Based on recent estimates of the planetary inventory of H_2O on Mars, it
has been suggested that Mars may possess subpermafrost groundwater systems of
regional (1) and possibly even global extent (2,3). If so, then the processes
of polar basal melting (4) and groundwater mound development (5) will result
in the creation of a pole-to-equator gradient in hydraulic head, that could
drive the equatorward flow of a significant quantity of subpermafrost
groundwater over the course of Martian geologic history. The equatorward flow
of this groundwater may be balanced at mid- to equatorial latitudes by a net
vertical migration of H_2O vapor, driven by the Martian geothermal gradient,
from the warmer depths to the colder near-surface regolith (6,7). In this way,
equatorial ground ice that is lost by sublimation to the atmosphere may undergo
a continuous process of subsurface replenishment (2,3,6,7).

The necessary permeability requirements for pole-to-equator groundwater
flow on Mars can be readily assessed on the basis of established models of
unconfined and confined steady-state well flow. As discussed in (5), a polar
groundwater mound will reach an equilibrium profile when the radial discharge
of groundwater within the aquifer system finally balances the amount of
recharge derived from basal melting (Figure 1). In this analysis the radius
of the well 'R_w' is analogous to the radius of the recharge (basal melting)
area discussed in (5); while, as before, the groundwater mound height is taken
to be the difference between the maximum and minimum hydraulic heads ($h_m - h_i$).
The distance 'R' to the region of lowest hydraulic head represents the
separation between the regions of net vertical recharge (polar) and discharge
(equatorial), and is taken here to be of the same scale as the planetry radius
of Mars. These relationships are illustrated in Figures 2 and 3.

The governing equation and appropriate boundary conditions for steady
unconfined well flow are (8):

$$\frac{\partial}{\partial r}\left[r\,\frac{\partial(h^2)}{\partial r}\right] = 0 \qquad\qquad (1)$$

$$h^2 = h_i^2 \quad (r=R)$$

$$Q = 2\pi r h v \quad \text{(conservation of mass)}$$

where v is the specific discharge (the discharge per unit area) given by
Darcy's law:

$$v = -\frac{kg}{\nu}\frac{\partial h}{\partial r} \qquad\qquad (2)$$

Solving Equation (1) in light of the above boundary conditions, we obtain:

$$h^2 = h_i^2 + \frac{Q\nu}{\pi kg}\ln(R/r) \qquad (R_w \leq r) \qquad (3)$$

Evaluated at $r=R_w$ Equation (3) yields an expression for the maximum hydraulic
head, from which we can obtain the following necessary permeability requirement
for unconfined steady-state well flow:

$$k = \frac{Q\nu}{\pi g(h_m^2 - h_i^2)}\ln(R/R_w) \qquad\qquad (4)$$

Of course, the possibility exists that the groundwater mound of an
initially unconfined aquifer could grow to the point of contact with the base
of the polar cryosphere; in this event, the aquifer may undergo a transition

MARS: PERMEABILITY REQUIREMENTS FOR GLOBAL GROUNDWATER FLOW
Clifford, S. M.

21

between confined conditions at the poles to unconfined conditions closer to the equator. Indeed, the planetary inventory of H_2O on Mars may be sufficiently large that the subpermafrost aquifer has been confined at the poles from the very outset of basal melting. Given either case, the solution presented in Equation (4) will no longer apply.

To analyse the possibility of confined flow, we solve the steady confined well equation, given by (8):

$$\frac{\partial}{\partial r} \left[r \frac{\partial h}{\partial r} \right] = 0 \qquad\qquad (5)$$

and which is subject to the boundary conditions:

$$h = h_i \;\; (r=R) \qquad Q = 2\pi r h_i v$$

Solving for the permeability in the same fashion as before, we find:

$$k = \frac{Qv}{2\pi h_i g (h_m - h_i)} \ln(R/R_w) \qquad\qquad (6)$$

In Table 1, permeabilities calculated from Equations (4) and (6) are presented for a reasonable range of polar recharge volumes and net hydraulic heads. The results indicate that a recharge volume of 1 km^3 of H_2O per Martian year, introduced into a 1 km thick aquifer at the Martian poles, could drive the flow of a similar volume of water to the Martian equator, given a regolith permeability of 25 darcies and a groundwater mound height of 100 m. If the recharge volume is lowered to 10^{-2} km^3 of H_2O per Martian year, and if we permit a net hydraulic head equivalent to the lithostatic pressure exerted by a 3 km thickness of ice-rich permafrost, then the minimum permeability of the regolith required to support a global groundwater flow system falls to approximately 10^{-3} darcies, a value which lies within the lower extreme of permeabilities for fractured igneous and metamorphic rock (Figure 4).

The significance of these minimum regolith permeability requirements can be placed in perspective by comparing them with the regolith value assumed by Carr (1) in his discussion of the possible role of confined aquifers in the formation of Martian flood features. Based on the measured permeability of a number of basalt aquifers on Earth, Carr (1) concluded that a reasonable estimate of the permeability of the Martian megaregolith might be of the order of 10^3 darcies, a value that is roughly 10^2 to 10^6 times greater than that required to support a Martian groundwater flow system driven by polar basal melting. It is important to note that these numbers represent effective permeabilities. Therefore, if only a very small fraction of the Martian regolith possesses a permeability as high as that estimated by Carr (1), then the necessary minimum permeability requirements for global groundwater flow on Mars will have been satisfied.

If the present planetary inventory of H_2O on Mars exceeds, by more than a few percent, the quantity required to saturate the pore volume of the Martian cryosphere, then a subpermafrost groundwater system of global extent is likely to exist. If so, then the long-term deposition of dust and H_2O in the Martian polar regions will eventually lead to basal melting and the development of groundwater mounds at both poles. Given a geologically reasonable value for the permeability of the Martian crust, the gradient in hydraulic head created by the presence of these groundwater mounds could drive the pole-to-equator flow of substantial quantities of H_2O. From such a system, equatorial ground ice could be readily and continuously replenished; obviating the need for the

MARS: PERMEABILITY REQUIREMENTS FOR GLOBAL GROUNDWATER FLOW
Clifford, S. M.

22

improbable scenario required of any atmospheric replenishment model (9).
Subpermafrost groundwater transport may therefore play an important role in the
long-term cycling of H_2O between the Martian atmosphere, polar caps, and deep
regolith.
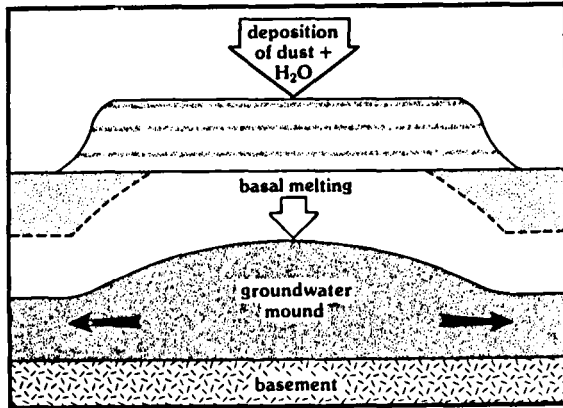
Figure 1.
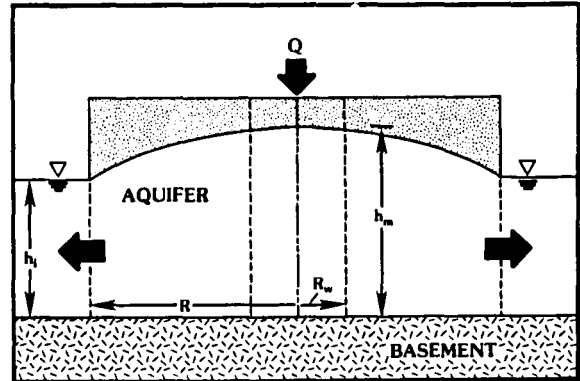
Figure 2.
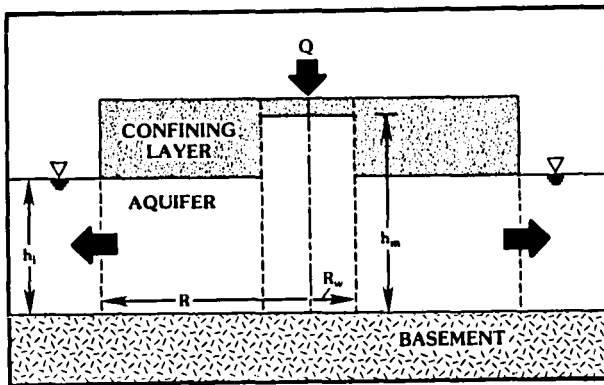
Figure 3.
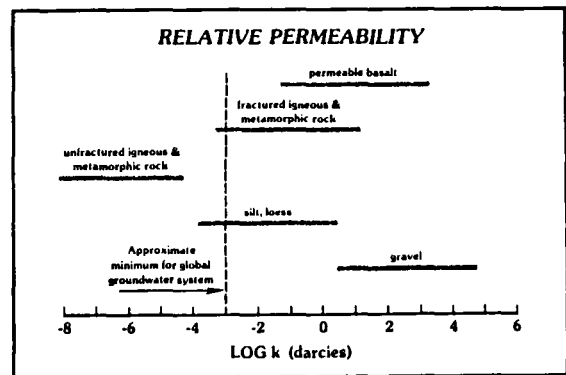
Figure 4.

Table 1. Minimum regolith permeability requirements for steady-state flow.

	Q (km³/yr)	Mound Height (m)	k (darcies)
UNCONFINED:	1	10^2	25
	10^{-2}	10^4	2.5×10^{-1}
CONFINED:	1	10^2	26
	10^{-2}	10^2	2.6×10^{-1}
	10^{-2}	10^4	2.6×10^{-3}

REFERENCES: 1) Carr, M. H. (1979) Formation of Martian flood features by release of water from confined aquifers, J. Geophys. Res., 82, 4039-4055. 2) Clifford, S. M. and Huguenin, R. L. (1980) The H_2O mass balance on Mars: Implications for a global subpermafrost groundwater flow system, NASA TM 81776, 144-146. 3) Clifford, S. M. (1984) A model for the climatic behavior of water on Mars, Ph.D. dissertation, Dept. of Physics and Astronomy, University of Massachusetts, 286 p. 4) Clifford, S. M. (1984) Polar basal melting on Mars, submitted to J. Geophys. Res.. 5) Clifford, S. M. (1984) Mars: Groundwater mound development in response to polar basal melting, these abstracts. 6) Clifford, S. M. (1980) Mars: Ground ice replenishment from a subpermafrost groundwater system, in: Proc. 3rd Colloq. Planet. Water, 68-67. 7) Clifford, S. M. (1982) Mechanisms for the vertical transport of H20 in the Martian regolith, in: Papers presented to the Conference on Planetary Volatiles, 23-24. 8) Todd, D. K. (1959) Groundwater Hydrology, John Wiley & Sons, New York, 336 p. 9) Clifford, S. M. (1984) Equatorial ground ice on Mars: A comparison of potential atmospheric and lithospheric replenishment models, in preparation.

RADIATION-DOMINATED SNOWMELT ON MARS

Gary D. Clow, U.S. Geological Survey, Menlo Park, CA 94025

The currently favored hypothesis for the formation of the martian valley networks is that they were cut by the action of running water. Carr (1) has shown that liquid water can flow hundreds of kilometers in ice-covered streams and that this behavior is remarkably insensitive to climate. However, the generation of sufficient volumes of liquid water to initiate streamflow remains a significant problem. Several global-climatic models (2,3,4,5) have shown that greenhouse warming will not lead to surface temperatures near the melting point of water until surface pressures are approximately 1 bar. The existence of the valley networks, coupled with the results of these studies, has been taken as evidence that the climate on Mars differed radically when the valleys formed. Furthermore, a recent study by Postawko (6) appears to make generation of liquid water on Mars through the greenhouse effect even more difficult. In her latitudinally resolved climatic model, Postawko demonstrates that meridional heat transport will prevent equatorial temperatures from reaching 273 K for pressures as high as 3 bars, unless the planetary albedo was much lower than the present value or gases in addition to CO_2 and H_2O were responsible for the greenhouse effect.

Nonetheless, microclimatic conditions may have occasionally existed on Mars which were more conducive to the generation of liquid water than those suggested by global-climatic studies. The present study is concerned with the melting of snow in the equatorial zone during periods of low winds, such that sensible and latent heat losses from the snow to the atmosphere are minimized. The model developed for this investigation incorporates a CO_2- H_2O atmosphere over a snow layer of arbitrary thickness and a rocky substrate. Sensible heat and water vapor are transferred through the atmospheric boundary layer by a combination of molecular diffusion and stability-dependent eddy diffusion based on the Businger parametrization (7). Above the boundary layer, the atmosphere is assumed to be saturated with water vapor and to have an approximately adiabatic temperature gradient. Downward traveling infrared fluxes due to the CO_2 and H_2O emission bands are calculated over the spectral range 50–2000 cm^{-1}. The model also includes penetration of sunlight into the snow, the temperature- and density-dependent thermal conductivity of snow, and downward migration of meltwater within the snowpack.

The results can be viewed at several levels. All calculations have been made at latitude 30°S under relatively "clear" skies (atmospheric optical depth, 0.16), using the present martian orbital parameters and solar constant. The snow's albedo and density have been set at 0.5 and 0.25 g cm^{-3} respectively. The windspeed at the top to the boundary layer was set at 1 m s^{-1} to minimize sensible heat transfer to the air. At the first level, mean annual surface temperatures were calculated for various atmospheric pressures. As expected, mean annual surface temperatures remain quite low (less than 205 K) for pressures lower than 100 mbars. However, at 300 mbars the net radiative flux at the surface is so intense

that snowmelt is pervasive. Steady-state solutions for the temperature profile within a snowpack reveal that the profile becomes nearly isothermal at depths greater than a few optical pathlengths in snow and that the deep-snow temperature is enhanced above the surface value by an amount dependent on the total solar flux absorbed by the snow and on the ratio of the snow's optical pathlength to its thermal conductivity. Under clear skies, steady-state deep-snow temperatures can exceed surface temperatures by 35-55 K in the equatorial zone if the optical pathlength is 10 cm. Although this effect is large, it is still insufficient to allow melting at depth for a 100 mbar atmosphere under mean annual conditions. Finally, the effect of seasonal solar insolation changes were considered by starting with the mean-annual-temperature profile at aerocentric longitude 180° and allowing Mars to proceed through its orbit for 200 days. A 66-cm-thick snow layer was selected for this simulation. By midsummer, extensive melting occurred for a 100 mbar atmosphere despite the cold temperatures deep within the rocky substrate. The 273-K isotherm was also reached for a 30 mbar atmosphere, although the melt volume appears to be too small to allow downward migration of liquid water.

For a radiation-dominated regime, snow in the equatorial zone could have melted at pressures considerably lower than 1 to 3 bars. The exact atmospheric pressure at which this could have occurred is sensitive to the ratio of optical pathlength to thermal conductivity for snow and depends on the prevalence of low windspeeds for a significant fraction of the martian year.

References

(1) Carr, M.H., 1983, Stability of streams and lakes on Mars, Icarus, 56, p. 476-495.
(2) Pollack, J.B., 1979, Climatic change on the terrestrial planets, Icarus, 37, p. 479-553.
(3) Cess, R.D., Ramanathan, V., and Owen T., 1980, The martian paleoclimate and enhanced atmospheric carbon dioxide, Icarus, 41, p. 159-165.
(4) Toon, O.B., Pollack, J.B., Ward, W., Burns, J.A., and Bilski, K., 1980, The astronomical theory of climatic change on Mars, Icarus, 44, p. 552-607.
(5) Hoffert, M.I., Callegari, A.J., Hsieh, C.T., and Ziegler, W., 1981, Liquid water on Mars: an energy balance climate model for CO_2/H_2O atmospheres, Icarus, 47, p.112-129.
(6) Postawko, S.E., 1983, Martian paleoclimate, Ph.D. thesis, University of Michigan, 147 pp.
(7) Businger, J.A., Wyngaard, J.C., Izumi, Y., and Bradley, E.F., 1971, Flux-profile relationships in the atmospheric surface layer, J. Atmos. Sci., 28, p.181-189.

MARS: LONG TERM CHANGES IN THE STATE AND DISTRIBUTION OF H_2O.

F.P. Fanale, J. R. Salvail, A.P. Zent, and S.E. Postawko; Planetary Geosciences Division, Hawaii Institute of Geophysics, University of Hawaii, Honolulu, Hawaii 96822

A model for H_2O distribution and migration on Mars has been formulated which takes into account: 1) thermal variations at all depths in the regolith due to variations in obliquity, eccentricity and the solar constant; 2) variations in atmospheric PH_2O caused by corresponding changes in polar surface insolation; and 3) the finite kinetics of H_2O migration in both the regolith and atmosphere. Results suggest that the regolith H_2O transport rates are more strongly influenced by polar-controlled atmospheric PH_2O variations than variations in pore gas PH_2O brought about by thermal variations at the buried ice interface. The configuration of the ice interface as a function of assumed soil parameters and time is derived. Withdrawal of ice proceeds to various depths at latitudes $< 50^{\circ}$ and is accompanied by filling of regolith pores at latitudes $> 50^{\circ}$ and transfer of H_2O to the polar cap. The transfer has a somewhat oscillatory character, but only $< 1g/cm^2$ is shifted into and out of the regolith during each obliquity cycle. The net irreversible and inexorable transfer of H_2O to higher latitudes involves between $1 \times 10^6 km^3$ and $1 \times 10^7 km^3$ of H_2O over the history of Mars for most reasonable sets of assumptions. This mass is comparable to the amount of material removed from deflated terrain at mid and low latitudes and to the mass of the polar cap. We conclude that this process combined with periodic thermal cycles played a major role in development of the fretted terrain, deflationary features in general, patterned ground, the north polar cap and the layered terrain.

SOURCES AND SINKS OF PRESENT DAY WATER WITHIN THE MARTIAN REGOLITH:
EVIDENCE FROM A TERRESTRIAL ANALOG OF MARTIAN WEATHERING PROCESSES-THE DRY
VALLEYS OF ANTARCTICA.   Everett K. Gibson, Jr., SN4, Experimental Planet-
ology Branch, NASA Johnson Space Center, Houston, Texas 77058 (Presently at
Dept. of Earth Sciences, The Open University, Walton Hall, Milton Keynes,
England)

Initial information about the water abundances of the Martian regolith
was obtained from the gas chromatograph-mass spectrometer (GC-MS) experiment
on board the two Viking landers. Anderson and Tice (1979) noted that the
total amount of water released from Martian soils was estimated to range from
1.0 to 1.9 percent by weight. Small amounts of water were lost by the soils
at 200°C (<0.2 o/o), but at 350° and 500°C significant amounts(0.1 to 1.4 o/o)
were detected during pyrolysis of soil samples. Water released during the
higher temperature interval was thought to be associated with decomposition
of hydrate minerals. Kotra et al. (1982) reviewed the release of volatiles
from possible Martian materials and noted the wide variety of minerals that
could be present within samples analyzed by Viking. Their studies noted that
the manner in which the Viking's volatile release information was obtained
may not account for significant amounts of volatiles or volatile-bearing
secondary minerals present within the Martian regolith.

It is well known that secondary minerals within soils and regoliths may
be reservoirs for significant amounts of volatiles. The nature of the authi-
genic secondary minerals in soils from the terrestrial analog for the Martian
regolith found in the Dry Valleys of Antarctica has been reviewed by Gibson
et al. (1983). In common with soils from other arid parts of the world (El
Baz and Prestel, 1980), soluble salt concentrations are characteristic of Dry
Valley soils. The origins of the water soluble ions forming the Dry Valley
salts is controversial: proposed origins include chemical weathering of rocks,
hydrothermal fluids, marine aerosols, and the evaporation of water from
marine incursions. Gibson et al. (1983) noted that the molar ratios of the
water soluble ions reflect the nature of the secondary minerals present. For
example, when the Na^+ and Cl^- molar ratios are equal (i.e. 1:1) the presence
of halite is indicated. Similarily, when the Ca^{2+} to Cl^- ratio is 1:2, ant-
arcticite ($CaCl_2 \cdot 6H_2O$) is present.

Most silicate mineral and lithic fragments in the Dry Valley soils exhibit
some degree of alteration. A major problem is in determining which alteration
effects are caused by in situ weathering and which are the result of other pro-
cesses. Some alteration resulted from hydrothermal activity in the source
rock-epidote and sericite, for example, are hydrothermal minerals, and some
amphiboles have been replaced by biotite. In addition, weathering may have
occurred prior to deposition at the soil sites. It is also possible that some
of the diagenesis occurred during the subaqueous history of the soils.

There is, however, good evidence for present day weathering in the Dry
Valley soils.   The sharp increase in iron oxide near the surfaces, especially
relative to fresh ferromagnesian minerals, demonstrates increased oxidation
towards the surface (Gibson et al., 1983). This phenomenon has been noted
previously by Bockheim (1979). Evaporites indicate ionic migration and
chemical activity even in the permanently frozen zones. Halite abundances,
for example, decrease systematically from the salt layer near the surface to
the bottom of a one meter deep soil pit. Even though halite abundances are
very low near the bottom, there is no indication of a break at the boundary of
the permanently frozen zone. Secondary calcite abundances increase with
depth; the reason for this is not presently understood. The presence of these

evaporites also indicates that chemical weathering of rocks and possibly soils has been active within the soil profiles becasue some of the water soluble ions (Ca^{2+}, Mg^{2+}, K^+, and CO_3^{2-}) in the evaporites originated by rock weathering (Keys and Williams, 1981).

Individual silicate mineral fragments in both the active and the permanently frozen zones show evidence of chemical weathering (Gibson et al.,1983). The characteristic effect of chemical weathering on the surfaces of minerals in temperate climates is dissolution along crystallographically-controlled zones of weakness (Berner et al., 1980). Such dissolution features are common on the surfaces of susceptible silicate fragments (feldspars, amphiboles, and pyroxenes) throughout the Dry Valley soils studied. Differential weathering along exsolution lamellae is present in some pyroxenes. Because such delicate features would probably not survive sedimentary transport, they are evidence for in situ chemical weathering.

Zeolites are well known for their ability to store volatiles. Zeolites have been found in Dry Valley soils and their occurrance and habit shows their fragile nature. They are euhedral, unabraded, and unfractured, which strongly suggests in situ formation. Their presence in the Dry Valley soils is another indication that diagenetic processes are active throughout the soils. Pedogenic zeolites are not usually found in Antarctic soils. Chabazite and other zeolites have been identified in rock cores from the Dry Valley Drilling Project (DVDP), but their origin is attributed to hydrothermal processes (Berkley and Drake, 1981). Zeolites of sedimentary or pedogenic origin are fairly common in other terrestrial climates. The presence of chabazites in the Dry Valley soils is consistent with other occurrences in that they form in an arid environment under saline, alkaline conditions (Hay, 1977).

Weathering of planetary surface materials results from both chemical and physical interactions of the planet's surface with the atmosphere and, if present, the hydrosphere and biosphere. The net result of weathering is to modify the original surface materials and produce secondary materials that are the products of an approach to equilibrium between the atmosphere and solid body. The detailed study of the soils from the Dry Valleys of Antarctica has produced an idealized soil profile which should be applicable to the Martian regolith. The soil profile would be composed of four basic zones: (1) aeolian zone; (2) salt zone; (3) active zone; and (4) permanently frozen zone. Processes operating within each of these zones tend to modify the original surface materials. The three zones above the permanently frozen zone are the regions where most of the chemical and physical weathering occurs.

It is known that Martian surface conditions may be favorable for chemical weathering (Gooding, 1978; Booth and Kieffer, 1978). The primary silicates would be expected to be reactive minerals such as pyroxenes, olivines, and feldspars. Because of the possible existence of an extensive sub-surface system of water ice or even liquid water (Clifford, 1981), water is probably available to assist in the weathering of the reactive minerals. Such weathering would result in the formation of clays, sulfates, carbonates, hydrates, and zeolites. The formation of pedogenic zeolites under cold, arid Antarctic conditions opens the possibility that zeolites may also form in the Martian regolith. Terrestrial zeolites are especially common in soils derived from volcanic ejecta (Hay, 1977), and such soils may be common on Mars. Zeolites are well known for their volatile exchange and storage properties. Consequently, the possible presence of a significant abundance of zeolites in the Martian regolith may have a profound effect on the volatile budget of Mars. Specifically, zeolites could be a repository of atmospheric gases including CO_2, O_2, and H_2O. Changes in pressure and temperature might induce Martian zeolites to take up or release significant quantities of volatiles.

Gibson, E.K. Jr.

In summary, Martian soil subjected to chemical weathering processes could contain the following likely constituents: (1) fresh primary silicate material; (2) partially altered primary silicates; (3) secondary minerals, possibly including clay minerals, evaporites, carbonates, sulfates, hydrates and zeolites; and (4) altered volcanic glass or impact glass. The soil may also include palogonite and other alteration products and secondary minerals. It is unlikely therefore that an equilibrium assemblage of minerals would be present. From the detailed study of the soils from the Dry Valleys of Antarctica, it is obvious that the complex processes in operation produce major changes in the parent materials, depending upon where the constituents reside and the degree to which weathering and diagenesis operates. It is furthermore, clear that natural near-surface environments, even in very cold and dry regions, may produce extremely complex soils. It seems obvious that for any analysis conducted by a remote instrument, extreme caution must be taken when interpreting the results and drawing conclusions, especially about possible processes operating in regoliths in cold, arid environments similar to those of the Dry Valleys or Mars.

References

Anderson D.M. and Tice A.R. (1979) J. Mol. Evol. 14, 33-38.
Berkley J.L. and Drake M.J. (1981) Icarus, 45, 231-249.
Berner R.A. et al. (1980) Science 207, 1205-1206.
Bockheim J.G. (1979) Soil Science 128, 142-152.
Booth M.B. and Kieffer H.H. (1978) J. Geophys. Res. 83, 1809-1815.
Clifford S.M. (1981) Third Inter. Colloq. on Mars, (abstracts), pp. 44-45.
El Baz F. and Prestel D. (1980) Lunar and Planet Sci. XI, 254-256.
Gibson E.K. Jr. et al. (1983) Proc. Lunar and Planet Sci. Conf., 13th, J. Geophys. Res., Suppl. A912-A928.
Gooding J.L. (1977) Icarus 33, 483-513.
Hay R.L. (1977) Mineralogy and Geology of Natural Zeolites, pp. 53-66, M.S.A. Publication.
Keys J.R. and Williams K. (1981) Geochim. Cosmochim. Acta 45, 2299-2309.
Kotra R.K. et al. (1982) Icarus 51, 593-605.

WATER AND ICE IN THE MARTIAN REGOLITH: DEPENDENCE OF STABILITIES ON REGOLITH MINERALOGY.   J. L. Gooding, SN2/Planetary Materials Branch, NASA/Johnson Space Center, Houston, TX 77058 USA.

Introduction. Water on Mars can be expected to interact with the Martian regolith in the following three ways:
(a) adsorption/absorption (on free surfaces or within cavities of particles),
(b) condensation (as liquid or quasi-liquid films or as ice),
(c) chemical reaction (by weathering to form new minerals or mineraloids).
Interactions of types (a) and (b) might be reversed by warming of the regolith during diurnal, seasonal, or climatic temperature cycles. Interactions of type (c), though, may be irreversible if the hydrous weathering products are stable or metastable with respect to dehydration under ambient conditions. However, all three processes should be interdependent because types (a) and (b) can be expected to vary not only with particle size and porosity but also with phase composition of the regolith. Specifically, abundances of both adsorbed water and of "unfrozen" water (quasi-liquid water below the nominal freezing point of pure, bulk water [1,2]) should depend on the specific surface area of the substrate. To better delineate the dependence of process (b) on regolith mineralogy, new experiments on freezing and melting of wet rocks were conducted with minerals that are common alteration products of mafic rocks on Earth and with samples of various regoliths formed on terrestrial basalts.

Samples and Methods. In each experiment, a granular, 10-12 mg sample was wet with 4 mg of water (yielding a mass ratio of 0.29-0.41 g water/g dry "rock") and then equilibrated at 300 K under a constant flow of dry carbon dioxide in the sample block of a microcomputer-automated Perkin-Elmer DSC-2C differential scanning calorimeter. After cooling at 5 K/min to 200 K and re-equilibration at that temperature, the sample was re-heated at 5 K/min to 300 K. Energy flow was recorded during both cooling and heating cycles. Individual minerals, characterized by x-ray diffractometry and electron probe microanalysis, occurred naturally in a variety of crystal sizes but were pulverized to a common size range of approximately 10-60 μm before analysis. For each "regolith" sample, the >63,<125-μm sieve fraction was used as an approximation to the estimated median particle size of the "soil" (<1-mm) fraction of the global Martian regolith [3]. Previously documented regolith samples included glacial-outwash debris and weathered tephra from the summit of Mauna Kea volcano, Hawaii, (3B,5B[4]), a subglacial palagonite tuff from Gaesafjoll volcano, Iceland (G13[5]), and dune sand from the Ka'u Desert region of Kilauea volcano, Hawaii (K1980-8B [6]).

Freezing Effects. Each sample undercooled prior to heterogeneous nucleation and freezing and exhibited an enthalpy of freezing (integrated freezing peak) that was less than the enthalpy of melting (integrated melting peak during heating cycle). The amount of undercooling, T(uc), was defined as the difference between the extrapolated-onset temperatures of melting and freezing. The enthalpy of freezing divided by the enthalpy of melting provided an ice-conversion ratio, R(ic), that is an index of the relative efficiency with which ice crystallized from the undercooled water. For pure water, R(ic) < 1 because, after initial freezing, water persisted for an additional 13-K undercooling in a metastable form having a heat capacity that is different than that of stable ice. Values of R(ic) < 1 for rock/water mixtures can be interpreted either in terms of undercooled metastable ice (as for pure water) or in terms of mineral/water complexation that withdraws part of the water inventory into a form that resists segregation into ice [1,2].

The latter interpretation is supported by occurrence of additional small peaks in the cooling or heating curves of most samples. Variations in T(uc) indicate the relative ice-nucleation abilities of the samples whereas variations in R(ic) indicate the relative water-complexation abilities of the samples (Fig. 1). A possible weathering-sequence trend of R(ic) vs. T(uc) is defined by a series of lithologically similar "regoliths," including relatively unweathered dune sand (basalt glass + olivine + lithic fragments), palagonite tuff (basalt glass + palagonite), and heavily weathered tephra (basalt glass + allophane + 7-A phyllosilicate) (Fig. 1). Zeolites (chabazite, analcime) and goethite extract significant amounts of water into unfrozen forms and plot along the tephra/dune sand trend although smectite- and chlorite-type clay minerals plot well away from that trend. A tenuous trend from pure water to dune sand to moderately weathered glacial outwash (lithic + mineral fragments) suggests that igneous minerals may be more efficient at nucleating and retaining ice than is basalt glass.

Melting Effects. Each frozen mixture melted over a temperature range defined by the lower- and upper-temperature limits of the melting peak (identified by first-derivative inflections of the heating curve). "Melting" at temperatures below the lower limit for pure ice indicates the formation of "unfrozen" water [1,2] and, as expected, depends significantly on substrate mineralogy (Fig. 2). Clay minerals produced the most profound effects although structures with exchangeable interlayer sites (e.g., nontronite) seem to be more potent in this repect than are structures without such sites (e.g., chlorite), an observation that is consistent with the contrast between the unfrozen-water efficacies of smectite and kaolinite [2]. "Melting" intervals that extend to temperatures above the upper limit for pure ice (e.g., chabazite, palagonite tuff) indicate melting of ice plus release of water from mineral/water complexes having transition temperatures that are only slightly greater than that of ice.

Survival, Storage, and Migration of Water in the Martian Regolith. Although expandable clay minerals (e.g., smectites) are favored in some mineralogical models of Martian surface fines, they are less efficient at nucleating ice than are non-expandable clay minerals. Consequently, frost formation on Mars, by heterogeneous nucleation on either the surface or on atmospheric dust, should be relatively unfavorable unless there exist abundant, fine-grained minerals other than smectites. However, debris flows fluidized by water (lobate crater ejecta, channel or slope mudflows, etc.) should survive longer if the suspended load is dominated by smectites or other minerals of low ice-nucleation efficacy. Once an icy regolith has formed, though, an abundance of clay minerals (especially smectites) would favor formation and migration of interfacial water at temperatures well below 273 K. However, an abundance of strong water-complexing phases such as chabazite or palagonite should be expected to extract significant amounts of water into forms that would be thermally more stable than ground ice and, hence, might constitute a portion of the Martian water budget that is inaccessible to the atmosphere/regolith water cycle.

References: [1] Anderson D. M. (1966) Res. Rep. 219, U. S. Army Cold Regions Research and Engineering Laboratory, Hanover, NH, 31 p. [2] Anderson D. M. (1968) Israel J. Chem., 6, 349-355. [3] Gooding J. L. (1981) Papers Presented to Third International Colloquium on Mars, LPI Contr. 441, Lunar and Planetary Institute, Houston, TX, 95-97. [4] Japp J. M. and Gooding J. L. (1980) Reports Planet. Geol. Program -1980, NASA Tech. Memo. 82385, 212-214. [5] Allen C. C., Gooding J. L., and Keil K. (1981) Icarus, 45, 347-369. [6] Gooding J. L. (1982) J. Geol., 90, 97-108.

DYNAMIC FREEZING OF ROCK / WATER COOLED 5 K/MIN UNDER CO₂
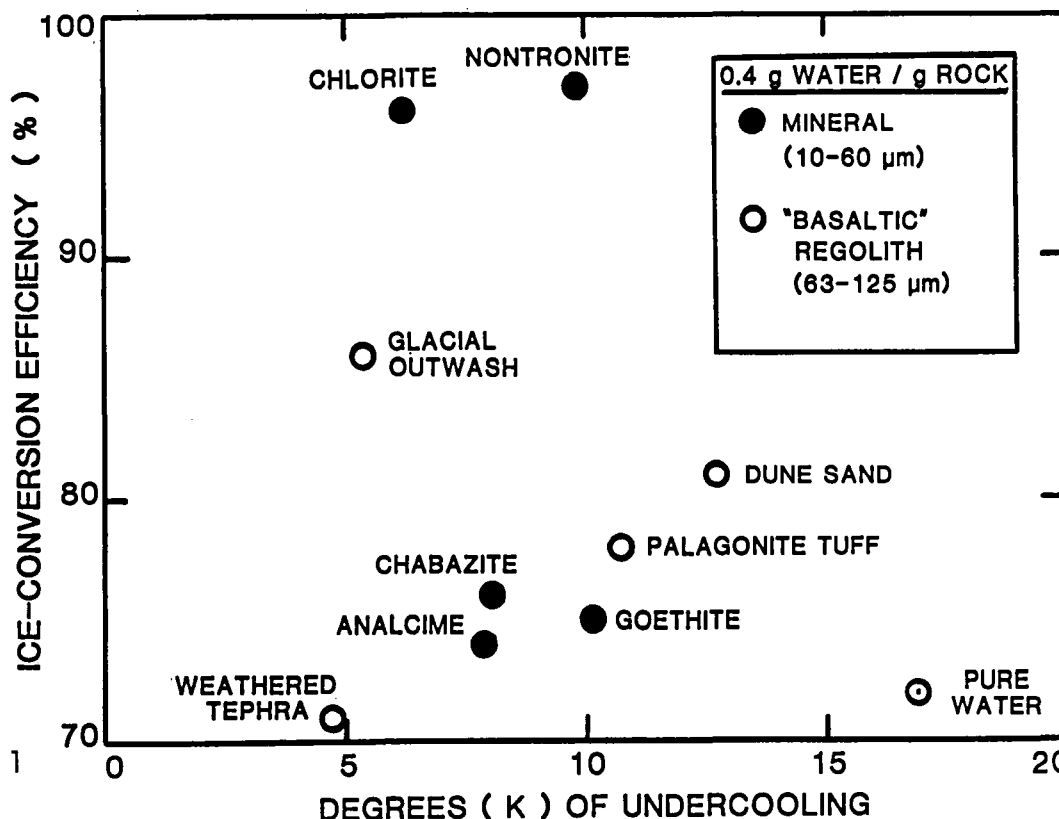
Figure 1

Figure 2

DYNAMIC MELTING INTERVALS OF ROCK / ICE
HEATED 5 K/MIN UNDER CO₂
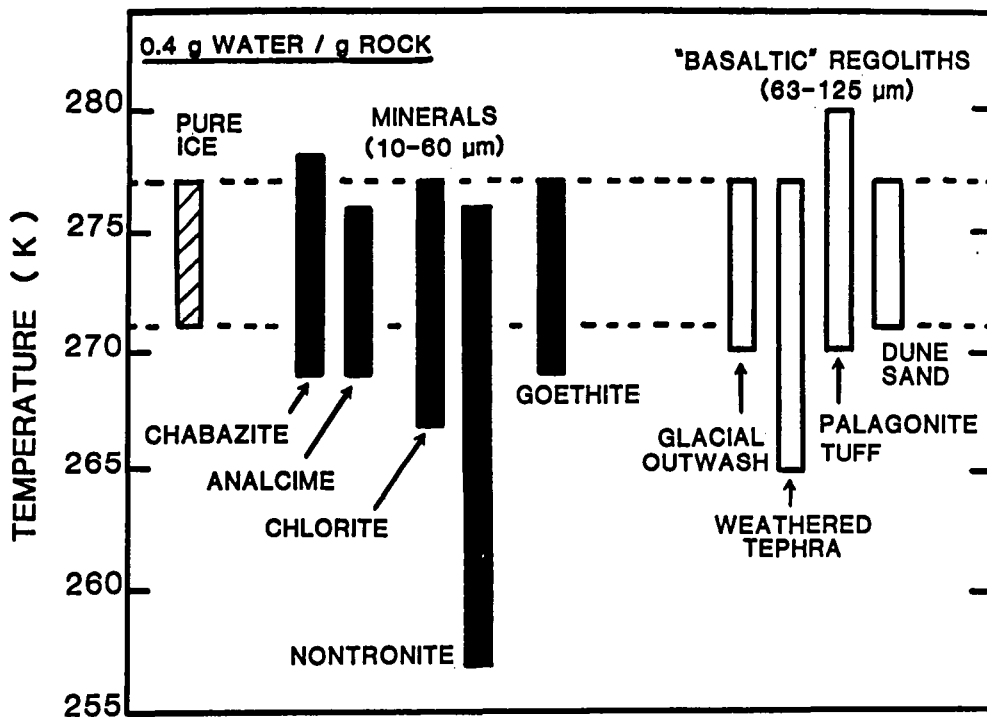
ON THE LATITUDINAL DISTRIBUTION OF DEBRIS IN THE
NORTHERN HEMISPHERE OF MARS; E. A. Guinness, C. E. Leff, and R. E.
Arvidson, McDonnell Center for the Space Sciences, Department of Earth
and Planetary Sciences, Washington University, St. Louis, MO 63130

Examination of Mariner 9 images showed evidence of debris mantling on
Mars. The evidence included craters that appeared to be filled with debris
and an apparent lack of small craters. Based on such data, it has been
suggested that a circumpolar debris mantle exists poleward of about 30N and
30S latitudes (1). The presence of a debris layer has important implications
for the modulation over time of atmospheric pressure by the
cap-regolith-atmosphere system. Several studies (e.g., ref. 2) have modelled
the effects of the regolith as a storage reservoir for volatiles. Each of
these studies, however, has lacked a quantitative assessment of the thickness
and distribution of debris mantling. In this abstract we discuss our
preliminary efforts in providing constraints on the thickness and distribution
of debris. Our initial approach is to examine crater size-frequency data for
selected regions on Mars, later expanding the study to include an inventory of
aeolian features and other direct indicators of debris deposition.

Thus far we have determined the crater size-frequency distributions for
ten regions between latitudes 20N and 80N and covering a range of longitudes
(Table 1). Crater data were derived from Viking Orbiter images with
resolutions of between 26 and 75 meters/pixel. Data for the Viking One (VL1)
landing site (3) and a similar crater distribution for a region northeast of
VL1 (28N, 46W) were used as a standard distribution for a crater production
population. Viking Orbiter images of these regions show no buried or filled
craters. Viking Lander images show that the surface at VL1 is free from a
thick, fine-grained debris layer. Thus, the VL1 data provide a reasonable
sample of a production population.

Assuming that the debris deposits are young relative to the craters and
that the debris simply filled or buried craters, the crater size-freqeuncy
distribution curves for debris-mantled areas should show a reduction of slope
compared to unmantled areas (4). Small craters can also be lost due to the
modulation transfer function of the imaging system. Thus, any slope reduction
occurring at diameters of less than about six times the image resolution were
ignored. We would also expect atmospheric hazes would reduce the slope of the
crater size-frequency distribution at small crater sizes because the
modulation transfer function of the atmosphere would preferentially reduce the
contrast of small craters. Evidence of atmospheric obscuration was checked by
using the cloud and haze catalog generated by Kahn (5).

Five of the count areas provide a generally north-south trend north of
our control areas in Chyrse Planitia. Two areas are in Acidalium Planitia
(37N and 47N latitude). Both of these areas have crater size-frequency
distributions that parallel the VL1 data, but suggest a somewhat younger
surface (Figure 1). The other three areas in the north-south transect are at
latitudes between 71N and 78N. The crater size-frequency distributions for
these three areas show a reduction in slope for small crater sizes (Figure 2).
The frames used to acquire crater data, however, were taken during the
northern early spring and mid-summer seasons, times that have a reasonable
probability of haze, as suggested by the cloud and haze data base. In fact, a

large cloud can be seen to the north of one of the count areas. Thus, there is a reasonable possibility that the slope reductions are due to atmospheric obscuration.

In order to check whether the results from the previous transect are representative of the northern hemisphere, we examined several areas in the mid-latitudes and polar regions at a variety of longitudes. Two of the areas east and west of the Elysium volcanic province have crater size-frequency distributions that are very similar to VL1 (Figure 3). A third count area north of Elysium (33N, 238W) has a distribution that shows a lack of small craters. The images of this region show clear indications that the region is partially covered by younger lava flows, which could have removed small craters by burial. As an additional check on atmospheric effects in the crater data, we determined crater size-frequency distributions for an area (75N, 167W) at two different seasons, mid-spring and early summer. Both distributions show a slope reduction for small craters, but the break in slope occurs at different diameters. The cloud and haze data base suggests that both times have a reasonable chance for hazes. In fact, the images at both times have streak-like structures that are suggestive of atmospheric clouds or haze.

In general, the crater data discussed in this abstract show no indications of a wide-spread increase in debris thickness with increasing latitude. The high resolution of the images examined (26-75 meters/pixel) suggests that a recently mobile debris layer of greater than several hundred meters is not likely. Still, our small sample size cannot rule out the possibility of a longitudinally-complex system for the distribution of debris. Clearly, examples of craters that appear to be filled with debris can be found throughout the planet. One possibility that our crater data cannot address is the presence of a thick regolith that pre-dates the majority of impact events. Finally, atmospheric haze can be an important factor in modifying the shape of crater size-frequency distributions.

REFERENCES CITED
1. Soderblom, L. A., Kreider, T. J., and Masursky, H. (1973),
    J. Geophys. Res., 78, 4117-4122.
2. Fanale, F. P., Salvail, J. P., Banerdt, W. B., and Saunders, R. S. (1982),
    Icarus, 50, 381-407.
3. Dial, A. L. (1978), NASA Tech. Mem. 79729, 179-181.
4. Chapman, C. R. and Jones, K. L. (1977), Ann. Rev. Earth Planet. Sci., 5,
    515-540.
5. Kahn, R. (1984), J. Geophys. Res., 89, 6671-6688.

REGION	LAT/LON	Ls	SCALE (m/pix)	NUM CRATERS	AREA (sq. km)	Frames
Chryse	28N/46W	74.2	45	1160	19799	668A34-42
Acidalium I	37N/27W	20.9	59	484	34933	225S01-7,9,10
Acidalium II	47N/23W	141.2	75	77	1195	71B71-76
Polar I	71N/60W	38.4	26	71	4730	525B01-07
Polar II	76N/93W	141.2	58	22	18253	71B42-46,61-64
Polar III	78N/72W	140.7	58	11	35952	70B06-10,27-34
Elysium I	24N/216W	65.9	32	612	9733	649A38-45
Elysium II	26N/180W	67.6	35	489	12714	653A34-42
Elysium III	33N/239W	49.6	72	225	31510	612A43-47
Vastitas I	75N/167W	50.0	35	103	10186	551B83-87
Vastitas II	75N/167W	117.3	75	15	23183	703B40-43

TABLE ONE
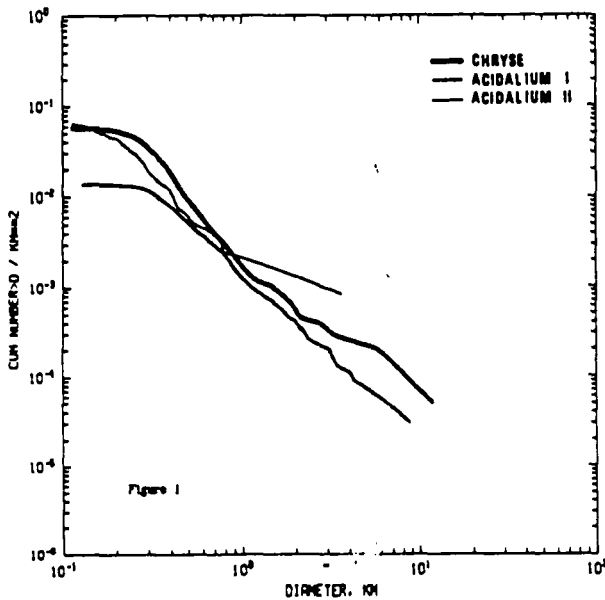
Figure 1.
Crater size-frequency distribution for Acidalium Planitia are compared to Chryse Planitia (northeast of VL1). The distribution for Acidalium II is highly uncertain between diameters of 1 and 10 km because of the small number of craters counted.
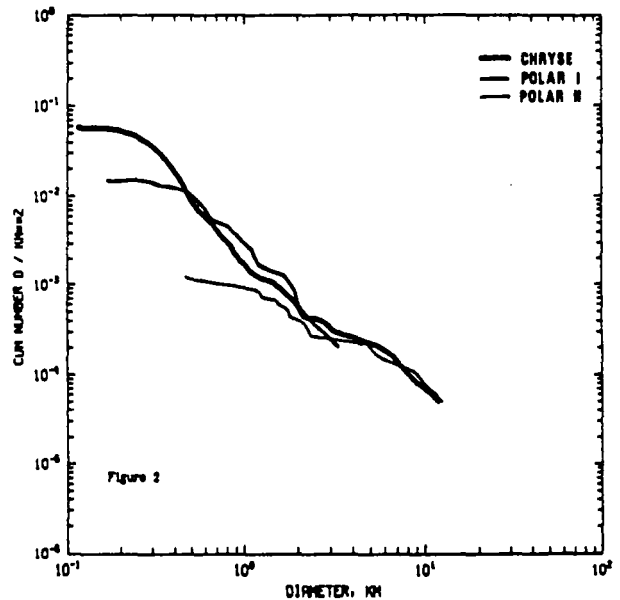
Figure 2.
Crater size-frequency distribution for two polar regions are compared to the Chryse data. The data for the polar regions show a slope reduction at different diameters.
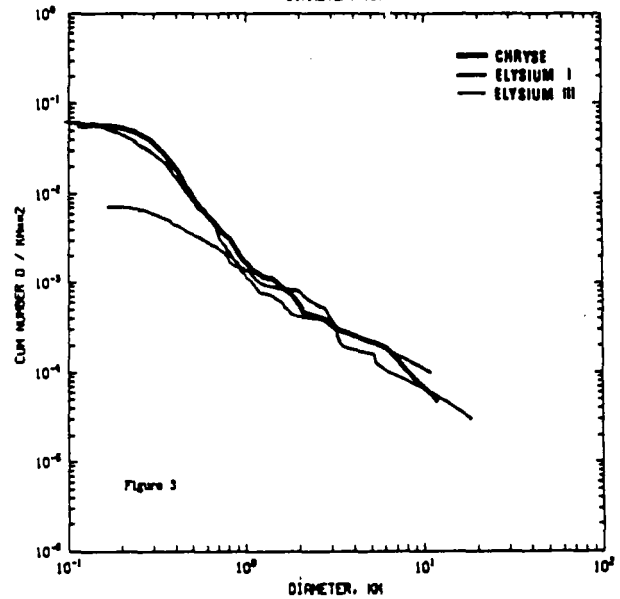
Figure 3.
Crater size-frequency distributions for the Elysium volcanic province are shown Again, the Chryse data are shown for comparison.

NUMERICAL SIMULATION OF THE CURRENT WATER CYCLE ON MARS;
R.M. Haberle (NASA/Ames Research Center, Moffett Field, CA) and T. Herdtle
(I.M.I. Inc., San Jose, CA).

Previous modeling efforts to simulate the current water cycle on Mars
have represented atmospheric transport as a diffusive process with latitud-
inal exchange being proportional to the gradient of vertically integrated
vapor abundance (1,2). The results, therefore, are sensitive to an arbitrary
and unknown exchange coefficient making it difficult to determine the role
of atmospheric transport in the observed water cycle. In this paper the
current status of a Mars water cycle model that has a more realistic treat-
ment of atmospheric transport is described, and some of its preliminary
results are presented and discussed.

The basic approach is to use numerical methods to solve a continuity
equation for water vapor in the meridional plane (latitude vs. height). At
present the only sources and sinks for atmospheric water vapor are those
associated with evaporation from surface ice deposits and precipitation from
the atmosphere itself. The wind field needed to evaluate the advective terms
in the continuity equation is calculated from a zonally symmetric general
circulation model (GCM) in which the effects of longitudinally asymmetric
motions, such as baroclinic waves, have been neglected (3). Consequently,
the computed circulation is the so called "diabatic" circulation which under
certain conditions is a reasonable approximation to the Lagrangian circula-
tion, i.e., the actual motion of air parcels (4). Because the small amount
of water vapor present in the Martian atmosphere has a negligible effect on
atmospheric heating rates, calculation of the wind field can be decoupled
from the transport calculations. This is desireable since the time for the
water cycle to come into equilibrium is much longer than the time needed for
the circulation to come into equilibrium.

Thus computation of the current water cycle takes place in two steps.
First, the annual cycle of the diabatic circulation is simulated by running
the GCM for several Mars years and outputing to tape all the information
needed to solve the transport part of the problem during the last simulated
year. This information includes diurnal as well as seasonal variations of
temperature. The transport code then accesses this tape as input and integr-
ates forward in time until equilibrium is reached.

The preliminary results to be discussed are based on an annual circu-
lation that ignores the effects of airborne dust heating. Several experiments
with the transport code are planned which test the sensitivity of the results
to the presence of a permanent CO_2 cold trap at the south pole, and the
transport of water in the condensed phase. These will be presented and dis-
cussed.

REFERENCES

1. Davies D.W. (1981). The Mars water cycle. Icarus, 45, 398-414.
2. Jakosky B.M. (1983). The role of seasonal reservoirs in the Mars water
   cycle.II. Coupled models of the regolith, the polar caps, and
   atmospheric transport. Icarus, 55, 19-39.
3. Haberle, R.M., C.B. Leovy, and J.B. Pollack (1982). Some effects of global
   dust storms on the atmospheric circulation on Mars. Icarus, 50,
   322-367.
4. Dunkerton, T. (1978). On the mean meridional motions of the stratosphere
   and mesosphere. J. Atmos. Sci., 35, 2325-2333.

STABILITY AND COMPOSITION OF CONDENSATE AT THE VIKING LANDER 2 SITE
ON MARS. H.M. Hart and B.M. Jakosky (Laboratory for Atmospheric and Space
Physics, University of Colorado, Boulder, CO 80309).

There has been much discussion of the composition and thickness of the
condensate observed at the Viking Lander 2 (VL2) site during both winters of
its operation. The candidate substances are CO_2 ice, H_2O ice, and CO_2-H_2O
clathrate. There are arguments against each of these being very abundant.
VL2 is located near the edge of the farthest extent of the winter north
polar cap. CO_2 ice would be marginally stable there, at best. Water ice
could probably be stable, but the large amounts suggested by estimates of
the thickness of the condensate (1) are not consistent with observations of
the seasonal appearance and disappearance of water vapor (2). Clathrate,
being composed primarily of water, has similar problems. We have examined
the surface energy balance at VL2 during the period that the condensate was
on the ground in order to determine the relative stability of CO_2 and H_2O
frost, and we have re-examined previous estimates of the amount of frost
present.

Three energy sources were considered in the energy balance: thermal
infrared emission from the atmosphere; direct and diffuse solar radiation;
and sensible heat flux from the atmosphere. Atmospheric temperature
profiles were derived from lander air temperatures, orbiter Infrared Thermal
Mapper (IRTM) 15μm temperatures, and radio occultation profiles. Infrared
optical depths for dust at 7, 9, 11 and 20μm were estimated from visible
optical depths measured at VL2 and from relationships between the IRTM band
measurements. The total solar flux absorbed at the surface was calculated
from the dust scattering model of Davies (3) and separated into direct and
diffuse components to distinguish shadowed and unshadowed regions. Sensible
heat flux was calculated from the air temperatures and winds measured at VL2
using the sublimation temperature of CO_2 as the surface temperature;
sensible heat flux was always less than 1% of the total energy.

The total surface energy, E_{total}, was calculated at 6 different times
during the period that the condensate was on the surface. CO_2 ice was
considered to be stable if the equilibrium temperature T_{eq} was less than the
sublimation temperature T_{sub} of CO_2 at 10 mb (T_{sub} = 150 K), where
$\sigma T_{eq}^4 = E_{total}$. The minimum nighttime flux was always marginally compatible
with CO_2 ice stability except during the height of the second dust storm
($L_s \approx 280°$). The maximum daytime flux never allowed CO_2 ice to be stable.
Daytime IR fluxes alone were enough to sublimate CO_2 ice, as were diffuse
solar fluxes alone. Sublimation (deposition) rates were calculated from
energy excesses (deficits). Nighttime deposition rates varied from 3-25 μm
of CO_2 ice per hour and daytime rates varied from 300-1300 μm/hr, such that
any ice deposited at night will sublime away within an hour or so during the
next day. The condensate is therefore probably water ice.

The thickness of the condensate has been previously estimated at
several tenths of a millimeter (1). This is equivalent to several hundred
precipitable microns of water vapor, which ought to show up as a pronounced
source during the period that the condensate was breaking up and
disappearing ($L_s \approx 305°$-360°). Mars Atmospheric Water Detector (MAWD)

observations show very little water during any part of this period (2). This result suggests either that the VL2 site is somehow unique in attracting condensate deposition or that the frost is not as thick as previously estimated. We have estimated the thickness of the frost from comparison of the observed spectral changes with those expected based on laboratory measurements of a frost-covered regolith. The change in the reflectance of cinder grains due to the addition of a 0.05 mm layer of ice on red cinder grains is 23% at a wavelength of $0.8\mu m$ (1). At $0.8\mu m$ the change in relative reflectance of the surface upon disappearance of the frost was 5% (4), suggesting that the layer of frost on the residual dust is about 0.01 mm thick. This value is equivalent to about 10 prμm of water vapor, which is consistent with the amount of water exchanged seasonally between the atmosphere and the regolith and seasonal polar cap combined (5), and can place a constraint on the amount of water vapor seasonally stored in each of these reservoirs.

References:

(1) Clark R.N. (1980). The Surface Condensates on Mars Observed by Viking: Frost Layers Several Tenths of a Millimeter Thick, Lunar and Planet. Sci., 160-161, Lunar and Planetary Institute, Houston.

(2) Jakosky B.M. and Farmer C.M. (1982). The Seasonal and Global Behavior of Water Vapor in the Mars Atmosphere: Complete Global Results of the Viking Atmospheric Water Detector Experiment, J. Geophys. Res., 87, 2999-3019.

(3) Davies D.W. (1979). Effects of Dust on the Heating of Mars' Surface and Atmosphere, J. Geophys. Res., 84, 8289-8293.

(4) Wall S.D. (1981). Analysis of Condensates Formed at the Viking Lander 2 Site: The First Winter, Icarus, 47, 173-183.

(5) Jakosky B.M. (1983). The Role of Seasonal Reservoirs in the Mars Water Cycle II. Coupled Models of the Regolith, the Polar Caps, and Atmospheric Transport, Icarus, 55, 19-39.

MARS: MINERALOGICAL CONSTRAINTS ON VOLATILE EVOLUTION
R. L. Huguenin, Remote Sensing Center and Dept. of Geology/Geography,
University of Massachusetts, Amherst 01003

Surface mineralogy provides important constraints on understanding the nature and distribution of sources and sinks for water on Mars. The mineralogy of chemically unweathered surface rocks and fines reveal information about oxidation state and volatile content of the source magmas. Mineralogy of weathering products constrain models of volatile incorporation, extent of equilibrium with present conditions, and whether alteration processes are contemporary or historical.

Reflectance spectra of areas on Mars that were measured during the 1978, 1973, and 1969 oppositions have been analyzed using a new multiple high order derivative analysis technique. With this technique absorption bands can be extracted from the spectra with accuracies of better than approximately 3% and with high sensitivity. The technique depends on no assumptions about band shape, and continuum contributions are suppressed. Processing is standardized and fully automated.

The 1978 spectra covered a wavelength range of 600-2600nm while the 1969 and 1973 spectra covered the range 350-1050nm. The 1978 wavelength range was the more useful for identifying silicate phases, while the earlier spectra were more useful for iron oxide phase identification.

A variety of silicate bands were extracted from the 1978 spectra. It is notable that these bands were evident in both dark and bright area spectra, with little obvious masking by dust. Simple inspection of the spectra would suggest that iron oxides dominate the spectral signature of the bright areas while dark areas contain visible absorption bands. With multiple high order derivative analysis, however, detection of bands is more sensitive to band width than band strength, and the extent of masking depends on how narrow the overlapping bands are rather than how strong they are. For the Mars data, silicate bands are extracted equally well from bright area and dark area spectra, which has significant implications for analysis of data from future orbiting spectrophotometer instruments.

Absorption features suggest the presence of Mg-olivine. Derivative analyses of laboratory olivine spectra reveal bands in the vicinity of 1260nm, 1035nm, and 862nm, with variations that are a function of the Mg/Fe ratio. Six of these spectra had sets of bands at these three positions, with ranges of 1220-1284nm, 1019-1040nm, and 848-868nm, consistent with relatively magnesian olivines.

Absorption features consistent with the presence of plagioclase feldspar were observed in all nine spectra. Laboratory spectra reveal band positions that range from 1100nm to 1350nm, depending on 2V (large 2V corresponds to short wavelength bands, and low 2V corresponds to long wavelength band positions). Band positions in the Mars spectra cluster near 1226-1347nm, suggesting a range of plagioclase compositions.

There are also features that are consistent with the presence of Ca-rich pyroxenes. Sets of bands near 756-802nm, 937-1003nm, and 1104-1202nm are similar to laboratory spectra of Fe^{3+} -bearing augite-diopsides, and occur in six of the 1978 areas. Five spectra have bands at 912-937nm that are consistent with low-Ca pyroxenes being present in those areas. Bands near 2000nm are consistent with these assignments, but their positions are probably modified by the strong atmospheric CO_2 absorption feature near those bands and their positions may not be accurate.

Among the other bands detected in the spectra are features that are

consistent with the presence of hematite and goethite. Laboratory spectra of
synthetic and natural goethites show principal absorption features near 900nm,
670nm, and 530nm. Multiple high order derivative analysis reveals that the
900nm feature consists of two absorption bands near 1064-1119nm and 181-862nm
that combine to form a composite feature near 900nm. The 670nm feature
consists of two bands near 689-700nm and 608-615nm, while the 530nm feature
is a single band near 521-540. For hematite, there are a pair of bands near
908-942nm and 797-815nm that combine to form a composite feature near 850nm.
There is a band near 626-684nm and one near 568-572nm. A weak band also
appears near 1093nm in some, but not all hematite spectra. The 1969 and
1973 spectra all contained bands consistent with mixtures of hematite and
goethite of varying proportions.

Notably absent were bands near 648-649nm, 720-727nm, and 773-791nm that
along with other bands characterize maghemite. Also missing were lepidocro-
cite bands. What was present, however, was a continuum curve shape that was
very close to the spectrum of ferric oxide plus magnetite. This suggests
that the magnetic iron oxide observed by the Viking magnetics experiment may
have been magnetite and goethite and hematite rather than maghemite.

While the band positions are well defined, assignments are not necessari-
ly unique. Some ambiguity exists in the assignments of isolated bands within
individual spectra, but when suites of bands coexist (3 olivine bands, 2-4
pyroxene bands, etc.) within spectra, assignments are strenghtened. For the
Mars spectra all but the plagioclase bands were assigned based on the
presence of suites of bands. The bands attributed to plagioclase were
residual after assignments of suites $(Fe_2O_3-FeOOH$, olivines, pyroxenes).
No bands were missing within suites, and no extraneous bands were left un-
assigned after the plagioclase assignments.

Additional support comes from derivative analysis of spectra of SNC
meteorites, which reveal sets of absorption bands that are similar to the
Mars bands. The meteorite bands are in the appropriate positions for the
known constitutent minerals, and the assemblages are very similar to those
derived for the Mars areas.

The derived silicate mineral assemblages suggest that several of the
areas may contain relatively low silica olivine basalts (or their coarse-
grained equivalents). Two spectra show two high-calcium pyroxenes with no
evidence for olivine, however, and one shows a low-Ca pyroxene and high-Ca
plagioclase assemblage with no evidence for olivine. The regions are large
and the minerals may not coexist within rocks or fines. The spectra may
instead represent composites of several rock types, and thus the observed
assemblages cannot be classified. The assemblages are, however, similar to
the SNC meteorite assemblages.

With respect to the iron oxides, it is notable that areas with the re-
latively larger goethite contributions were either within zones of ongoing
(certain 1973 areas) or historically frequent dust cloud activity. Areas
that had relatively smaller goethite contributions were outside the zones
of frequent dust cloud activity.

This suggests the possibility that the more hydrated phase may occur
within a mobile dust compoment, and that the less hydrated phase may be less
mobile. The latter compoment may correspond to the salt-encrusted duricrust
component, and the former may correspond to the unconsolidated drift compo-
nent that was observed at the Viking Lander sites.

In summary, the mineralogies of the primary silicates suggest that
source magmas may be relatively calcium-rich and iron rich. The prevalence

of mixed oxidation state charge transfer bands suggests that oxygen fugacities may be high in the magma source regions, and this suggests that volatile contents may be high. With volcanic units apparently spanning geologic time, volcanism may represent a continuing source of high-oxygen fugacity volatiles on the planet.

At the same time chemical weathering may represent an ongoing volatile sink on the planet. As has been discussed by several investigators, most recently Gooding, goethite is not a stable phase on Mars and should dehydrate over time. Goethite has been proposed to be a primary weathering product by Huguenin, however. The presence of goethite bands in the spectra supports the proposed formation of that phase; and the presence of hematite bands supports the proposed dehydration of that phase. This, combined with proposals that the salt-encrusted component may be an older evolutionary product of the younger unconsolidated compoment suggests that the goethite may be younger than the hematite. The instability of goethite further suggests that the goethite may be recently formed.

THE SEASONAL CYCLE OF WATER ON MARS: A REVIEW. B.M. Jakosky, (Laboratory for Atmospheric and Space Physics, University of Colorado, Boulder, CO 80309).

The behavior of water vapor in the Mars atmosphere is closely tied to the martian seasons, with changing surface and subsurface temperatures allowing the exchange of water between the atmosphere and polar caps and between the atmosphere and regolith, and with the circulation of the atmosphere acting to redistribute water vapor over the entire planet. If we can understand the nature of the processes responsible for the exchange of water between various reservoirs on the seasonal timescale and the role of each reservoir in supplying the seasonal supply of water vapor, then perhaps we can extrapolate this behavior to other epochs when the seasonal solar forcing was different. In this manner, we can quantitatively address some of the outstanding questions regarding water and climate on Mars -- the origin and evolution of the polar layered terrain and the formation of the channels and valley networks.

Recent additions to our understanding of the seasonal water cycle include: detailed observations of the spatial and temporal variability of atmospheric water from the Viking spacecraft and comparison with previous Earth-based observations spanning over six martian years; analysis of the distribution of clouds and hazes in the atmosphere which indicate saturation, also as observed from Viking; in situ measurements of the surface abundance of salts which may contribute to the presence of a liquid brine solution; observations and modeling of the seasonal advance and retreat of the polar caps; modeling of the exchange of water between the atmosphere and either the seasonal and annual polar caps or ice or adsorbed water in the regolith; modeling of the stability of ice or liquid water on or beneath the surface; and modeling of the role of atmospheric transport in redistributing the seasonal water.

Now is an appropriate time to summarize, synthesize, and critically examine these results. The upcoming Mars Geoscience/Climatology Orbiter will further address the issues involved in the seasonal cycle of water (among others), and a thorough discussion of previous results will aid considerably in framing the questions to be addressed. In reviewing the seasonal cycle, an effort has been made to address each of the constraints provided by the various observational data sets as well as by the models which have been constructed of individual water exchange and transport models. In this manner, previous results may be realistically synthesized, and areas for future observations, modeling, or laboratory measurements may be suggested.

MARS AT HIGH OBLIQUITY: POSSIBLE PRECIPITATION OF ICE AT LOW LATITUDES. B.M. Jakosky (Laboratory for Atmospheric and Space Physics, University of Colorado, Boulder, CO 80309) and M.H. Carr (U.S. Geologic Survey, Menlo Park, CA 94025).

A key question regarding the Mars climate involves the mechanism for formation of the valley networks on the old cratered highlands. They appear to have formed due to the presence of liquid water, either through groundwater sapping or by direct precipitation, and require volumes of water so great that some replenishment of surface water must have occurred. Greenhouse models of the atmosphere suggest that ~1 bar CO_2 is required for average temperatures to reach the melting point, and the current pressure of ~6 mbar is much too small to have a significant effect. We suggest another mechanism for resupplying water to the regolith that depends only on the abundant presence of polar ice and the large changes of obliquity which are known to occur.

The current obliquity is about 25°, and it oscillates between about 12° and 36° on timescales of 10^5 - 10^6 years. Prior to the formation of Tharsis, it reached extremes of about 9° and 46° (or more). At the highest obliquities, the greater insolation will readily remove the CO_2 cap each summer and heat up the residual water ice cap. Calculations have been done of the sublimation of water, and indicate that several centimeters may sublime each summer for 35° obliquity, and several tens of centimeters for 45° obliquity.

This water will be carried equatorward, as it is today during northern summer, where it will saturate the atmosphere and condense. Today's equatorial and mid-latitude atmosphere can hold up to several hundred precipitable micrometers (pr μm) of water without saturating; during dust storms, the temperatures are warmer but the atmosphere can still hold only several hundred pr μm at night. At higher obliquities, the region equatorward of about ±50° latitude will be cooler than at present and will consequently hold less water. Even if dust storms occur more frequently than today, saturation and condensation of water will tend to remove dust from the atmosphere and cool the atmosphere due to condensation and settling and due to the radiative feedback of the presence of surface and atmospheric ice.

During the subsequent winter, the equatorial atmosphere can still hold only several hundred pr μm of water, such that possible transport back to the pole will be down a gradient that is 5-50 times less than that away from the summer pole. Thus, water sublimed in summer and condensed onto the surface away from the pole will tend not to be transported back during winter. In 10^4 years, the approximate time spent at highest obliquity, as much as hundreds of meters (for an obliquity of 35°) to 2 km (obliquity of 45°) of ice may sublime from the pole, if such ice is present. Condensed in non-polar regions, this results in a layer of ice roughly meters to tens of meters thick. This water can either recharge a subsurface reservoir to promote sapping, or can, under certain conditions, melt to provide liquid runoff.

One appealing reason to invoke a polar source for equatorial water for carving the channels is that the valley networks were carved early in Mars history. At that time, the Tharsis bulge may not have reached its present size. As Tharsis grew and the maximum obliquity attained dropped, less water could be removed from the pole at highest obliquity. This decrease in the

supply of water may provide a shutoff mechanism for the formation of the valley networks, explaining the relatively old age of most of them.

Additionally, this result suggests that the major formation and reworking of the layered terrain occurred prior to the formation of Tharsis, with as much as the entire 2-km thickness being modified at each hot-pole high obliquity. Activity since then may have been limited to minor modification and redevelopment at the highest obliquities and to relatively minor modifications involving individual layers at moderate obliquities such as the present value.

HYDROLOGIC CYCLE ON MARS: EFFECTS OF CO_2 MASS FLUX ON GLOBAL WATER DISTRIBUTION; P.B. James, Physics Department, University of Missouri-St. Louis, 63121

One of the major differences between martian and terrestrial meteorologies is that on Mars the principal constituent of the atmosphere, carbon dioxide, precipitates in the planet's polar regions in response to seasonal changes in insolation. The latent heat of CO_2 is a major source for radiated energy during the polar winter and controls the rate of sublimation of the seasonal polar caps, which are mostly CO_2, in spring. Thus the seasonal martian climate and the CO_2 cycle are intimately connected and are, in fact, synonymous to a first approximation. The purpose of this work is to investigate the coupling between the CO_2 cycle and the hydrologic cycle on Mars.

The periodic condensation and sublimation of up to thirty percent of the atmosphere results in large scale mass motions which are controlled by the seasonal insolation changes. Equivalent wind speeds on the order of meters per second result near the edge of the subliming south polar cap. The CO_2 mass flux is strongly dependent upon season and latitude; and, because of Mars' large eccentricity, there are pronounced hemispheric and seasonal asymmetries in these currents. During certain seasons advection of water vapor due to these atmospheric motions may be the dominant mode of atmospheric transport. Depending upon the phasing between these motions and the release of water, this advection could influence water distribution on the planet.

In order to assess the consequences of asymmetric advection on the global distribution of martian water, a very simple model for the Mars water cycle is being studied. The atmospheric transport is modeled using a diffusion term following Davies (1) in addition to the advection. Sinks for water vapor in the form of surface ice and clouds are included; but the regolith, shown to be an important reservoir by Jakosky (2,3), is not yet included. The temperature and sublimation wind fields computed by a simple CO_2 cycle model (4) are used as input for these calculations. In addition to determining the importance of the advective transport in the current global distribution, numerical modeling of the changes which might be produced by changes in orbital parameters will be included in this study.

1. Davies, Donald W. (1981) The Mars Water Cycle. Icarus 45, p. 398-414.
2. Jakosky, Bruce M. (1983) The Role of Seasonal Reservoirs in the Mars Water Cycle. I. Seasonal Exchange of Water with the Regolith. Icarus 55, p. 1-18.
3. Jakosky, Bruce M. (1983) The Role of Seasonal Reservoirs in the Mars Water Cycle. II. Coupled Models of the Regolith, the Polar Caps, and Atmospheric Transport. Icarus 55, p. 19-39.
4. James, Philip B. and Gerald R. North (1982) The Seasonal CO_2 Cycle on Mars: An Application of an Energy Balance Climate Model: J. Geophys. Res. 87, p. 10271-10283.

OBSERVATIONAL CONSTRAINTS ON THE GLOBAL-SCALE WIND SYSTEMS
OF MARS; R. Kahn, Washington U., St. Louis, Mo. 63130

Wind direction observations set important constraints on the advection of volatiles, and on the schedules for release and deposition of condensates in the seasonal polar caps of Mars. In recent work by Kahn (1; 2), wind direction observations based on cloud features and surface dust streaks from all Viking and Mariner 9 images were collected and studied in light of the predictions of previously published circulation models. Several surprising results were obtained.

Figure 1 shows all known measurements for which there are strong temporal constraints, plotted as a function of latitude and season. The majority of these data are from lee wave clouds, though data from variable surface features, plume clouds, and apparent cloud motions have been included. In most cases, the tails of the wind direction arrows are located at the center latitude of the images in which the clouds appear, and arrows point in the apparent direction of the wind for a mercator projection with north at the top of the figure. Data from several Mars years are superposed, but the observations are too sparse to detect interannual variations. For orbits where several lee waves indicating a common wind direction occur in close spatial proximity, a single arrow is plotted. Thin dot-dashed lines are used to separate regions of distinctly differing wind direction.

The behavior of the winds in northern high latitudes during winter and spring is of particular interest for the volatile budget. Thermal wind shear, produced by the normal pole to equator temperature gradient, will drive prograde (west to east) winds, while the flow generated by mass flux due to sublimation of the seasonal cap will force retrograde winds. In the southern hemisphere, an abrupt reversal of wind direction near Ls= 180 degrees is consistent with the beginning of cap recession in southern spring. In the northern hemisphere, a similar reversal expected near Ls= 0 deg is not observed; the winds remain prograde until about Ls=40 deg, at which time retrograde winds are found, but only poleward of 75 deg latitude. Two dimensional modeling of the force balance was performed (1), using meridional temperature gradients measured by the IRTM instruments, and a mass flux constrained by the heat balance model of James and North (3). I find that the mass flux must be reduced by a factor of about 20 in early to mid northern spring to match the data. A halt in north polar cap recession is often observed during this season, and in 1984, condensate clouds at the cap edge were rare at this time, becomming more common in midspring (4), also suggesting reduced mass flux before Ls=40 deg.

In mid northern winter, during the 1977 global dust storm, the generally prograde winds at Viking Lander 2 (VL2) turned retrograde. Axisymmetric modeling of this situation, with atmospheric dust included, failed to reproduce the observations (5). However, atmospheric temperature measurements show sudden warming near the polar cap edge that is coincident with the wind reversal (6). The reversal of winds at VL2 may have been aided by cap sublimation mass flux flow induced by heating of the polar cap edge. Such heating is expected as a result of enhanced meridional circulation during the dust storm, and at least some years, late winter observations of the north

polar cap suggest patchiness south of 75 deg latitude at vis and infrared wavelengths. If the equatorward parts of the north polar seasonal cap were depleted of CO_2 by sublimation in the winter, the unexpected springtime behavior can be explained by a paucity of frost south of about 75 deg latitude.

Predictions of the cap formation and recession schedules are very sensitive to changes in the values of polar cap emissivity and albedo. Better observations of these quantities using existing data, coupled with wind direction measurements and the loose constraints on mass flux set by VL pressure data, could be used to develop an improved picture of seasonal polar cap behavior. More complete measurement of cap morphology, wind direction, and pressure, together, over one or several Mars years, as the MGCO mission may provide, would extend considerably our understanding of the distribution and transport of volatiles on Mars.

Acknowledgments

References

(1) Kahn, R. (1983) Some observational constraints on the global-scale wind systems of Mars. J. Geophys. Res., 88, 10,189-10,209.
(2) Kahn, R. (1984) The spatial and seasonal distribution of Martian clouds, and some meteorological implications. J. Geophys. Res., 89, 6671-6688.
(3) James, P.B., and G. North (1982) The seasonal cycle of CO_2 on Mars: An application of an energy balance climate model. J. Geophys. Res., 87, 10,271-10,283.
(4) Martin L., and P. James (1984) Mars 1984: the transition from polar hood to surface cap (abstract). Bull. Am. Astron. Soc., 16,673.
(5) Haberle, R., C. Leovy, and J. Pollack (1982) Some effects of global dust storms on the atmospheric circulation of Mars. Icarus 50, 322-367.
(6) Martin, T.Z. (1983) Mars atmosphere: details of dust storm induced north polar warming (abstract). Bull. Am. Astron. Soc. 15, 486.
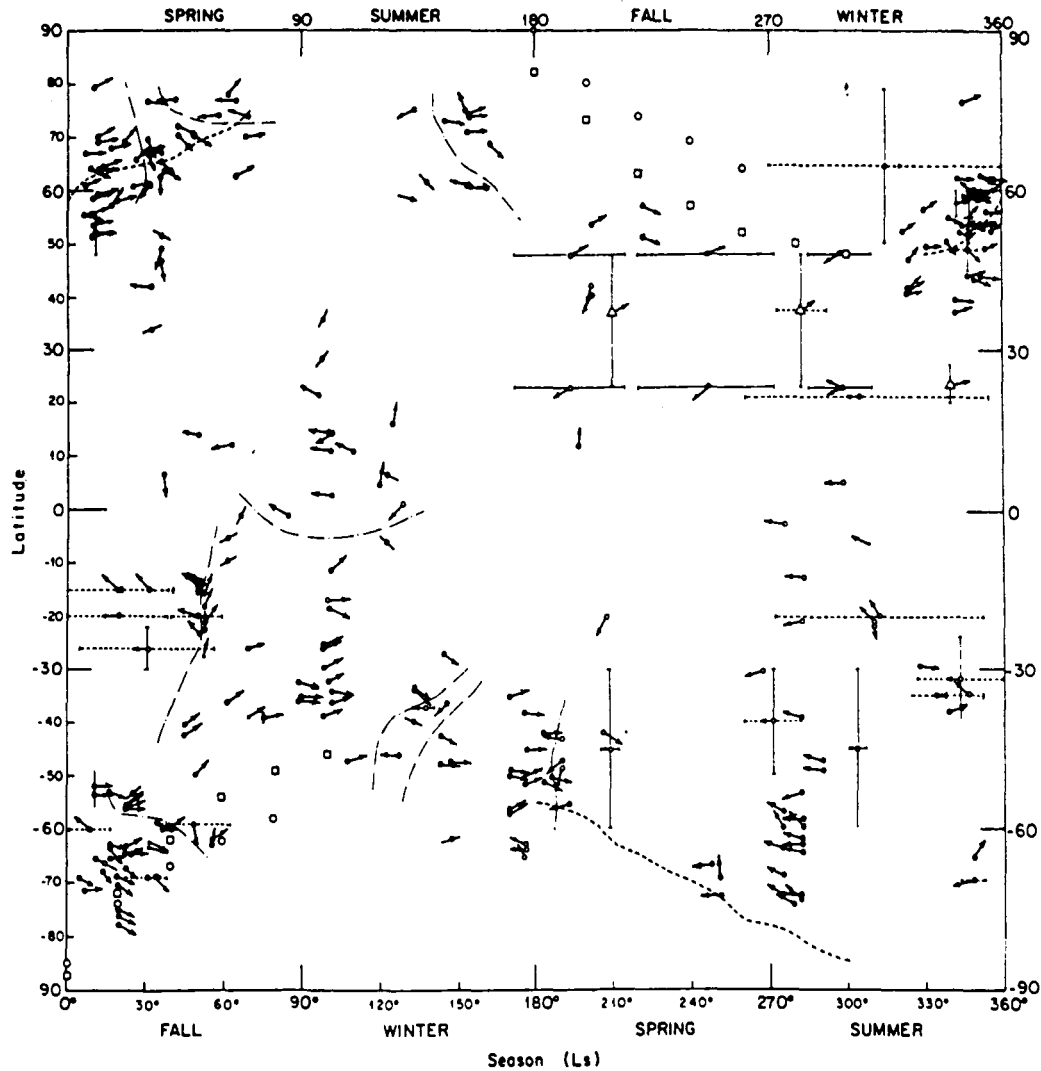
Fig. 1. Apparent near-surface wind directions for Mars. Measurements include arrows with closed circles (lee wave cloud data), arrows with open circles (plume cloud, proper cloud motion, and variable surface feature observations), and three arrows with triangles (upper level wind indicators). Solid bars designate ranges over which a given wind direction marker was observed, and dashed bars show ranges during which a change must have taken place. Dotted-dashed lines separate regions with similar wind direction observations. The polar cap edges during recession are drawn as dashed lines; during formation, open circles and open squares show predicted cap edge locations according to two theoretical models.

GROUNDWATER SAPPING AND ANCIENT VALLEY NETWORKS ON MARS
R. Craig Kochel, Dept. of Geology, Southern Illinois University, Carbondale, IL 62901 and Alan D. Howard, Dept. of Environmental Sciences, University of Virginia, Charlottesville, VA 22903.

Documenting valleys on Mars that have a high probability of having been formed by groundwater sapping has important implications for the interpretation of paleoclimates and paleo-hydrology on that planet. Global mapping of these sapping valleys will be important in assessing present and past hydro-logical conditions in the near-surface Martian regolith. Ground-water sapping via outflow from aquifers and along zones of increased permeability is an important process in escarpment retreat by basal undercutting. When concentrated, these ground-water flows can be important processes in valley formation. Sapping valleys typically retreat headwardly by sapping at the base of their valley headwalls. Terrestrial valleys in which sapping has been important in valley genesis and Martian valleys where sapping has been invoked as a major formative process share the following similarities in morphology: 1) valley walls are steep-sided, smooth, and contain sharp wall-floor junction angles; 2) valley floors are smooth with wide U-shaped profiles or narrow with V-shaped profiles; and 3) valleys display abrupt theater-like head terminations.

On Earth, groundwater sapping has been suggested to explain valleys with the above morphologies in many areas including: 1) valleys dissecting the Hawaiian volcanoes (1,2); 2) the Colorado Plateau (3,4,5); and 3) on beaches and various other areas (6,7). On Mars, sapping has been invoked to explain a variety of valley networks including: 1) dry valleys of the ancient cratered terrain (1,8,9); 2) medium-scale outflow channels with short, stubby tributaries like Nirgal Vallis (1,10); 3) slope valleys along major escarpments like the tributaries to Valles Marineris (2,11), along the cratered terrain boundary of the fretted terrain (12); and 4) along the floors and walls of the large-scale outflow channels as post-flood modifications along structural trends (13).

In order to accurately map the distribution of Martian valleys attributable to groundwater sapping, a suite of valley morphologic and network morphometric indices must be determined which can be readily mapped and interpreted. A combination of approaches is necessary to develop these morphometric criteria for recognition of sapping valleys on Mars. We are working with the following types of investigations in order to elucidate criteria to recognize sapping on scales available from Viking imagery: 1) experimental studies of valleys created in a variety of types of sediments and stratigraphic/structural settings; 2) comparisons of experimental and terrestrial valleys formed by sapping with terrestrial runoff networks and with probable sapping networks on Mars; 3) analog studies in the field and remotely of terrestrial valleys influenced by sapping; and 4) theoretical studies of the mechanics of sapping to help

ANCIENT GROUNDWATER SAPPING VALLEYS ON MARS

49

Kochel and Howard

understand the constraints for application of experimental
systems to Martian valleys.

Valley networks formed in our preliminary experimental net-
works (2, 14) share many common morphometric attributes with
terrestrial valleys where sapping processes appear to be impor-
tant. Many of these morphometric parameters such as channel
gradient are useful only in experimental or terrestrial settings
where detailed topographic data are available. However, our
initial studies show that sapping valleys have the following
attributes recognizable in Viking Orbiter images: 1) channel
junction angles are unusually acute compared to terrestrial run-
off channels; 2) drainage density is lower than in runoff net-
works; 3) higher drainage densities occur in headwater portions
of the sapping basins; 4) the ratio of channel area to basin
area is higher for sapping basins; and 5) there is commonly
marked structural control of sapping valleys.

We are investigating new morphometric indices as well as
dimensional and dimensionless combinations of new and standard
indices to enlarge the present suite of morphometric parameters
indicative of sapping processes. An example of combined para-
meters results from the measurement of eight linear attributes
of basin geometry and relief from topographic maps of Hawaiian
channels. Of the 44 Hawaiian valleys studied, 33 had no indica-
tion of sapping processes. The other 11 exhibited the typical
entrenched canyons with theater-like heads of sapping valleys.
Principal components analysis (PCA) plots of the first two sig-
nificant eigenvectors yielded a separation of morphologically
distinct valleys in the same region according to whether they
had been affected by sapping processes. Multivariate techniques
such as PCA may result in criteria that can be applied in dis-
criminating channels on Mars formed by sapping and surface
runoff. Other possible morphometric parameters include indices
of channel and basin width measured at various locations along
the main valley axis, channel gradient, and a ratio of lengths
of tributaries to the mainstream.

Our preliminary experiments with the new three-dimensional
sapping box show that sapping is a competitive process involving
capture of local groundwater by the most rapidly-growing channel
in the headward direction. Unlike surface runoff systems, when
capture takes place, the down-gradient tributaries become
inactive because their source of groundwater replenishment has
been intercepted and diverted into a more headwardly-located
tributary. This process contributes to short, stubby tributaries
like those found in Nirgal Vallis on Mars. Experimental sapping
channels enlarge headwardly at a rapid rate and then bifurcate
during later phases of their evolution.

Channel morphologies are typically U-shaped during active
sapping and have steep valley walls. After the run is terminated
and waters are drained, the valley walls dry out and adjust to
smooth angle-of-repose slopes as the valley cross-section
becomes V-shaped. These angle-of-repose slopes along valley

margins are strikingly similar to those in Valles Marineris tributaries, which implies that the Martian valleys may have undergone a similar two-stage development. The degree of adjustment to angle-of-repose slopes on the Martian channels may be a crude index of time since active sapping along channels.

References

(1) Baker, V.R. (1982), The Channels of Mars: Austin, Univ. Texas Press, 198p.

(2) Kochel, R.C., Howard, A.D. and McLane, C. (1984) in press, Channel networks developed by groundwater sapping in fine-grained sediments: Analogs to some Martian valleys: in Woldenburg, M. ed. Geomorphological Models, Boston, Allen and Unwin.

(3) Laity, J.E. (1980) Groundwater sapping on the Colorado Plateau: NASA Tech. Mem. 82385, p. 358-360.

(4) Laity, J.E. and Pieri, D.C. (1980) Sapping processes in tributary valley systems: NASA Tech. Mem. 81776, p. 271-273.

(5) Laity, J.E. and Saunders, R.S. (1981) Sapping processes and the development of theatre-headed valleys: NASA Tech. Mem. 84211, p. 280-282.

(6) Higgins, C.G. (1982) Drainage systems developed by sapping on Earth and Mars: Geology, v. 10, p. 147-152.

(7) Higgins, C.G. (1983) Piping and sapping: development of landforms by groundwater outflow: in Lafleur, R.G., ed., Groundwater as a Geomorphic Agent: London, Allen and Unwin.

(8) Pieri, D.C. (1980) Geomorphology of Martian valleys: in Advances in Planetary Geology: NASA TM 81979, p. 1-160.

(9) Malin, M.C. Laity, J.E. and Pieri, D.C. (1980) Sapping: Analog studies on Earth and Mars: NASA Tech. Mem. 81776, p. 298-299.

(10) Baker, V.R. (1980) Nirgal Vallis: NASA Tech. Mem. 82385, p. 345-347.

(11) Kochel, R.C. and Baker, V.R. (1981) Modifications of escarpments along channels and plateaus on Mars: NASA Tech. Mem. 84211, p. 321-323.

(12) Kochel, R.C. and Peake, R.T. (1984) in press, Quantification of waste morphology in Martian fretted terrain: J. Geophys. Res.

(13) Baker, V.R. and Kochel, R.C. (1979) Martian channel morphology: Maja and Kasei Vallis: J. Geophys. Res., v. 84, p. 7961-7983.

(14) Howard, A.D. and Kochel, R.C. (1984) Quantitative and experimental modelling of sapping networks: NASA Tech. Mem. 86246, p. 191-193.

INFLUENCE OF ATMOSPHERIC DUST LOADING AND WATER VAPOR CONTENT ON SETTLING VELOCITIES OF MARTIAN DUST/ICE GRAINS: PRELIMINARY RESULTS

Steven W. Lee, Geology Dept., Arizona State Univ., Tempe, AZ 85287

Previous studies have indicated that condensation of water vapor and/or CO_2 onto suspended dust grains can significantly increase the sedimentation rate of dust/condensate particles on Mars (cf. 1,2,3). This process was assumed to be particularly effective in the polar regions, especially in the northern hemisphere following global dust storms. However, recently reported thermal observations of the north polar region indicate that atmospheric temperatures are above the CO_2 condensation point everywhere except at the surface (4). In the absence of CO_2 condensation, the principal dust/volatile interaction affecting sedimentation rates on Mars will be the condensation of water ice onto dust grains.

Settling velocities of dust/ice grains have been modelled to investigate the influence of variable atmospheric dust loading and water vapor content on sedimentation rates. The model accounts for differing temperatures and elevations, determines the size and density of dust/ice grains produced assuming various initial dust loads, particle sizes, and water vapor abundances, and predicts the settling velocity of the resulting composite particles. Preliminary results (Figure 1) show that a composite particle rapidly increases in size and decreases in average density with condensation of only a few precipitable microns (pr μm) of water; atmospheric drag apparently reduces the settling velocity relative to that expected for a "naked" dust grain. With increasing atmospheric optical depth (and hence, dust loading), this process is effective at higher water vapor abundances. Under conditions prevailing during global dust storms (optical depths >1), the sedimentation rate is significantly reduced, even though each composite particle has grown to several times its initial mass. Under conditions of lower dust loading, increasing vapor content allows continued growth of particles, resulting in an increased settling rate following the initial decline.

This study indicates that under conditions of low dust loading, condensation of only a few pr μm of water vapor onto dust grains will reduce their sedimentation rate; availability of larger quantities of water vapor, however, will enhance the fallout of dust. With high dust loading (such as occurs during global dust storms), the sedimentation rate is reduced by the condensation of any available water vapor. This behavior implies that scavenging of dust by rapid fallout of dust/ice grains during major dust storms is not an effective process in the polar regions (or elsewhere). Subsequent to dust storm clearing, condensation of more than a few pr μm of water may enhance the dust sedimentation rate anywhere on the planet.

REFERENCES

(1) Pollack, J.B., D. Colburn, R. Kahn, J. Hunter, W. Van Camp, C.E. Carlston, and M.R. Wolf (1977). Properties of aerosols in the martian atmosphere, as inferred from Viking Lander imaging data. J. Geophys. Res., 82, 4479-4496.

(2) Pollack, J.B., D.S. Colburn, F.M. Flaser, R. Kahn, C.E. Carlston, and D. Pidek (1979). Properties and effects of dust particles suspended in the martian atmosphere. J. Geophys. Res., 84, 2929-2945.

(3) Cutts, J.A. (1973). Nature and origin of layered deposits of the martian polar regions. J. Geophys. Res., 78, 4231-4249.

(4) Jakosky, B.M. and T.Z. Martin (1984). Mars: Polar atmospheric temperatures and the net transport of water and dust. Submitted to Icarus.

SETTLING VELOCITIES OF MARTIAN DUST/ICE GRAINS
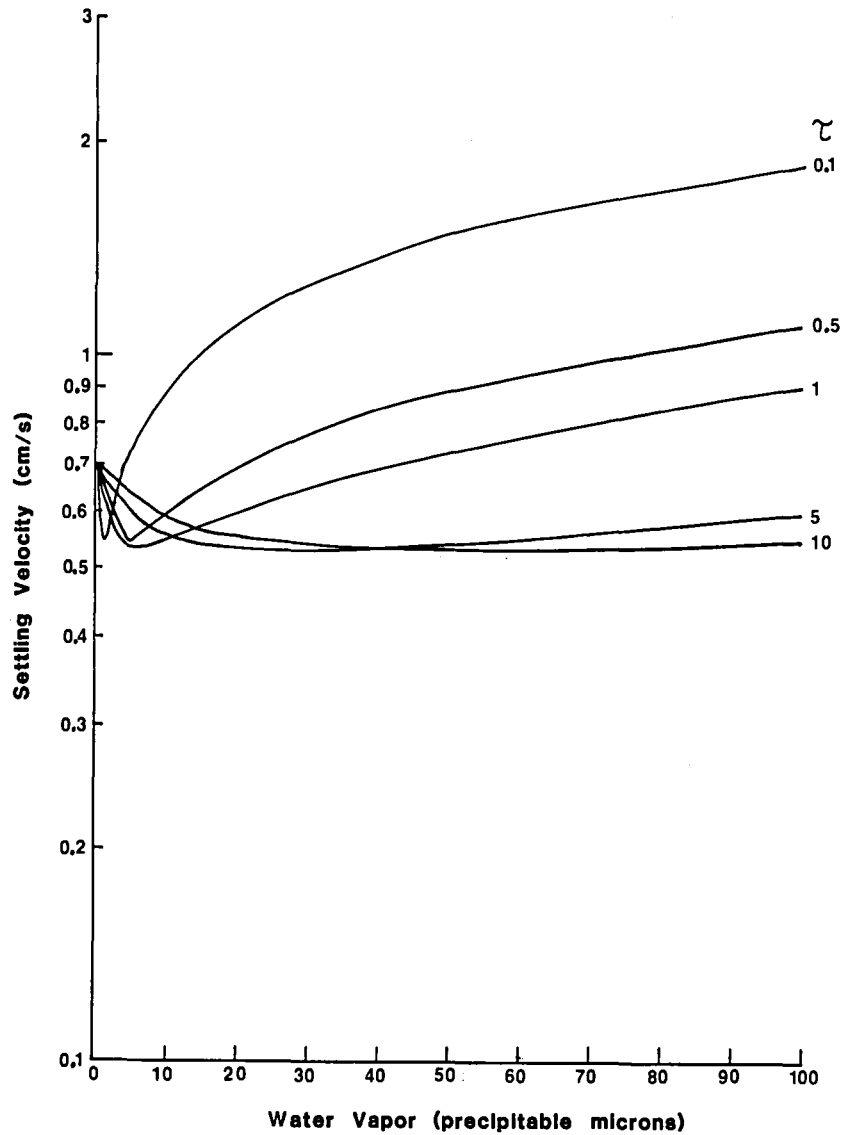Lee S. W.

Figure 1: Settling velocity of dust particles as a function of atmospheric water vapor content (complete condensation on the dust is assumed) and dust loading. The model assumes dust grains of 2.5 µm radius, a temperature of 180°K, and atmospheric pressure of 6.1 mb. Behavior for several different dust loading conditions (optical depth, τ = 0.1 to 10.0) is shown.

GROUND WATER IN THE EQUATORIAL REGION OF MARS: EVIDENCE FROM LANDSLIDES; B.K. Lucchitta, U.S. Geological Survey, 2255 N. Gemini Drive, Flagstaff, AZ 86001

Three fresh-looking landslides occur on the north wall of Ophir Chasma and shed debris southward into a north-south-trending trough that dissects mesas of layered deposits (Fig. 1). The trough extends across Ophir Chasma into central Candor Chasma, where it merges with a low, level plain. These slides clearly contained water, as the figure and accompanying discussions show. The morphologic similarity of these slides to other landslides in the Valles Marineris suggests that other slides were also lubricated by a liquid.

Figure 1 shows that the three slides consist of rugged deposits that extend 20 to 30 km from their detachment scars along the north wall of Ophir Chasma (1,2) and grade into smoother, longitudinally grooved deposits that extend an additional 40 km to their lower margins. Two slides (AA',CC') have conspicuous lobes that terminate inside the north-south-trending trough. The middle slide (BB') merges with a broad, flat debris apron that fills the trough and has a vaguely longitudinally textured surface. The apron extends southward to a barrier ridge of canyon-wall material that separates Ophir from Candor Chasma. The ridge is breached to the level of the top surface of the apron in a 2- to 5-km wide slot. The continuation of the trough in Candor Chasma contains a channel that has high, level terraces and a hilly floor deposit. Several of the hills are doughnut shaped. Their number increases southward toward a fault scarp that crosses the channel floor. South of the fault scarp, the channel floor is longitudinally fluted, apparently carved by erosion. Where the trough merges with the low, level plain in central Candor Chasma, the channel makes a sharp bend to the east and hugs the eroded base of a wind-fluted interior mesa. The channel and its deposits can be traced to the easternmost corner of the level plain, a total distance of about 250 km from the north wall of Ophir Chasma.

The channel and its deposits appear to be directly related to the landslides and their debris aprons. Apparently, the landslide debris generated an outwash fan emplaced by a fluid; the fan became dammed against the bedrock ridge. At the dam, the outwash dropped much of its load and became a debris-charged flood. The floodwaters lost more of their load at the fault scarp, and they eroded bedrock on the channel floor south of the scarp. The water followed a sharp eastward bend in the channel and eroded the base of its northern bank. Eventually the remaining debris came to rest as hummocky material on top of the level plain.

The landslide deposits, debris apron, and channel material must have been lubricated by water, as indicated by the following observations: the materials negotiated several bends and traveled a total distance of 250 km from their source on a gradient of 4 m/km. Most other landslides in the Valles Marineris travelled a maximum of about 100 km, a distance commensurate with their potential energy, as shown in a comparative study of large, mostly dry, terrestrial landslides and Martian slides (3). The materials were capable of erosion at considerable distances from their source; they breached a bedrock crossridge, carved flutes in the lower channel and eroded its banks. The bedrock breach is to the level of the debris apron; this level suggests erosion by spilling of a liquid. Finally, the doughnut-shaped hills resemble moraines with kettle holes,

which on Earth are formed by the melting of ice blocks. Water contained
within the landslide material probably was released catastrophically and
created a debris-laden flood. As the landslides originated from Valles
Marineris wall rock, some layers within the 7- to 10-km-high walls must
have contained water or ice.

The landslide deposit and outwash material appear to be young; their
surfaces show only a few small (up to 500-m-diameter) superposed craters.
The emplacement of these landslides appears to have been the latest event
in this region of Mars. In summary, water or ice must have been present in
the subsurface of this equatorial region of Mars in relatively recent time.

References

(1) U.S. Geological Survey (1984) Controlled photomosaic of part of the
        Valles Marineris region of Mars (experimental), MTM-05072. U.S.
        Geol. Survey Misc. Invest. Map I-1592, scale 1:500,000.
(2) Wu, S. S. C., Schafer, F. J., and Jordan, R. (1980) Topographic
        mapping of Mars: 1:2 million contour map series, in NASA Tech.
        Memo 82385, p. 458-461.
(3) Lucchitta, B. K., 1979, Landslides in the Valles Marineris, Mars.
        J. Geophy. Research, v. 84, no. B14, p. 8097-8113.

GROUND WATER IN THE EQUATORIAL REGION OF MARS
Lucchitta B. K.

55

Fig. 1
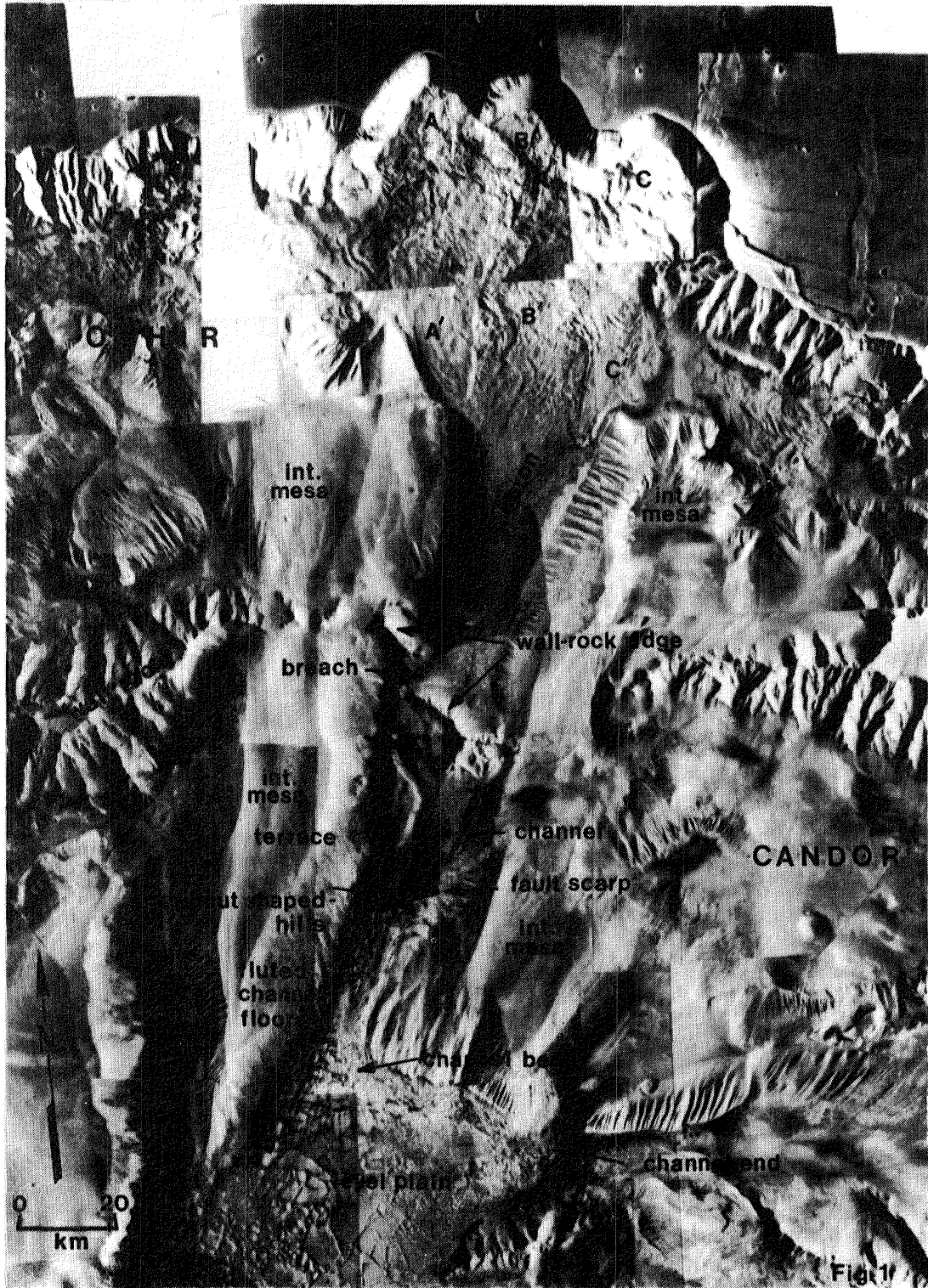
CLOUD PROPERTIES IN PAST MARTIAN CLIMATES; H.G. Marshall, J.C.G. Walker, W.R. Kuhn; Atmospheric & Oceanic Science Department, University of Michigan

Conditions for the existence of water clouds on Mars are explored along with their possible impacts on paleoclimates and precipitation. Our cloud model assumes a steady state array of periodic clouds with simplified vertical structure and internal dynamics. We estimate ice and water cloud fraction and precipitation as functions of relevant Martian climate parameters such as temperature and surface pressure. Limitations of these estimates and possible roles of precipitation events in Martian Channels are discussed.

THE POSSIBLE ROLE OF WATER IN THE RECESSION OF MARS' POLAR CAPS;
L. J. Martin, Planetary Reseach Center, Lowell Observatory; and P. B. James,
University of Missouri, St. Louis, and Lowell Observatory

Correlations between Viking observations and Earth-based photographs
through 1984 suggest that the polar caps are complex features whose seasonal
cycles are only partially understood. Even less known are the causes and
effects of annual variations within these cycles [1]. The resolution of Viking
observations provides the means for better interpretation of the more compre-
hensive and extensive Earth-based observations, which likewise give us the
basis to interpret the relatively few Viking images that included polar cap
phenomena.

We believe the observations support the theory that the seasonal polar
caps have an H_2O component as well as a CO_2 component. The CO_2 caps that begin
to form in fall are probably patchy [2] and not bright and therefore have not
been observed from Earth. As the CO_2 caps begin to sublime in late winter, a
bright ring of what may be water frost forms on their periphery. This bright
ring that retreats towards the poles each spring [1] is the "cap" that has
been recognized and measured from Earth for many decades [3]. It is also the
same cap boundary whose recessions have been measured on the Viking images
[1,2,4].

Because they have not been resolved using Earth-based telescopes, the
fall/winter CO_2 caps have not been well observed. They had been postulated on
the basis of models [5] and verified by Mariner 7 [6]; their existence is
supported by pressure measurements at the Viking lander sites [7]. Viking
orbiter pictures show some frost in those seasons [8], as do images from
Viking Lander II. Viking IRTM data may provide the best information on the
caps' growth periods but are yet to be fully analyzed. Throughout the fall and
winter, the north polar region is hooded by clouds, whereas the southern polar
hood does not appear until mid-winter (L_s 130°) [9]. This appearance may
coincide with the earliest phases of CO_2 cap sublimation, since the boundary
of the southern cap appears to move south about 15° of latitude before it
begins to appear as a bright ring in late winter (at about L_s 160° during the
1984 apparition) [9].

Water vapor measurements [10,11] suggest that H_2O may have been released
from the subliming CO_2 caps. This release could have provided a component of
the hood clouds during early stages of cap recession. We suggest that H_2O from
the hoods may have condensed on the perimeters of the receding CO_2 caps,
creating the visibly bright frost rings. As the CO_2 caps continue to sublime
(and release water vapor), their peripheral H_2O rings close inward as the caps
retreat towards the poles. Although the residual cap in the south was found to
contain CO_2 [12], its relatively high albedo [13] may result from a component
of water.

Recent observations of the North Polar Cap [14] provide additional
evidence for the presence of water: Analysis of Planetary Patrol photography
relevant to the late winter/spring season of the North Polar Cap has confirmed
a plateau in the regression curve between L_s = 20° and L_s = 45° in 1977-78.
This standstill was previously reported in analyses of Viking and terrestrial
data [2]. The notion of a relatively stationary cap boundary at roughly 65°
latitude is also consistent with the suppression of sublimation winds during

this season [15]. The resumption of cap recession at about L_s = 45° coincides with the relevant increase in water vapor in the north polar region, reinforcing the suggestion of released vapor from the edge of the retreating cap. Comparison of red and blue Earth-based images strongly supports this correlation between CO_2 sublimation and released water vapor. While the red and green pictures, which are sensitive to the surface cap, show an orderly regression commencing at L_s = 45°, the cloud-sensitive blue pictures show the formation and rapid southerly expansion of circumpolar clouds at the same time [14].

Although CO_2 is the major component of the seasonal caps, there is good evidence that water is also involved, perhaps to the extent of being the more visible constituent. If true, the caps must play a major role in Mars' water cycle, although not to the degree advocated by Percival Lowell.

References

[1] James, P. B., Briggs, G., Barnes, J., and Spruck, A. (1979). Seasonal recession of Mars' South Polar Cap as seen by Viking. **J. Geophys. Res.** 84, 2889-2922.

[2] James, P. B. (1979). Recession of Martian North Polar Cap: 1977-1978 Viking observations. **J. Geophys. Res.** 84, 8332-8334.

[3] Iwasaki, K., Saito, Y., and Akabane, T. (1984). Martian North Polar Cap and haze 1981-1982. **Publ. Astron. Soc. Japan** 36, 347-356.

[4] James, P. B. (1982). Recession of Martian North Polar Cap: 1979-1980 Viking observations. **Icarus** 52, 565-569.

[5] Leighton, R. B., and Murray, B. C. (1966). Behavior of carbon dioxide and other volatiles on Mars. **Science** 153, 136-147.

[6] Neugebauer, G., Munch, G., Kieffer, H. H., Chase, S. C., and Miner, E. D. (1971). Mariner 1969 infrared radiometer results: Temperatures and thermal properties on the Martian surface. **Astron. J.** 76, 719-749.

[7] Hess, S., Ryan, J. A., Tillman, J. E., Leovy, C. B., and Henry, R. M. (1980). The annual cycle of pressure on Mars measured by Viking Landers I and II. **Geophys. Res. Lett.** 7, 197-200.

[8] James, P. B. (1983). Condensation phase of the Martian South Polar Cap (abstract). **Bull. Amer. Astron. Soc.** 15, 846-847.

[9] Martin, L. J., and James, P. B. (1984). Mars 1984: Transition from polar hood to surface cap (abstract). **Bull. Amer. Astron. Soc.** 16, 673.

[10] Davies, D. W. (1982). Water vapor in Mars' arctic: Seasonal and spatial variability. **J. Geophys. Res.** 87, 10253-10263.

[11] Davies, D. W., and Wainio, L. A. (1981). Measurements of water vapor in Mars' antarctic. **Icarus** 45, 216-230.

[12] Kieffer, H. H. (1979). Mars south polar spring and summer temperatures: A residual CO_2 frost. **J. Geophys. Res.** 84, 8263-8288.

[13] James, P. B., and North, G. R. (1982). The seasonal CO_2 cycle on Mars: An application of an energy balance climate model. **J. Geophys. Res.** 87, 10271-10283.

[14] James, P. B., Pierce, M., Martin, L. (1984). Mars: North Polar Cap regressions, 1975-1982 (abstract). **Bull. Amer. Astron. Soc.** 16, 673.

[15] Kahn, R. (1983). Some observational constraints on global-scale wind systems of Mars. **J. Geophys. Res.** 88, 10189-10209.

SUBLIMATION RATES REQUIRED FOR STEADY-STATE GLACIERS, MARS

Henry Moore, U.S. Geological Survey, Menlo Park, CA., 94025

Glacier-like landforms are observed in the fretted terrain of Mars in the latitude belts near $\pm 42°$. Their origin and the climatic conditions required to sustain them are current problems. The velocity of flow within them and their growth rates are also current problems. If they are composed chiefly of water ice, the sublimation rate of ice onto the glaciers required to maintain a steady-state can be estimated.

The profile of a two dimensional steady-state glacier which ablates at the tip depends on the form of the flow law and the distribution of sublimation of ice onto the glacier (1,2). The rate of sublimation of ice onto the glacier required to maintain the steady-state form depends on the flow law parameter which, in turn, depends on the temperature of the ice (2). Thus, sublimation rates required to maintain martian glaciers could be estimated with the assumption that they are in a steady-state.

Procedures for estimating sublimation rates can be illustrated with a simple model. Flow of ice through the glacier is assumed to obey the following law (2):

$$\bar{V} = A \; \mathcal{T}^3 \; \frac{h}{5}$$

where $\bar{V}$ is the average velocity of the ice through a vertical section with thickness h. $\mathcal{T}$ is the stress at the base of the glacier and A is the flow law parameter.

For sublimation of a uniform thickness of ice, the steady-state profile of the glacier is:

$$\left(\frac{h}{H}\right)^{8/3} = 1.0 \; - \left(\frac{x}{X}\right)^{4/3}$$

where h is the thickness of the glacier at a distance, x, from the head. H is the thickness at the head and X is the length of the glacier. The sublimation rate (S) required to maintain the glacier is:

$$S = \frac{A}{5} \left(\frac{\rho g}{2}\right)^3 \left(\frac{H^2}{X}\right)^4$$

where ρ is the density of the glacier and g is the acceleration of gravity. The flow law parameter is related to the temperature (2):

$$A = A_o \; \exp \frac{-E}{RT}$$

where E is the activation energy for creep (73.4 kJ/mol), R is

the gas constant, T is the temperature, and A_o is a constant (0.58 kPa^{-3} s^{-1}).

Sublimation rates required to maintain a martian glacier with a maximum thickness (H) of 0.9 km and a length (X) of 25 km are markedly dependent on temperature (fig. 1) (e.g. 3). At 210°K, the sublimation rate on the glacier required to maintain the steady-state profile is only 14 microns/year. Average velocities of ice within the glacier are low. Midway they are only about 0.2 mm/yr and 250 m from the tip they are 2 mm/yr. Ablation must be 36 cm/yr at or near the tip.

There are countless other scenarios. If ice is introduced at the head of the glacier above at a rate 36 cm/yr and the flow law and flow law parameter are the same, the steady-state shape is a parabola. Ice is sublimed from the parabolic glacier along its length and the velocity of the tip is zero. A composite of the two shapes can be devised for which ice is sublimed onto the upper part, away from the lower part, and the velocity of the tip is zero.

Martian rock glaciers at the bases of cliffs (3) composed chiefly of ice that are in a steady-state will increase in size according to the net increase in added material. Thus, the velocity of the rock glacier will depend on the rate at which the rock and ice are added.

References Cited

(1)   Vialov, S. S., 1958, Regularities of glacial shields
            movement and the theory of plastic viscours flow: in
            Symposium of Chamonix, 16-24 Sept. 1958, International
            Assoc. of Scientific Hydrology, Publ. 47, p. 266-275.

(2)   Paterson, W. S. B., 1981, The physics of glaciers, 2nd ed.,
            Pergamon Press, 380 p.

(3)   Squyres, Steven W., 1978, Martian fretted terrain: flow of
            erosional debris: Icarus, v. 34, p. 600-613.

(4)   Lucchitta, Baerbel K., 1984, Ice and debris in the fretted
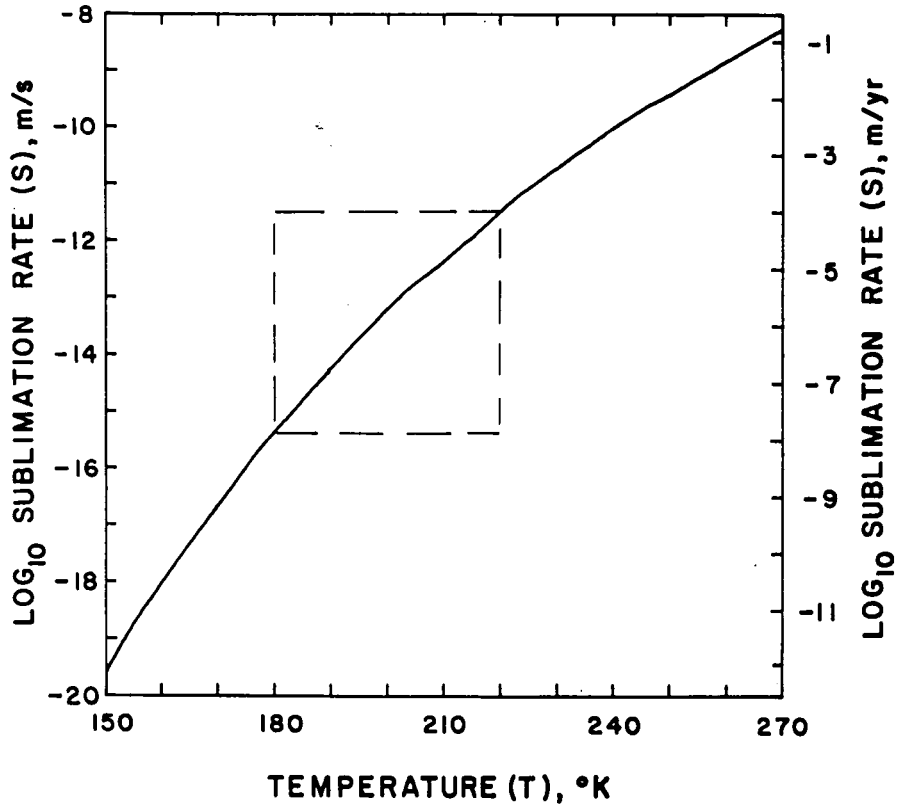   terrain, Mars: Jour. Geophys. Res., v. 89, p. B409-
            B418.

Figure 1. Sublimation rates required to maintain a steady state martian glacier as a function of temperature. Details appear in text. Rectangular box indicates martian conditions for ice near the 42° latitude belts where glacial forms are observed (3,4).

MAPPING OF THE WATER VAPOR DISTRIBUTION ON MARS; A MICROWAVE SPECTROMETER AND RADIOMETER FOR MG/CO; Duane O. Muhleman (Caltech), R.T. Clancy (U. of Colorado), F.P. Schloerb (U. of Mass.), L. Riley and W.G. Wilson (Jet Propulsion Laboratory)

A very intense line of H_2O exists at 183.31 GHz (λ = 1.64 mm) which is optically thick at the line center everywhere in the Mars' atmosphere where the column water vapor content is greater than a few precipitable micrometers. Over the warm surfaces of the planet the spectral line appears in absorption of the background continuum; it appears in emission over regions where the ground temperatures is significantly lower than that of the atmosphere, e.g., the polar regions.

We are developing a Microwave Spectrometer and Radiometer (MSAR) which will be proposed for the MG/CO mission. The primary goal of our instrument is to map the column content of water vapor over the entire planet or a daily basis. The instrument will be sensitive to a column content greater than 0.1 μm (pr). In regions and epochs where the column content exceeds 1 or 2 μm, the spectra will be inverted to obtain some information about the altitude distribution of the water vapor. The microwave technique has several advantages other methods of measuring the H_2O distribution:

(1) The measurements are completely independent of the atmospheric dust content due to the relatively long wavelength of 1.64 mm, i.e. in all cases the dust column is very optically thin.

(2) The measurements are unaffected by ice clouds or any other aerosols for the same reason.

(3) The measurements do not require solar illumination and the instrument sensitivity is not degraded at the coldest points on Mars.

(4) The detectors do not require cooling, i.e. they will operate at room temperature.

(5) The instrument is nadir-looking which is ideal for mapping.

(6) A H_2O spectrum will be measured in 10 seconds with a foot-print of 10 km cross and 40 km along the orbit track.

(7) The instrument will also measure the first 2 rotational lines of CO (ubiquitous on Mars) which will be inverted for the temperature-pressure profiles, also independent of the atmospheric dust content.

Synthetic water vapor spectra appear below. The left panel show the instrument responses for a constant mixing ratio of H_2O corresponding to 10 μm of H_2O over the polar regions where the ground temperature is ~150 K (upper curve, primarily in emission) and over mid-latitude regions (lower curve, primarily in absorption). The right panel shows the effect of distributing the entire 10 μm in the lower 5 km (upper curve, emission) and, again, the spectrum of uniform mixing. The sensitivity to the altitude distribution is made obvious by these curves! The absorption spectra for 1.0 and 0.1 μm of H_2O are indicated by the (+) signs at the line center. For 0.1 μm the continuum absorption at line center (res = 1 MHz) is 1.5% which for the average continuum temperature of 200 K corresponds to 3 K of absorption. The system design goal has a 1 MHz channel sensitivity of ±1.0 K in the 10 sec integration. Thus, 0.1 μm of precipitable water vapor causes a 3 σ feature in the center channel of the spectrometer. We feel we can map the H_2O content whenever the column is greater than 0.1 μm.

The proposed experiment has several other very important goals. The instrument has three radiometer channels at 115 GHz (λ 2.7 mm), 183 GHz (λ

1.6 mm), and 230 GHz (λ 1.3 mm) which will measure the Mars' surface brightness temperatures to an absolute accuracy of ± 2.0 K over 10 x 10 km foot prints. These temperatures will correspond to the effective temperatures at depths of about 10 wavelengths for the Mars regolith and about a factor of 5 deeper for polar ice cover. These measurements combined with similar radiometer brightness temperatures at cm-wavelength made with the radar-altimeter antenna will yield subsurface temperature maps of the regolith and ice cover over depths from 2 cm to about 1 meter. Both the diurnal and annual temperature waves in the surface will be studied. The millimeter radiometer channels will map the surface temperatures at the polar cap boundries over the small footprints. Since these frequencies are in the Rayleigh-Jeans domain <u>surface</u> temperatures will be linearly averaged over the footprints and this technique should be nearly optimum for mapping the latitude of the CO_2 frost point with the least confusion from low albedo ''warm spots.''

Finally, spectra of O_2 and O_3 will be simultaneously measured with the CO spectra and maps will be generated for all the species (H_2O, CO, O_2, and O_3) in the basic photochemical cycle of the Mars atmosphere. Ozone has been seen over the polar region on Mars. An abundance of 40 μm-atm of O_3 over cold regions creates an emission feature of 1.5% of the continuum or about 3 K. The area under such a line would be determined to about $\pm 10\%$ with a corresponding error in O_3 column abundance with a 1 minute integration (180 km strip along the orbit). Much longer integrations of a few hours would be required to detect O_3 all over the planet at the 5 μm-atm level.
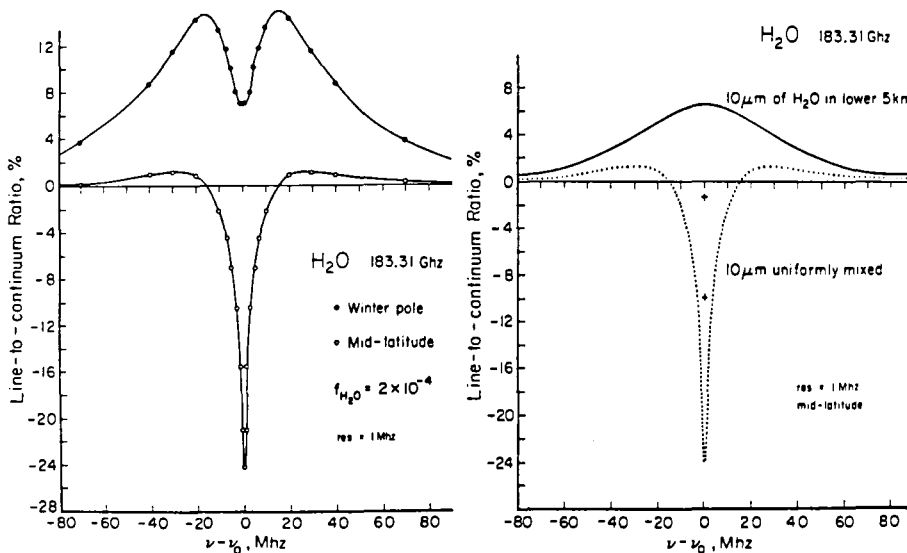
GEOLOGY OF LAYERED DEPOSITS IN THE VALLES MARINERIS. S.S. Nedell, Department of Geology, San Jose State University, San Jose, CA, 95192, and S.W. Squyres, Space Science Division, NASA Ames Research Center, Moffett Feld, CA 94035.

We have performed detailed geologic mapping of the floors of the Valles Marineris on Mars using high resolution Viking Orbiter images (125 to 25 m per picture element). The primary targets of the mapping were the layered deposits that are found in the lower elevations of the canyons. These deposits are widespread in the canyons, and exhibit fine rhythmic horizontal layering that is continuous over large areas. The goals of the mapping were to establish the geographic distribution and thickness of the deposits, to establish the stratigraphy of all major the geologic units within the canyons, and to choose among candidate hypotheses for the origin of the layered deposits.

The layered deposits form erosional remnants that once may have covered larger areas of the valley floors. These remnants most commonly take the form of plateaus up to 5 km high with exposed layering on their steep faces. The greatest total thicknesses of deposits are found in Candor, Ophir and Melas Chasmas. Individual layer thicknesses measured to date range from 170 m in Candor Chasma to 220 m in southeast Melas Chasma. The maximum lateral extent that an individual layer has been traced is ∼50 km. At the best image resoutions, no angular unconformities were detected in the layers.

Typical consequences of erosion and weathering of the layered deposits include fine eolian fluting along steeper faces, and production of a light and dark mottled pattern on subhorizontal surfaces. The mottling may be produced by differential weathering of layers of differing albedo. Because a clear relationship between rhythmic layering and the mottled surface pattern was established in well-exposed remnants, occurrence of the layered deposits was in some cases mapped in areas where there was distinct mottling, but no clear exposure of layers. The canyon walls generally exhibit spur-and-gully topography that is quite distinct from the eolian fluting of the layered deposits. Eolian fluting is not observed on the canyon walls. In many locations the walls have also undergone extensive landsliding. In contrast, no landslides formed in the layered deposits, even on the steepest surfaces. We infer from these differences that the material of the layered deposits is markedly different from that of the canyon walls.

A deep "moat", or trough, commonly separates the layered deposit from the canyon walls. Formation of the moats by eolian erosion is unlikely because of their great depth (over 5 km in Ophir and Hebes Chasmas) and the difficulty of producing deep erosion along canyon walls while leaving the sediments farther from the walls virtually untouched. Rapid release of ponded water by overtopping divides in the canyons has been suggested by Lucchitta (1) as a mechanism of forming outflow channels, and the streamlined sides of some layer remnants is consistent with some fluvial erosion of sediments within the canyons. However, draining of putative lakes accompanied by deep fluvial erosion is not a viable candidate for all moat formation. Hebes Chasma is a completely enclosed basin, but it has a well-developed moat that must have formed without any rapid drainage. The deep moats most probably formed subsequent to deposition of the adjacent layers, primarily by collapse of the canyon walls due to removal of large amounts of ground ice. There is strong evidence elsewhere in the canyons (e.g., in Noctis Labyrinthus) for substantial enlargement of the canyons by sapping and wall collapse. This collapse and subsequent mass wasting formed the spur-and-gully topography of the canyon walls.

In a few instances no moat is present and the layered deposits lap directly against and partially bury the spur-and gully-topography of the canyon walls. In these cases the

Nedell, S.S., and Squyres, S.W.

deposition of the layers clearly postdated local canyon enlargement by wall collapse, so we infer that layer deposition and wall collapse took place in more or less the same period of martian history.

The history of the Valles Marineris began with formation of tectonic grabens, followed by sapping, collapse, and weathering of the walls to form spur-and-gully topography. The layered deposits were emplaced during roughly the same period. Further local canyon wall collapse and perhaps deep erosion of the deposits in some areas followed, producing the present remnant and canyon wall geometry. The outlfow channels associated with the Valles Marineris may date from this epoch of erosion. Sediments have been identified in Eos Chasma with no layering and a gently undulating surface. These may be products of the layer erosion, redeposited when water flowing westward through the narrow Coprates Chasma lost the capacity to carry much of its load as the canyons widened into Eos and Capri. Landsliding postdates the formation and deep erosion of the layered deposits. Evidence for this temporal relationship is supplied by slides diverted by erosional plateaus in Ophir Chasma, and slides deposited over topographically subdued remnants in Candor Chasma. Eolian erosion responsible for the fluting has been volumetrically minor, and could be continuing up to the present.

We have considered four possible hypotheses for the origin of the layered deposits: *(1)* that they are eolian deposits, *(2)* that they are remnants of the same material that makes up the canyon walls, *(3)* that they are explosive volcanic deposits (ref. 2), or *(4)* that they were deposited in standing bodies of water. The eolian hypothesis is inconsistent with the distribution of the sediments, which lie only in the lower elevations of the canyons. The higher elevations, canyon walls, and surrounding uplands are completely free of any similar deposits. The clear differences in morphology and weathering style exhibited by the layered deposits and the canyon walls show that the two materials are in fact quite different. There are several objections to the volcanic hypothesis. First, the morphology of the deposits is inconsistent with typical styles of explosive vulcanism. Ash fall deposits, like eolian deposits, would not show such a limited geographic distribution. Ash flows, on the other hand, would not tend to form such regular layering, and would require a substantial number of widely spaced volcanic calderas. No unequivocal volcanic calderas have been identified in the Valles Marineris system, and many exensive layered deposits *(e.g.,* in Hebes Chasma) are clearly not associated with any observable volcanic vents. The horizontality, lateral continuity, great thickness, and stratigraphic relationships of the layered deposits are consistent with deposition in standing bodies of water. For most reasonable models of the evolution of the martian atmosphere, we would expect large lakes on Mars at the time of the layer deposition to be ice-covered. Perenially ice-covered lakes exist on Earth in the Dry Valleys of Antarctica. The annual sedimentation rate in antarctic Lake Vanda has been estimated at 0.06 mm yr^{-1} (3), and a similar rate would produce deposits of the thickness observed on Mars in $\sim 8 \times 10^7$ yr. We plan to investigate the processes of sedimentation in ice-covered lakes in detail, and to consider the applicability of such processes to the sediments in the Valles Marineris.

(1) Lucchitta, B.K. (1982) NASA Tech. Memo. 85127, 233-234.

(2) Lucchitta, B.K. (1981) NASA Tech. Memo. 84211, p.419-421.

(3) Love, G., Virginia Polytechnic Institute (1984) *personal communication.*

THE MARS GEOSCIENCE/CLIMATOLOGY OBSERVER (MGCO) MISSION. Frank Don Palluconi, Jet Propulsion Laboratory, California Institute of Technology, Pasadena, CA 91109, and Arden L. Albee, California Institute of Technology, Pasadena, CA 91125

The Mars Geoscience/Climatology Observer Mission is to be the first in a series of modest cost inner planet missions. Launch is planned for the August/September 1990 Mars opportunity with arrival at Mars one year later. The Geoscience/Climatology objectives are to be met over the course of a one Mars year (687 day) mapping mission. The mapping orbit will be near polar (93 degree orbital inclination), sun-synchronous (2 PM sunward equator crossing), and near circular (350 km orbit altitude, 116 minute period). The spacecraft, to be selected in late 1985, will be a modified version of an existing commercial design which in the mapping orbit will maintain a nadir orientation. Experiments and instruments will be selected through an Announcement of Opportunity (AO) process with release of the AO in April 1985 and selection in early 1986.

The completeness of the global and seasonal coverage afforded by this mission is ideal for improving our understanding of the Martian Climate. The specific measurement objectives for the mission involve:

1. Determining the time and space distribution, abundance, sources, and sinks of volatile material and dust over a seasonal cycle.
2. Exploring the structure and aspects of the circulation of the atmosphere.
3. Determining the global elemental and mineralogical character of the surface.
4. Defining globally the gravitational field and surface topography.
5. Establishing the nature of the magnetic field.

To provide assistance in identifying spacecraft requirements and defining the mission a strawman payload has been defined which includes the following experiments/instruments: Gamma Ray Spectrometer, Visual and Infrared Mapping Spectrometer, Pressure Modulator Infrared Radiometer, Radar Altimeter, Ultraviolet Spectrometer, Ultraviolet Photometer, Magnetometer and Radio Science. Many of these experiments/instruments and others that have been suggested will contribute to both geoscience and climatology. It is expected that the experiments carried by MGCO will be highly synergistic and will make extensive use previous earth-based and spacecraft-based Mars observations.

Understanding in space and time the sources and sinks, vertical distribution and transport of CO_2, H_2O and dust along with the structure and circulation of the atmosphere will provide an opportunity to address in a substantial way many climate questions. The selected orbit will provide only limited diunal coverage so the full range of atmospheric behavior will not be accessable. In this sense MGCO should be viewed as a beginning experimental effort to understand the Mars atmosphere.

The climatology objectives of the MGCO mission are intended to improve our understanding of the current climate of Mars. If we are able to understand the current climate, we may more confidently project this knowledge backward in time to periods when the Mars orbit and axial characteristics and the atmospheric pressure were different. This is another step in deepening our knowledge of terrestrial planet evolution.

NEW GCM SIMULATIONS OF TRANSPORT INTO THE POLAR REGIONS;
James B. Pollack and Robert M. Haberle, NASA/Ames Research Center,
Jerome White and Kenneth Bilski, Informatics Inc.

We have made a number of significant improvements to our Mars General
Circulation model (GCM). These include incorporation of the radiation
properties of dust, an increase in the number of vertical layers (from 3 to
~9), better treatment of the exchange integral in the thermal radiative
fluxes, and an improved treatment of turbulent transport in the free
atmosphere. Simulations have been performed for global averaged dust optical
depths of 0, 1, and 5 at L_s=270 (southern hemisphere solstice). Results
from these simulations are analyzed to assess the amount of transport by
atmospheric eddies into the polar regions at times of varying dust loading.
This information is relevant for understanding the ability of atmospheric
winds to move water into and out of the polar regions.

CONTROLS ON PRECIPITATION OF VARIOUS IRON OXIDES AND HYDROXIDES: RELEVANCE TO MARS.

J. Posey-Dowty, L. B. Tanenbaum, B. M. Moskowitz, D. A. Crerar, R. B. Hargraves
Dept. of Geological and Geophysical Sciences, Princeton University

The red coloration of the Martian surface is presumably due to the presence of ferric iron. With respect to the inventory and history of Martian volatiles, the mineralogic forms in which the ferric iron occurs - specifically, whether or not hydrated ferric oxides are present - is of obvious importance.

Our investigation of the causes of the high magnetic susceptibility of the surface material[1,2] has focused on two general possibilities:

(1) that the magnetism is carried by superparamagnetic particles in "metanontronite" (nontronite transiently heated to very high temperatures (and dehydrated) perhaps by shock[1,2,3]).

(2) that the magnetism is caused by a thin, red, magnetic, ferric oxide or hydroxide coating on otherwise nonmagnetic silicate (or other) mineral particles[1,2].

To explore this second possibility we have been experimenting to evaluate the importance of anion species on the precipitation of ferric oxides/hydroxides by rapid oxidation of ferrous iron from solutions, at rigorously controlled neutral pH, in the presence of different mineral substrates. The products of these experiments have been analyzed by x-ray, transmission I.R., and thermomagnetic properties.

Our tentative current conclusions are:

(1) Ferroxyhite ($\delta FeO \cdot OH$), is excluded because its precipitation requires extremely rapid, and strong oxidation, (which we consider unlikely), and its saturation magnetization is too low (<10 emu/gm) to be compatible with the apparent magnetic properties of the Martian surface.

(2) Lepidocrocite ($\gamma FeO \cdot OH$) is the predominant hydrated ferric oxide phase precipitated by rapid oxidation of Fe^{2+} at neutral pH from blank perchlorate, chloride, and sulfate solutions. By analogy with the behavior of goethite ($\alpha FeO \cdot OH$)[4] we believe that variations in the amount of maghemite present are primarily related to the grain size of the precipitates, coarser grains of lepidocrocite inverting more rapidly to γFe_2O_3.

(3) Mineral substrates strongly influence the phase precipitated in a manner consistent with their isoelectric points (IEP)[5] (see Table, specifi-

CONTROLS ON PRECIPITATION OF IRON OXIDES AND HYDROXIDES
Posey-Dowty et al.

69

cally: minerals with low IEP (e.g. feldspars) favor lepidocrocite, those with high IEP (e.g. calcite) promote goethite.

(4) Quartz is a conspicuous exception, in that although it has low IEP, it strongly promotes the precipitation of goethite. This fact may relate to the predominance of αFe^{3+} weathering products on earth.

(5) Primary lepidocrocite, eventually dehydrating to maghemite, is the most plausible model for the production of magnetic, Fe^{3+}-coated grains. Should this be the explanation for the magnetic properties of the Martian surface material, we therefore would not expect water still to be present in any form of hydrated ferric oxide; (OH) in other minerals, however, is not precluded.

1.
Hargraves, R. B., Collinson, D. R., Arvidson, R. E. and Spitzer, C. R., 1977, The Viking Magnetic Properties Experiment: Primary Mission Results. J. Geophys. Res., v. 82, p. 1315-1324.
2.
Hargraves, R. B., Collinson, D. R., Arvidson, R. E. and Cates, P. M., 1979, Viking magnetic properties experiment: Extended Mission Results. J. Geophys. Res., v. 84, p. 8379-8384.
3.
Moskowitz, B. M. and Hargraves, R. B., 1984, Magnetic Cristobalite(?) - a possible new magnetic phase produced by the thermal decomposition of nontronite. Science, v. 225, p. 1152-1 54
4.
Langmuir, D., 1971, Particle size effect on the reaction: Goethite = Hematite + Water. Am. J. Sci., v. 271, p. 147-156.
5.
Parks, G. A., 1975, Adsorption in the marine environment. in "Marine Geochemistry" (2nd ed.), vol. 1, J. P. Riley and G. Skirrow, eds., Academic Press, N.Y., p. 241-308.

CONTROLS ON PRECIPITATION OF IRON OXIDES AND HYDROXIDES
Posey-Dowty et al.

70

				PRECIPITATE		
Substrate	IEP*	G(IR)	L(IR)	L(mag) relative %	M(IR)	H(IR)
Quartz	1.5-2.0	✓	✓	3.0	tr(p)	✓
Albite	2.0-2.4	X	✓	6.9	✓(s,p)	tr(p)
Orthoclase	2.0-2.4	X	✓	13.6	✓	tr(p)
Na Plag.	2.0-2.4	X	✓	6.4	✓	tr(s,p)
Rutile	4.7-6.2	X	✓	0.5	✓	✓
Augite	4.5-6.5	tr	✓	3.4	✓	X
Basalt (qtz rich)	<<6.0	✓	✓	4.6	✓	tr
Basalt (qtz poor)		X	✓		✓	✓
Montmorillonite (contained qtz)	<2.5	✓	✓	1.6	X	tr
Olivine	4.0-8.9	X	✓		tr(c)	✓
Calcite	9.5-10.8	✓	✓	3.0	tr(c,p)	tr
αAl_2O_3	9.0-10.0	✓	✓	3.8	X	tr
$MgO(syn)$[1]	12.4	✓	✓	2.4		tr
Fe_3O_4	6.5±.2					
γFe_2O_3	6.7±.2					
$\alpha FeO \cdot OH$	6.7±.2					
$\gamma FeO \cdot OH$	7.4					
αFe_2O_3	8.0-9.0					
$Fe(OH)_3$	8.5					
$Fe(OH)_2$	12.0±0.5					

*From Parks, 1975

Results apply to all starting salts unless restricted to certain salts indicated in parenthesis.

s = ferrous sulfate, c = chloride, p = perchlorate

    ✓ = present

    X = absent

    tr = trace

1 Experiments with ferrous sulfate starting salt only

RADAR AND THE DETECTION OF LIQUID WATER ON MARS; L. E. Roth and R. S. Saunders, Jet Propulsion Laboratory, California Institute of Technology, Pasadena, California 91109; G. Schubert, Department of Earth and Space Sciences, University of California, Los Angeles, California 90024.

Detection (1) of the seasonally variable radar reflectivity in the Goldstone Mars data (2) (the 'Solis Lacus radar anomaly' (1)) and the proposed interpretation in terms of the near-surface presence of liquid water (1) created a controversy in the planetary science community. We previously expressed skepticism about that interpretation and, because of the potential significance of the observed phenomenon, attempted to develop alternate interpretations (3,4). After further analysis, we have come to support the liquid-water hypothesis.

In the course of the 1971 and 1973 oppositions, the Goldstone radar scanned Mars along (constant-latitude) tracks within the -14° to -22° lat. band. By coincidence, a few scans were taken along almost identical latitudes during both the 1971 and 1973 experiments. Detailed analysis (1) showed that there are significant differences between the two data sets, particularly in the general location of the Sinai Planum. The data exhibiting these differences are presented in Figs. 1(a) through (c). The graphs show smoothed radar reflectivity vs. longitude for three pairs of scans, each pair along almost identical latitudes. The pairs are arranged in the order of the increasing magnitude of ΔL_s, i.e. in the order of the increasing difference in areocentric solar longitude, L_s, of the two scans forming a pair. In this context, ΔL_s is a measure of the time interval, relative to Martian seasons, separating the scans of each pair. It is seen that reflectivity in all three plots follows the same trend, viz., it is low in the S hemisphere spring (lower L_s), high in the S hemisphere summer (higher L_s). In Fig. 1(a) (1971/1973, $\Delta L_s = 15.80^\circ$) this trend is not pronounced or may even reverse itself. However, the data in Fig. 1(c) (1971/1973, $\Delta L_s = 47.48^\circ$) leave no doubt. In the area of Sinai Planum higher radar reflectivity has been recorded deeper into the S hemisphere summer. It is this phenomenon, the seasonally variable radar reflectivity over Sinai Planum, that was termed the Solis Lacus radar anomaly (1) and that calls for elucidation. The data in Fig. 1(b) (1973/1973, $\Delta L_s = 23.50^\circ$) are even more tantalizing since they hint at a possible reflectivity increase taking place during the same opposition. Unfortunately, the coverage is incomplete.

In our attempt (3,4) to interprete the Solis Lacus anomaly we have approximated the Martian surface with a stack of layers (dust, duricrust, thawed permafrost) resting on a homogeneous half-space (frozen permafrost). The goal was to match the model reflectivities of various multi-layer configurations to the data in Fig. 1(c). It should be pointed out that the question of applicability of the idealized, planar models to the real-world geologic surfaces remains still unresolved (5,6). There is some evidence from both the passive- and active-microwave experiments (7,8,9,10) that the interference effects predicted by the planar models have been observed. This raises the possibility that the planar models have at least a limited applicability to the bland topographies in which the dominant morphogenic processes have been the eolian/fluvial erosion/deposition.

Of all the multi-layer models tested, the one-layer models match (at $\lambda 12.6$ cm) the data in Fig. 1(c) with the greatest ease. The models with three

and more layers cannot be made to match the data at all. The anticipated 'paradoxical situation...when each improvement in the model [i.e., inclusion of larger number of layers] will introduce additional ambiguities in the data interpretation' (4) has not been reached. One-layer models approximate the following situations: Thawing of permafrost under a layer of overburden (variable dielectric constant of the half-space) or redistribution of dust over a homogeneous half-space (variable depth of the layer). Removal or deposition of a uniform layer of dust, ~1.x10^{-1}cm to ~1.5x10^{-1}cm in depth, can arbitrarily closely mimic the data in Fig. 1(c) (4). The Viking Landers observations (11,12,13) indicate that deposits of 'up to hundreds of micrometer' (~10^{-2}cm) might be associated with a global dust storm. The polar dust deposition rates have been estimated at 4.x10^{-2}cm/yr (14). In the absence of reliable data it is a matter of opinion whether the estimated rates of ~10^{-2}cm/yr fall short of the required rates of ~10^{-1}cm/yr. However, a more serious objection can be raised against the layered-surface models of the Solis Lacus anomaly. The 1971 data in Figs. 1(a) and (c) were taken on 20 Sept 71 and 24 Sept 71, respectively. The 1973 data were taken on 10 Sept 73 and 6 Oct 73. The 1971 global dust storm started 22 Sept 71 (15). Thus, there is one major dust-depositing event, the 1971 storm, between the two scans in each pair, (Figs. 1(a), (c)). It is reasonable to expect that a global storm would have associated with it a regionally uniform dust deposition rate and that this uniform rate would, in turn, produce deposits causing reflectivity changes uniform over the entire region, and certainly over a region covered by two pairs of scans separated by only ~30 km in latitude. Figs. 1(a) and (c) indicate that this is not so. Furthermore, between the times the scans in Fig. 1(b) were taken, 18 Aug 73 and 5 Oct 73, there has been no major storm reported; the 1973 global storm commenced 13 Oct 73 (16). Yet there is a suggestion in the data (Fig. 1(b)) that reflectivity changes might have been present. Thus, it appears that the radar reflectivity variations observed over Sinai Planum had to be caused by a subsurface agent. Thawing of permafrost at shallow depths below the surface is the only candidate. Eolian effects cannot be ruled out, but their contribution was not decisive.

Conclusions: (a) In theory, both the liquid-water model (1) and the layered-surface model (3) are equally likely to account for the Sinus Lacus anomaly. The presently available Mars S-band radar data may not be sufficient to decide with finality in favor of either of the proposed interpretations. The circumstantial evidence, particularly the incomplete scans in Fig. 1(b), favors the liquid-water hypothesis. (b) Since the evidence is incomplete, the results reported here make the case for a program of multi-frequency radar observations of Mars even more compelling. If the reflectivity at lower frequencies (S-,L-bands) displays the familiar seasonal pattern, the planet behaves as a homogeneous half-space; liquid water is present. In the frequency interval from ~1 GHz to ~30 GHz, the magnitude of the dielectric constant of liquid water drops from ~80 to below ~8, the range shared by many common rocks (17). If the reflectivity at higher frequencies (S-,X-,K-bands) displays a seasonal pattern, the planet behaves as a layered half-space; the reflectivity variations are due to redistribution of dust. (c) To examine the validity of the multi-layer models for planetary surfaces in general, and for the Martian surface in particular, it would be advisable to carry out scatterometer experiments over the variable-roughness, variable-moisture-content, layered testbeds on Earth.

Fig. 1
Light lines: 1971 data
Heavy lines: 1973 data
(a) 1971: -15.47° lat.
    1973: -15.42°
(b) 1973: -15.75°
    1973: -15.84°
(c) 1971: -15.93°
    1973: -15.94°
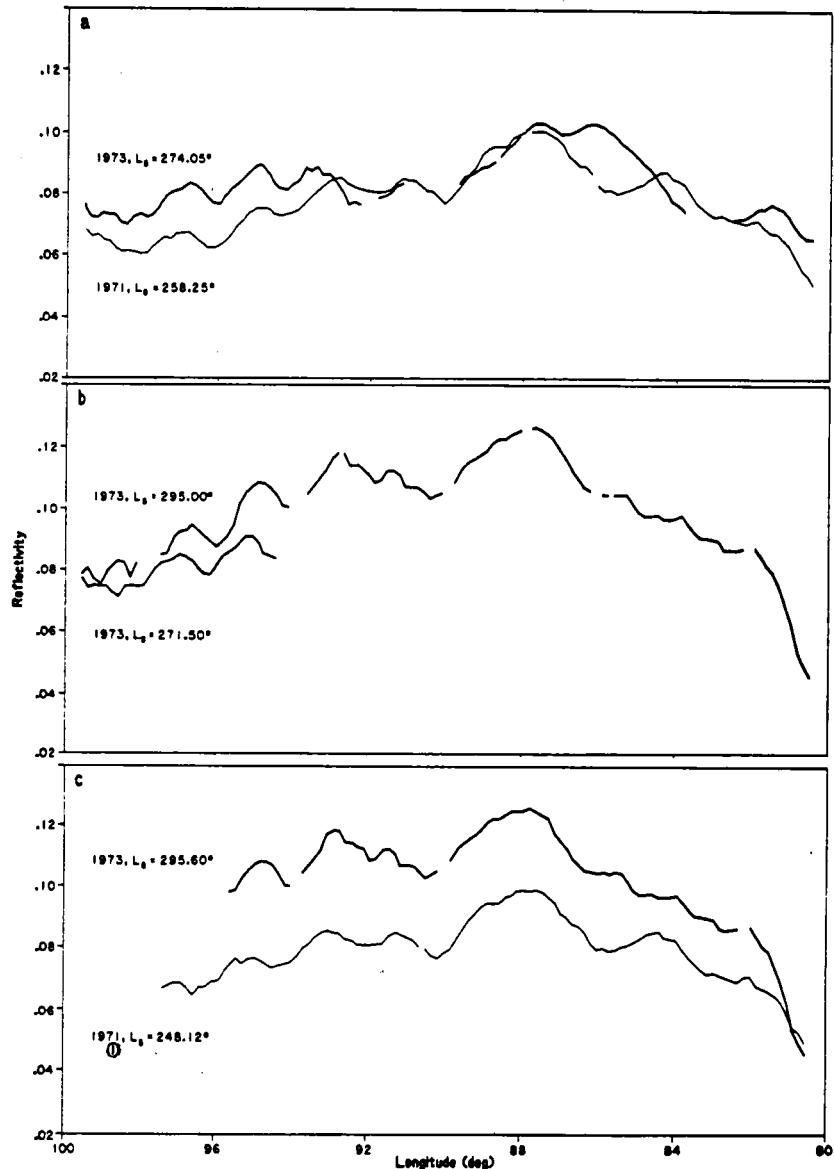
References: (1) Zisk, S. H. and Mouginis-Mrk, P. J. (1980). Anomalous region on Mars: Implications for near-surface liquid water. Nature 288, 735. (2) Downs, G. S., Reichley, P. E., and Green, R. R. (1975). Radar measurements of Martian topography and surface properties: The 1971 and 1973 oppositions. Icarus 26, 273. (3) Roth, L. E. and Suanders, R. S. (1984). Microwave reflectivity of the multilayer models of the Martian surface (abstract). Lunar Planet. Sci. XV, 693. (4) Roth, L. E. (1984). Is there radar incidence for liquid water on Mars? NASA TM 86246, 274. (5) Zisk, S. H. and Mouginis-Mark, P. J. (1981). Alternate models for the Solis Lacus radar anomaly on Mars. Papers 3rd Int'l Colloq. Mars, 294. (6) England, A. W. and Johnson, G. R. (1977). Microwave brightness spectra of layered media. Geophysics 42, 514. (7) Blinn, J. C., Conel, J. E., and Quade, J. G. (1972). Microwave emission from geologic materials: Observations of interference effects. J. Geophys. Res. 77, 4366. (8) Annan, A. P., Waller, W. M., Strangway, D. W., Rossiter, J. R., Redman, J. D., and Watts, R. D. (1975). The electromagnetic response of a low-loss 2-layer dielectric Earth for horizontal electric dipole excitation. Geophysics 40, 285. (9) Rossiter, J. R., Strangway, D. W., Annan, A. P., Watts, R. D., and Redman, J. D. (1975). Detection of thin layers by radio interferometry. Geophysics 40, 299. (10) Sadeghi, A. M., Hancock, G. D., Waite, W. P., Scott, H. D., and Rand, J. A. (1984). Microwave measurements of moisture distribution in the upper soil profile. Water Resources Res. 20, 927. (11) Jones, K. L., Arvidson, R. E., Guinness, E. A., Bragg, S. L., Wall, S. D., Carlston, C. E., and Pidek, D. G. (1979). One Mars year: Viking Lander imaging observations. Science 204, 799. (12) Guinness, E. A., Leff, C. E., and Arvidson, R. E. (1982). Two Mars years of surface changes seen at the Viking landing sites. J. Geophys. Res. 87, 10051. (13) Arvidson, R. E., Guinness, E. A., Moore, H. J., Tilman, J. and Wall, S. D. (1983). Three Mars Years: Viking Lander 1 imaging observations. Science 222, 463. (14) Pollack, J. B., Colburn, D. S., Flasar, M., Kahn, R., Carlston, C. E., and Pidek, D. (1979). Properties and effects of dust particles suspended in the Martian atmosphere. J. Geophys. Res. 84, 2929. (15) Martin, L. J. (1974). The major Martian yellow storm of 1971. Icarus 22, 175. (16) Martin, L. J. (1976). 1973 Dust storm on Mars: Maps from Hourly Photographs. Icarus 29, 363. (17) Hoekstra, P. and Delaney, A. (1974). Dielectric properties of soils at UHF and microwave frequencies. J. Geophys. Res. 79, 1699.

THE INFLUENCE OF H_2O ON VOLCANIC DEGASSING OF AEROSOL FORMING ELEMENTS S, Cl, AND F;

M.J. Rutherford and M.R. Carroll, Dept. of Geol. Sci., Brown University, Providence, RI 01912

A growing body of theoretical and experimental evidence indicates that volcanically derived sulfate and possibly halogen aerosols produced during volcanic eruption on earth may exert considerable influence on the earth's climate (Pollack et al., 1976; Sigurdsson, 1982; Rampino and Self, 1982; Devine et al., 1984). Has the Mars climate been similarly affected? In order to evaluate this question, it is first necessary to determine the nature and abundance of volcanic additions of sulfur and halogens into the Martian atmosphere. The problems of aerosol formation, the lifetime of aerosol particles and their climatic importance can then be evaluated. In fact, Settle (1979) assumed that S was available from volcanic degassing on Mars and made a theoretical analysis of these questions concerning aerosols and their climatic effects. This paper deals with the question of volcanic degassing, and some of the variables that might affect the degassing of S, Cl and F on Mars. In particular, it deals with the effects of H_2O and magma bulk composition on the degassing of these elements.

The amount of S, Cl and F that will be released from a volcanic rock as it reaches the surface of a planet will depend on several factors. First, is the element in question bound in a solid phase such as graphite, FeS, apatite or a mica, and if so, does that phase remain stable? Secondly, what are the factors affecting the solubility of S and halogens in the melt phase? Finally, is there an excess fluid phase associated with the magma, and if so, how are S, Cl and F partitioned into this phase. We have been experimentally investigating these questions by analysis of glass-phenocryst assemblages produced experimentally under controlled P, T, and f_{O_2} etc. conditions, and by analysis of similar natural volcanic assemblages. Experiments have now been done on two natural magma compositions, a dacite and an andesite, with the major emphasis being on S-solubility and composition of coexisting melt and fluid phases. The following points can be made on the basis of these experiments.

(1) The effect of decreasing pressure on S-solubility in silicate melts appears relatively minor. Therefore, the simple fact that the pressure on a magma decreases as it rises toward a planetary surface is not likely to cause major S-loss.

(2) S-solubility is partially dependent on magma compositon, increasing with increased FeO and TiO_2 in the melt. However, significant variations in FeO + TiO_2 in a fractionating magma occur only after very large degrees of crystallization, and are not likely to be an important factor leading to S-degassing.

(3) Sulfur-solubility in magmas is strongly affected by f_{O_2}. In all compositions investigated experimentally, the S solubility is high (i.e., 1000-2000 ppm) at low f_{O_2}, goes through a minimum at f_{O_2}'s equivalent to the QFM and NNO buffers, and then increases to equally high values at high f_{O_2}'s. The high solubility at low f_{O_2}'s appears to represent S^{-2} in the melt. At high f_{O_2}'s, the increased S solubility is correlated with high P_{SO_2}. Thus it is possible that some S-degassing could be associated with oxidation of a reduced magma as it rises toward a planetary surface. Oxidation of the appropriate magnitude and range appears common as magmas rise in the earth, because of re-equilibration with a C-O gas or graphite (Mathez, 1984), and it may also occur on Mars.

(4) S-solubility (Carroll and Rutherford, 1984) and Cl-solubility (Kilinc and Burnham, 1972) increase with increased H_2O in the silicate melt. These experimental data are supported by the analytical data of Devine et al., (1984) which contrasts the glass inclusions trapped in phenocrysts in volcanic rocks with matrix glasses in the same rock. No experimental data exists yet for F, but Burnham (1979) theorizes that F^- will coordinate with Si^{4+} in the melt, and its solubility will not be as dependent on P and P_{H_2O} as Cl and S.

VOLCANIC DEGASSING ON MARS
Rutherford, M. J. and Carroll, M.

75

Other experiments (Hamilton et al., 1964; Rutherford et al., in press) show that H_2O is strongly partitioned into silicate melts at depths of 1 km and more, but is concentrated in a coexisting fluid phase at surface pressures, a phase which will be readily lost at least from surface flows. These two pieces of evidence indicate that the presence of H_2O in the original magma will facilitate the degassing process, and probably will increase the amount of S, Cl and F(?) lost to the atmosphere in a volcanic episode.

(5) Experimental studies and analyses of volcanic glasses and volcanic gases at Mount St. Helens (Rutherford et al., in press; Gerlach et al., 1982) indicate that H_2O loss from magma beneath a volcano is likely to continue after the eruption. This H_2O carries H_2S and HCl from crystallizing magma, and probably more importantly, oxidizes FeS in the crystallized magma and surrounding rocks to form additional H_2S which will also be lost to the atmosphere.

(6) While H_2O is strongly partitioned into silicate melts at pressures >0.5 Kb, CO_2 is strongly partitioned into melts at pressures >20 kb (i.e., see Wyllie, 1980). A magma originating at greater than 20 kb would contain significant quantities of dissolved C-O gas if C was present in the source, and this C-O gas would exsolve as the magma moved towards lower pressures. However, calculations and experiments both indicate (Rutherford and Fogel, ms) that S and Cl would not partition into a CO-CO_2 fluid phase unless it contained significant H_2O. The origin of magmas at very high pressure will thus aid in the degassing of CO_2, but the addition of appreciable S and Cl to the fluid appears to depend on the presence of H_2O.

In conclusion, the available data all seem to suggest an extremely important role for H_2O in the degassing of S, Cl and to a lesser extent F from magmas. In fact, if H_2O were absent from a terrestrial-type planet, it appears the main force available (potentially) to drive the degassing of these elements would be oxidation. Near-surface oxidation appears to be likely on Venus, but there is no compelling evidence that it was important on Mars. The importance of H_2O as a degassing agent goes beyond the volcanic process. If, as has been proposed, the early formed atmospheric H_2O became entrapped in the regolith and surface rocks, this H_2O would potentially be available to form subsurface hydrothermal circulation systems around igneous intrusions much like those found on earth. These systems serve to bring S and Cl from the intrusion and surrounding rocks to the surface and atmosphere. Unfortunately, the bulk H_2O content of Mars is still unknown even though there are geological indications that H_2O has been present on the surface in significant amounts compared to present (i.e., Anderson et al., 1981).

REFERENCES:

(1) Arvidson, R. E. et al., 1980, Rev. Geophys. Space Phys., 19, 13-41. (2) Burnham, C. W., 1979, in *Geochemistry of Hydrothermal Ore Deposits*, H. L. Barnes, ed., Wiley. (3) Carroll, M. P., and Rutherford, M. J., 1984, Lunar and Planet. Sci. XV., 139-140. (4) Devine, J. D. et al., 1984, Jour. Geophys. Res., 89, 6309-6325. (5) Gerlach, T. M. et al., 1964, EOS, 63, 1142. (6) Hamilton, D. L. et al., 1964, Journ. of Petrlogy, 5, 21-39. (7) Kilinc, I. A. and Burnham. C. W., 1972, Econ. Geol., 67, 231-235. (8) Mathez, E. A., 1984, Nature, 310, 371-375. (9) Pollack, J. B., et al., 1976, Jour. Geophys. Res., 81, 1071-1083. (10) Rampino, M. R. and Self, S., 1982, Quat. Res., 18, 127-183. (11) Rutherford, M. J., *in press*, J. Geophys. Res. (12) Settle. M., 1979, J. Geophys. Res, 84, 8343-9354. (13) Sigurdsson, H., 1982, EOS, 63, 601-602. (14) Wyllie, P. J., 1980, J. Geophys. Res., 85, 6902-6910.

SEDIMENT - WATER DEPOSITION AND EROSION IN THE MARTIAN POLAR REGIONS.

R. Stephen Saunders, Timothy J. Parker, James B. Stephens, and Eric G. Laue, Jet Propulsion Laboratory, California Institute of Technology, Pasadena, CA 91109; Fraser P. Fanale, University of Hawaii, Honolulu, HI 96822

Sedimentary materials in the polar regions of Mars may be, in part, composed of clay-size mineral grains co-deposited with water ice. We have examined the properties of particle aggregates formed by sublimating a dispersion of sub-micrometer size grains of silicates in water ice. The properties of sublimate residues are of considerable interest in studies of the thermal modeling of Martian surfaces (Cutts et al, 1979; Fanale and Salvail, 1984). To understand these properties, a series of low temperature vacuum experiments was run during which dirty ices that might be expected to be found in Martian polar caps were made and then freeze-dried. In addition to using particulate material of appropriate grain size and mineralogy, particle nucleated ices were simulated by dispersing the particulates in the ice so that they did not contact one another.

Vacuum sublimation of the ice out of a solid dispersion (1:1000) of submicron montmorillonite clay particles (or quartz glass smoke, "Cabosil" particles) in water ice has produced a low density (0.001 g/cm^3) filamentary sublimate residue. These constructs, as seen in SEM micrographs, are formed of long network chains of the clay particles. The particle bonding forces are strong and produce a mechanically tough and resilient low density material. Lumps of the material will adhere to one another with forces approaching the original tensile strength. The material is porous and will allow vapors to diffuse through it, but the thermal conductivity and the visible light transmissivity are very low. These three features dramatically increase the time it takes to sublime away the ice because the incoming radiant and conducted heat is carried away by the out-flowing water vapor (Scheidegger, 1974). The vapor probably leaves the surface at nearly the temperature of the outer surface.

The experimental demonstration that a credible Martian "sand" may be formed from dust-bearing ice provides a possible source of material for some of the observed Martian aeolian landforms. Aggregates of fine particles have been suggested to explain at least some of the circumpolar dune fields (Thomas, 1982), with the polar deposits providing the material. But Thomas doubted that the particles would have enough strength to survive the saltation distances involved and argued that the dark color of the dunes indicates a

dust and a source other than the poles. For the "sand" to be credible it should be of low density and be mechanically soft so that it would produce little aeolian erosion of geologic features even over billions of years (Arvidson et al, 1979). Yet the "sand" must also be able to survive transportation over hundreds of kilometers without disintegrating. Its color must be that of the relatively dark circumpolar dunes and intra-crater dunes found on Mars (Thomas, 1984; Tsoar et al, 1979).

If, as we observe in our experiments, a light-weight fluffy rind is formed on the polar caps, it could provide material easily entrainable by Martian winds, which generally blow equatorward from the poles (Thomas, 1984; Tsoar et al, 1979). These winds would peel the fluffy rind from the surface of the sublimating summer polar caps and from the equatorward slopes of the polar troughs. These pieces of material would then be rolled into lumps (of high sail area/mass ratio) by the wind. They could form dune structures because they are hydraulically equivalent to sand particles.

To experimentally demonstrate that the filamentary sublimate residue could survive the saltation stresses induced by transportation for hundreds of kilometers, two apparatus were constructed. A Mars environment tumbling drum that can make several lumps of sublimate residue saltate "gravitationally" for long distances was used to demonstrate their strength. The tumbling drum is a glass jar that is coated with a thin coating of montmorillonite clay to simulate a surface composed of compacted sublimate residue. The lumps both roll and slide as the drum rotates. A rotary wind tunnel that can also cause the lumps to saltate for long distances was also used. In this apparatus the rotating fan blades produce a circumferential wind in the bowl that causes the lumps to saltate around continuously. The actual distance traveled by the lumps is difficult to determine in this apparatus. These devices were used in a simulated Martian atmosphere to test the durability of the lumps of sublimate residue. The lumps in both cases were capable of surviving for many tens of kilometers without any evidence of deterioration. Another observation was that the larger lumps would cannibalize the smaller lumps after a few hours of tumbling. Once the larger lumps (.5 to 1 cm) had incorporated the smaller lumps they would not aggregate further.

A major problem with any proposal of pole-derived dust aggregates as the material of circumpolar dunes is that these deposits appear to be darker than any polar source areas. However, data are lacking on the color and precise photometric properties of these deposits. Our experiments demonstrate that aggregates capable of being saltated for great distances can be produced from the sublimation residue of reasonable analogues of the polar deposit material.

REFERENCES

Arvidson, R., Guinnes, E., and Lee, S., Differential aeolian
    redistribution rates on Mars. Nature, Vol. 278, 5 April
    1979, pp. 533-535.

Cutts, James A., Blasius, Karl R., and Roberts, W. James,
    Evolution of Martian polar landscapes: Interplay of long-term
    variations in perennial ice cover and dust storm intensity.
    J. Geophys. Res., Vol. 84, No. 86, 1979, pp. 2975-2994.

Fanale, F. P., and Salvail, J. R., An idealized short period
    comet model: Surface insolation, H_2O flux, dust flux and
    mantle evolution.   Submitted to Icarus, Aug. 1984.

Scheidegger, A. E., The Physics of Flow through Porous
    Medica, 3rd ed., Univ. Toronto Press, p. 243-245, 1974.

Thomas, Peter, Present wind activity on Mars: Relation to
    large latitudinally zoned sediment deposits. J. Geophys.
    Res., Vol. 87, No. B12, 1982, pp. 9999-10008.

Thomas, Peter, Martian intracrater slotches: Occurrence,
    morphology, and colors. Icarus, Vol. 57, 1984, pp. 205-227.

Tsoar, Haim, Greeley, Ronald, and Peterfreund, Alan R., Mars:
    The north polar sand sea and related wind patterns. J.
    Geophys. Res., Vol. 84, No. B14, 1979, pp. 8167-8181.

POLAR WANDERING ON MARS AND THE DISTRIBUTION OF WATER-ICE THROUGH
TIME. Peter H. Schultz, Department of Geological Sciences, Brown
University, Providence, RI 02912.

Polar wandering (the geographic migration of the pole with
respect to a fixed spin axis) was a popular concept for explaining the
record of temperate-equatorial fossils in presently polar conditions
on the Earth. Although the well-documented evidence for plate
tectonics lessened the relevance of "true" polar wandering on the
Earth over the short term, the theoretical basis for expecting this
process on a planet remains (1, 2). A planet in near-isostatic
equilibrium would be particularly susceptible to polar wandering if a
redistribution of mass occurred over a sufficiently short-time
interval (formation of an impact basin, lava flooding, mantle
overturn, etc.). Although it has been argued that the lithosphere
presently may be too rigid to permit polar wandering (3), this result
at best reflects conditions relatively late in martian geologic
history. The extremely ancient surface record still preserved on Mars
raises the possibility that the consequences of polar wandering may
not have been avoided (4, 5).

One important consequence of polar wandering may be localized
trapping of water-ice insulated within deposits analogous to the
layered deposits found at the present poles. As a first step, we have
generated paleo-climate zones based on the working hypothesis that the
thick-layered terrains presently near the equator represent remnants
of ancient polar locations, thereby providing approximate ages, paths,
and relative residence times of the poles with respect to each point
on Mars. The paleo-climate maps delineate regions that were largely
within cold climate zones over the last 3.5-4.0 billion years;
therefore, they may indicate localizations of water/ice-related
features and processes. The present-day climate of Mars can be
divided into three latitude-dependent zones: polar (70°-90°
latitude), glacial/periglacial (40°-70°) and temperate/equatorial
($<40^\circ$). The polar zone contains thick air-fall accumulations of
frozen water/ice and dust that rest unconformably on pre-existing
terrains. The glacial/periglacial zones collar the polar zones and
contain features and deposits reflecting alternating periods of
mantling and stripping perhaps in response to obliquity variations.
Water-ice is in equilibrium with the atmosphere in this zone (6),
thereby favoring water-ice deposits perhaps represented by an
assortment of present-day latitude-dependent features (7, 8, 9).

The pole-distance of each quarter-degree element on Mars was
determined throughout the sequence of polar wandering. Each position
of the pole was subjectively weighted from 1 to 4 on the basis of the
thickness of relict deposits between longitudes 150° and 270°. These
weights simulated relative residence times of the pole positions.
Additionally, a relative preservation weighting function was applied
such that features associated with more recent pole locations would be
more heavily weighted. The preservation function was assumed to
reflect an exponentially decreasing amount of erosion with time.
Thus, more recent cold-climate features rapidly erode initially but
erode less rapidly as feature size and erodability decrease.

The resulting paleo-climate maps of the polar zones obviously
will reflect the occurrence of the equatorial-layered terrains between

150° and 270° used as input. The usefulness of this exercise, however, is for tracing the surrounding glacial/periglacial zones and for examining both zones in the opposite hemisphere. The plausibility of the scenario is tested by comparing such zones with the distribution of features commonly found in current polar and glacial/periglacial regions on Mars (Figures 1 and 2). Figure 1 shows the occurrence of: zones historically under polar conditions; polar-like remnants; areas once containing large reservoirs of water; location of ancient pole points inferred from the orientations and locations of grazing impacts (5); and regions of low thermal inertia (10). Inferred post-Tharsis polar zones generally correlate with processes and consequent features typical of the present-day polar regions. Such processes include the strikingly disparate erosion rates for unconformable deposit perhaps related to a relatively high content of interstitial ices. Inferred pre-Tharsis polar zones are heavily eroded near 200°W but correlate with the source regions of the circum-Chryse outflow channels in the opposite hemisphere. This contrast in expression may be understood by a marked change in the fate of volatiles as a function of time. Early in martian geologic history (but after the time when narrow valley networks were formed) polar-trapped volatiles were incorporated in the underlying mega-regolith due to basal melting controlled by boundary conditions of the internal thermal gradient and the external atmospheric temperature. Igneous intrusions associated with Tharsis subsequently released these locally trapped reservoirs. In more recent times, the slow release of volatiles was primarily through sublimation and diffusion to the atmosphere. The relatively recent outflows, however, in Amazonis (11), the Mangala Vallis system (12), and the outflow channels/sources comprising Medusa Fossae all may be related to volatile reservoirs trapped in relict polar-layered terrains. Here it appears that outflow channels first carved through the equatorial layered terrains and eventually to the underlying terrains.

Figure 2 illustrates a similar comparison between regions historically within glacial/periglacial zones and the global distribution of inferred ice-related flows (7) and unconformable etched plateaus. It reveals that the longitudinal as well as latitudinal distribution of such features might be understood in terms of inactive, active, and recharged deposits.

The perspective provided by a polar wandering scenario suggests the following: first, over the last 3.5 billion years large quantities of water-ice stored in relict dust-laden, polar-layered terrains were both gradually released through diffusion/ablation and catastrophically released through basal melting. Second, prior to 3.5-3.8 billion years ago pole-trapped water-ice was locally absorbed/adsorbed in the megaregolith through basal melting and migration as well as trapping by ongoing surface processes such as impact basin ejecta emplacement and flood basalts.

(1) Goldreich P. and Toomre A. (1969) J. Geophys. Res. 74, p. 2555-2569. (2).Melosh H. J. (1980) Icarus, 44, p. 745-751. (3) Willemann R.J. and Dawson, C. Lunar and Plan. Sci. XVI, p. 912-913. (4) Schultz, P.H. and Lutz-Garihan A.B. (1981) In Abstracts for Third Internat. Colloq. on Mars, p. 229-231. (5) Schultz P.H. and Lutz-Garihan A.B. (1982) Proc. Lunar Planet. Sci. 13th in J. Geophys. Res., 87, p. 84-A96. (6) Fanale F. (1976) Icarus, 28, p. 179-202. (7) Squyres S.W. (1979) J. Geophys. Res., 84, p. 8087-8096. (8) Luchitta B.K. (1981) Icarus, 45, p. 264-303. (9) Rossbacher L.A. and Judsen S. (1981) Icarus, 45, p. 39-59. (10) Zimbelman J.R. and Kieffer H. (1979) J. Geophys. Res., 84, p. 8239-8251. (11) Moore H.J. (1982) NASA TM-85127, p. 213-214. (12) Masursky et al., (1977) J. Geophys. Res., 82, p. 4016-4038.
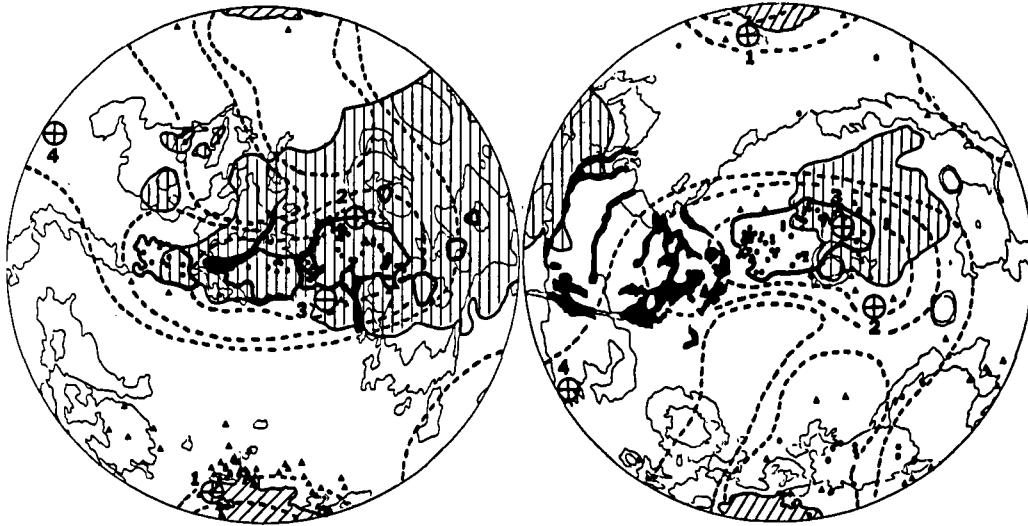
Figure 1. Comparison of regions subjected to polar paleo-climates (within 20° of pole) and selected features (Lambert Azimuthal projections centered at 180° and 0° longitudes, left and right respectively). Dashed lines indicate contours where polar features most likely would remain preserved. Dark boundaries indicate location of equatorial layered deposits. Polar-like features are represented by large pedestal craters (dots) and craters containing large unconformable deposits (triangles). The numerous but small (<5 km diameter) pedestal craters surrounding the present polar terrains (slanted hachures) are not shown. Chaotic terrains and major outflow channels are indicated by solid-filled areas. Vertical hachures indicate regions of low thermal inertias from (10). Circles with crosses correspond to possible pole positions determined from grazing impact craters (5) with 1 indicating the youngest position and 4 the oldest.
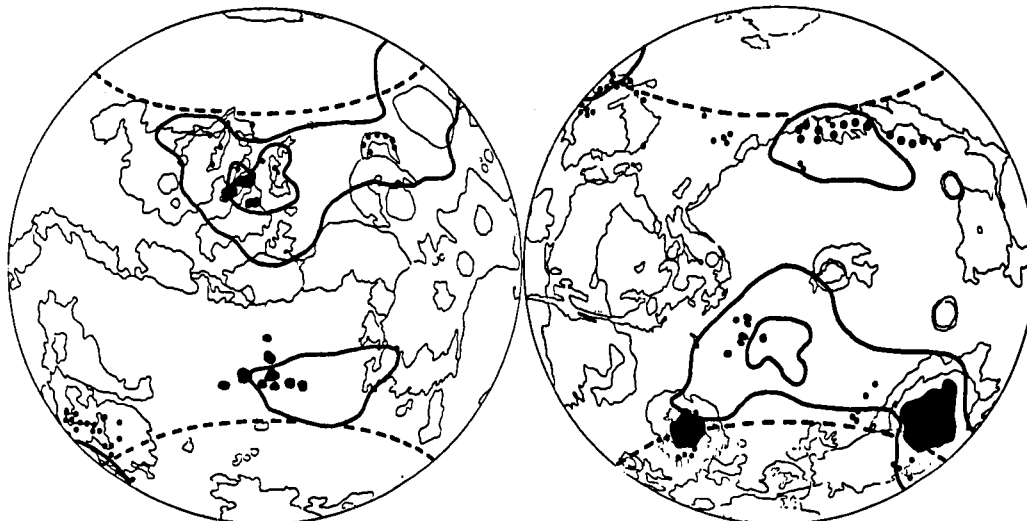

Figure 2. Comparison of regions subjected to glacial/periglacial climates (between 25° and 50° of poles) through time (solid contours) with the distribution of lobate debris aprons (dots) and unconformable etched terrains (solid-filled areas). Dashed lines indicate latitudes of ± 50° poleward which contain evidence for recent episodic mantling and stripping.

EROSION OF MARTIAN IMPACT BASINS AND THE CHANGING WATER CYCLE. Peter
H. Schultz, Department of Geological Sciences, Brown University,
Providence, RI 02912; John Rogers, American Petrofina Co., Houston,
TX 77002; Susan Haber, Hofstra University, Hempstead, NY 11550.

Pre-Viking views of Mars indicated that the number of large
(>300 km) impact basins was deficient relative to the Moon and
Mercury, but more recent studies indicate that this apparent
deficiency is largely an expression of very active but ancient
gradational processes (1,2,3). The purpose of this contribution is to
review the changing style of erosional processes on Mars as revealed
by the preservation of impact basins. A significant change in both
the rate and style of inferred water erosion apparently occurred
either prior to or contemporary with the formation of the Argyre
basin. Although Argyre is smaller than other impact basins on Mars,
the timing of this event may have been critical for subsequent
climates.

Pre-Argyre: Prior to the formation of the Argyre basin, large craters
and basins were extensively dissected by narrow valley networks as
described in numerous studies (4,5,6). The Isidis and Ladon basins
permit comparing the style and formation rate of run-off channels,
narrow-valley networks, and massif erosion. Crater statistics (3)
indicate that Isidis and Hellas basins were nearly contemporary, but
the present equatorial position of Isidis and high-resolution image
coverage provide a basis for more detailed study. Ladon is slightly
older than Isidis, but crater statistical uncertainty, evidence for
re-surfacing, and relatively small size (<1000 km) prevent resolving
the pre-Argyre record. The Isidis basin contains a complex system of
narrow-valley networks, catchment basins, and run-off channels. About
58% of the non-plains regions in MC-21NE are cut by narrow-valley
networks within the boundary scarp. One of the largest network
densities occurs in basal massif aprons where the system typically
merges with major channels that weave between basin massifs. The
larger channels commonly become wider, shallower, and more sinuous in
intermassif plains. Channel drainage densities (channel-length/area)
vary as a function of resolution and selected areas (Fig. 1). Channel
densities for non-plains areas are as high as $0.1km/km^2$, and the
channel density for intermassif drainage basins is typically
$0.06km/km^2$. High-resolution images reveal drainage densities as high
as $0.18km/km^2$. These values are slightly higher than those obtained
for Ladon. The drainage pattern in Isidis suggests an integrated
system of run-off that varies in expression. Intermassif regions
contain shallow, wide, and sinuous channels in floodplain-like valleys
that approach a mature pattern, whereas hummocky inter-ring zones have
parallel or convergent/divergent systems. It is clear that we are
seeing only a partial record of drainage patterns owing to subsequent
erosion and deposition. Narrow valleys 1-2 km across have been
preserved since the basin-forming epochs. Features smaller than 1 km
on the Moon have been destroyed over approximately the same time
interval.

Basins much older than Isidis are nearly destroyed by both
deposition and erosion. Such features are presently delineated by
drainage-pattern directions, structural patterns, and relict massifs.
On the Earth, even arid regions have ephemeral erosional processes

high enough that mountain relief can be removed in tens of millions of years. We cannot yet firmly establish a comparable rate for pre-Argyre Mars but rates were apparently high enough for planation within hundreds of millions of years. Thus the pre-Argyre epoch was characterized -- at least at Isidis -- by integrated drainage systems and massif erosion by valley dissection.

Post-Argyre: Narrow-valley networks on the ejecta facies of Argyre are relatively rare and are even rarer within the boundary scarp analogous to the Isidis boundary scarp. In contrast with the integrated system of Isidis, narrow-valleys emerge from scarps (north and northwest) or diverge from central locations (west). The number of craters larger than 40 km and 60 km on Argyre is about half that of Isidis (3). Although large run-off channels do occur, the narrow-valley networks are missing. In Figure 1, the crater-statistical slopes have been extrapolated back to 10 km for comparison with other, but smaller, post-Argyre craters. The density of narrow valleys on the ejecta facies of such craters is comparable to that on Argyre even though this superposed-crater age is much younger. The style of the narrow valleys is also different: they are typically singular (without tributaries).

Discussion and Summary: Although the drainage density of pre-Argyre narrow-valley networks does not approach the typical terrestrial value, this disparity may reflect selective preservation of the less mature and deeper (incised) systems associated with the formation of contemporary smaller craters or the re-use of buried, more ancient major run-off courses. The drainage density and style of post-Argyre narrow valleys indicate a major change in the available quantity of (assumed) water and the release primarily as springs. Much later basin-controlled release of large quantities of inferred water (catastrophic outflows) reveals an additional role of impact basins as reservoirs, but such release appears to require additional igneous/tectonic activity (1). The drastic change between pre-Argyre and post-Argyre drainage patterns and the style of massif erosion suggests that the Argyre impact permanently altered the martian climate and water cycle from an active lithosphere-atmosphere exchange to an inactive exchange primarily controlled by lithospheric conditions (local geotherm). The sensitivity of the martian atmosphere to this event and not to the earlier onslaught of impacts remains an enigma. Perhaps the outgassing of Mars was essentially complete and it could not recover from effects of the relatively late Argyre impact.

(1) Schultz P.H. et al., (1982) J. Geophys. Res., 87, p. 9803-9820.
(2) Schultz P.H. and Rogers J. (1982) In Abstracts for Conf. on Planetary Volatiles, p. 155-156, Lunar and Planetary Institute, Houston. (3) Schultz P.H. and Rogers J. (1984) Lunar Planet. Sci. XV, p. 734-735. (4) Pieri D.C. (1980) Science, 210, p. 895-897. (5) Carr M. and Clow G.D. (1981) Icarus, 48, p. 91-117. (6) Baker V. P. and Partridge J.B. (1984) Lunar Planet. Sci. Conf. XV, p. 323-24.
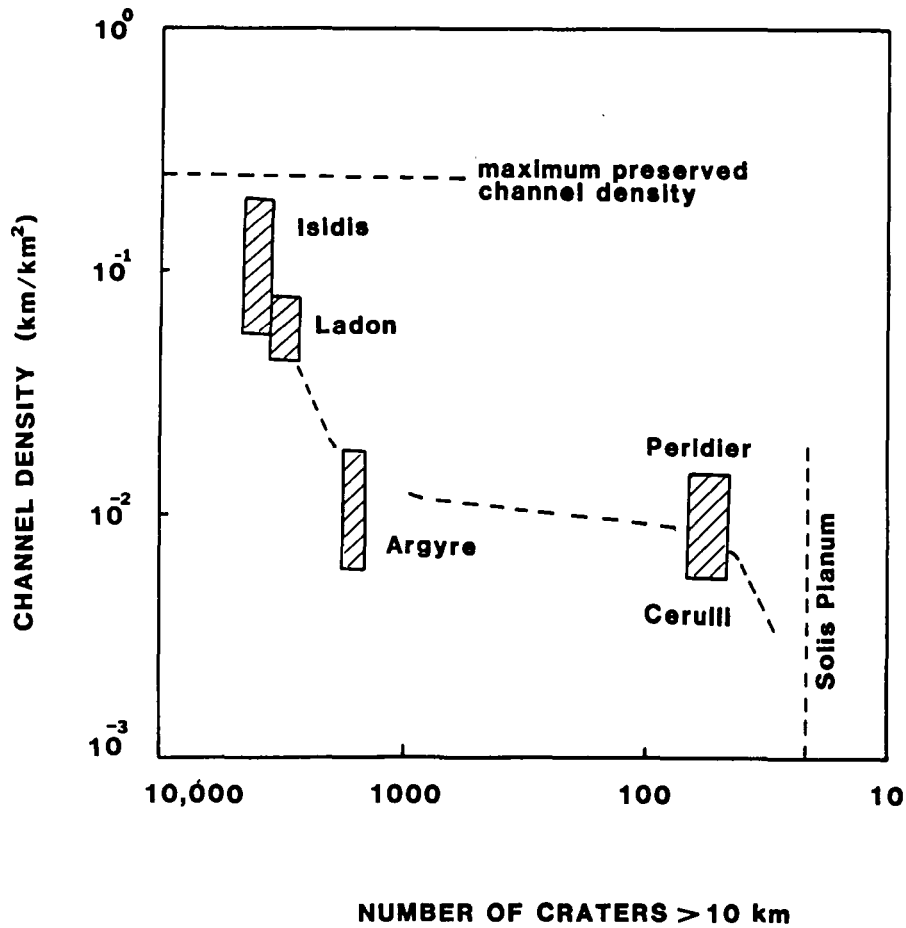
Figure 1. Channel densities (length/area) on impact basins and craters as a function of time. The approximate range in observed channel densities on relevant units is indicated by the height of each box, whereas the approximate uncertainty in crater-age is indicated by the width of each box. Channel densities do not include valleys on the scarps or walls of craters.

Direct Detection of Minor Clay Mineralogy on Mars

Robert B. Singer, Pamela D. Owensby (Planetary Geosciences, HIG, U. Hawaii), and Roger N. Clark (USGS Geophysics, Denver)

A magnesian clay-type mineral or other hydroxylated magnesian phase has recently been detected in the martian regolith from Earthbased spectrophotometry. However, the observed hydroxylated mineral is either a minor soil component or is not totally crystalline.

Near-IR (0.65-$2.55\mu m$) spectral observations of regions on Mars (~ 1000 km dia.) were obtained in April 1980 using the Mauna Kea 2.2m telescope. Some of these data are shown on the right side of Figure 1, with error bars, for the 1.7- to 2.55-μm spectral range. The deep composite absorption near $2\mu m$ is due to Mars atmospheric CO_2. The spectral features under discussion are weak but definite absorption bands centered near 2.35 μm. The 2.15- to 2.55-μm spectral region is free from other potentially complicating absorptions, such as from adsorbed, solid, or gaseous H_2O and CO_2. Extreme care was taken in data reduction to insure the validity of these weak absorptions, which have band depths less than about 3%. The absorption band positions and widths are like those produced by combined OH stretch and Mg-OH lattice modes and are diagnostic of minerals with structural OH such as clays and amphiboles (1,2).

Laboratory spectra of some representative clay minerals, as well as a palagonite and carbonate, are also shown in Figure 1 (left side). The absorption bands near $1.9\mu m$ are in all cases due to molecular H_2O adsorbed or included in various sites. For the clays and the palagonite the reflectance dropoff towards $2.55\mu m$ is due to the broad wing of intense water fundamentals around $3\mu m$. The bands near $2.2\mu m$ in both kaolinite and montmorillonite are highly diagnostic of the structural Al-OH bonds in these dioctohedral clays. Nontronite, an Fe^{3+} analog of montmorillonite, has a prominant Fe-OH absorption just shortward of $2.3\mu m$. Magnesian (trioctohedral) clay minerals, as well as some Mg-amphiboles, display similar bands generally centered in the 2.3-2.35-μm region (1,2). The palagonite spectrum shown is for a poorly crystallized altered basaltic glass from Mauna Kea, apparently not totally amorphous as are most other Mauna Kea palagonites (3). Note the weak Al-OH band near about $2.25\mu m$. Carbonates also have a band near $2.35\mu m$, due to CO_3 overtones, but accompanied by a stronger overtone absorption near $2.55\mu m$ (4,2), the first half of which is apparent as a very steep reflectance drop longward of $2.4\mu m$ in the example at the bottom of Figure 1.

Based on the wavelength position of the bands observed for Mars, one (or more) hydroxylated magnesian mineral is indicated. Likely candidates include the clay minerals serpentine, talc, hectorite, and saponite, and possibly Mg-amphiboles such as anthophyllite or tremolite. Further study is underway to more specifically identify the responsible phase(s). There is no evidence for aluminous hydroxylated minerals such as kaolinite and montmorillonite. Carbonates also appear ruled out as the source of the observed 2.35-μm band since there is no evidence of the expected stronger absorption near $2.55\mu m$. The general flatness of the Mars data longward of $\sim 2.2\mu m$ also indicates a high degree of dessication of the observed weathered materials.

High-albedo regions such as Elysium, Utopia, and Arabia have relatively strong bands near $2.35\mu m$, as would be expected for weathered soils. Low-albedo regions such as Iapygia show weaker but distinct bands, consistent with moderate coatings, streaks, and splotches of bright weathered soil or dust mixed with less altered crustal materials. The deepest band observed was for Hellas basin, which contained some dust clouds

at that time (5). This implies that aerosol suspension enhances the depth of this absorption, which is reasonable from optical considerations. In all areas observed, the 2.35-μm absorption is at least 3 times weaker than would be expected if well-crystallized clay minerals made up the bulk of bright soils on Mars. Two possible explanations are: 1) crystalline clays are a minority phase mixed with other materials (e.g. palagonites), or 2) the bright soils are more homogeneous but not fully crystallized into clay minerals. Further work is required to investigate these alternatives and place a quantitative upper limit on crystalline clay content for the observed regions.

Whichever of these possibilities is more correct, formation of the clay or clay-like soil component almost certainly required somewhat more water and higher temperatures than presently available on the martian surface. This may constitute additional evidence for significant climate change in martian history. It is also feasible, however, that the necessary conditions were provided within low-temperature hydrothermal systems associated with volcanism (e.g. 6). The magnesian composition determined here is fully consistent with the low Al/Mg ratio measured at both Viking landing sites and with the basaltic spectral characteristics observed in martian low-albedo regions. Serpentine, for example, is a common alteration product of pyroxene and olivine on Earth. This evidence strongly supports suggestions for a predominantly mafic or ultramafic martian crust.

(1) Hunt, G.R. and J.W. Salisbury, Visible and near-infrared spectra of minerals and rocks: I. Silicate minerals, *Mod. Geol. 1*, 1970, 283-300.

(2) Hunt, G.R., Spectral signatures of particulate minerals in the visible and near-infrared, *Geophysics 42*, 1977, 501-513.

(3) Singer, R.B., Spectral evidence for the mineralogy of high-albedo soils and dust on Mars, *J. Geophys. Res. 87*, 1982, 10159-10168.

(4) Hunt, G.R. and J.W. Salisbury, Visible and near-infrared spectra of minerals and rocks: II. Carbonates, *Mod. Geol. 2*, 1971, 23-30.

(5) L. Martin, Lowell Observatory, personal communication.

(6) Allen, C.C., J.L. Gooding, M. Jercinovic, and K. Keil, Altered basaltic glass: A terrestrial analog to the soil of Mars, *Icarus 45*, 1981, 347-369.

Figure 1 (next page). Left Side: representative laboratory reflectance spectra for a number of clay minerals, a poorly crystalline palagonite (altered basaltic glass) and a crushed limestone. Right Side: spectral reflectance for a number of surface regions on Mars observed in April, 1980. The Mars data consist of multiple observations averaged prior to any scaling or normalization, and include error bars. These data are presented relative to the standard star β Virgo; eventual calibration to the sun or a solar analog will slightly change the overall slopes but not the spectral details. All data, laboratory and telescopic, have been scaled for this figure to allow more direct comparisons of band depths.

Singer, R.B., _et al._

Scaled Reflectance (left panel, top to bottom): Kaolinite, Montmorillonite, Nontronite, Palagonite, Limestone

Scaled Reflectance (right panel, top to bottom): Utopia, Elysium, Arabia, Hellas, Iapygia — **1980 Mars**

Wavelength (μm)   Wavelength (μm)
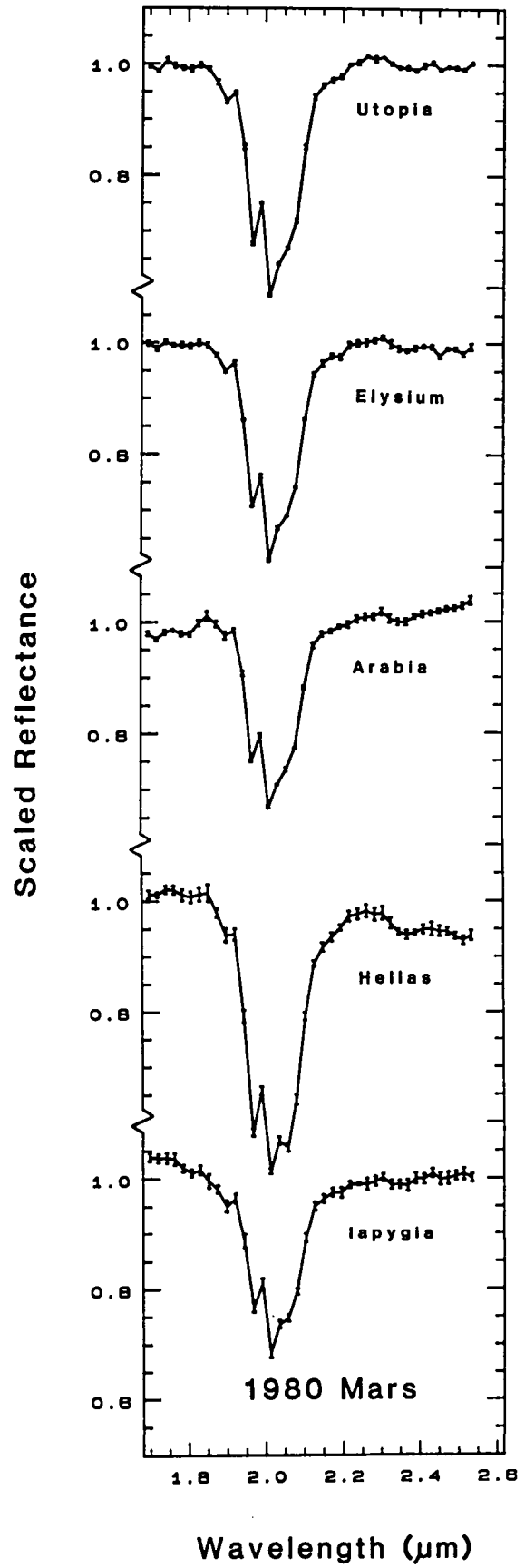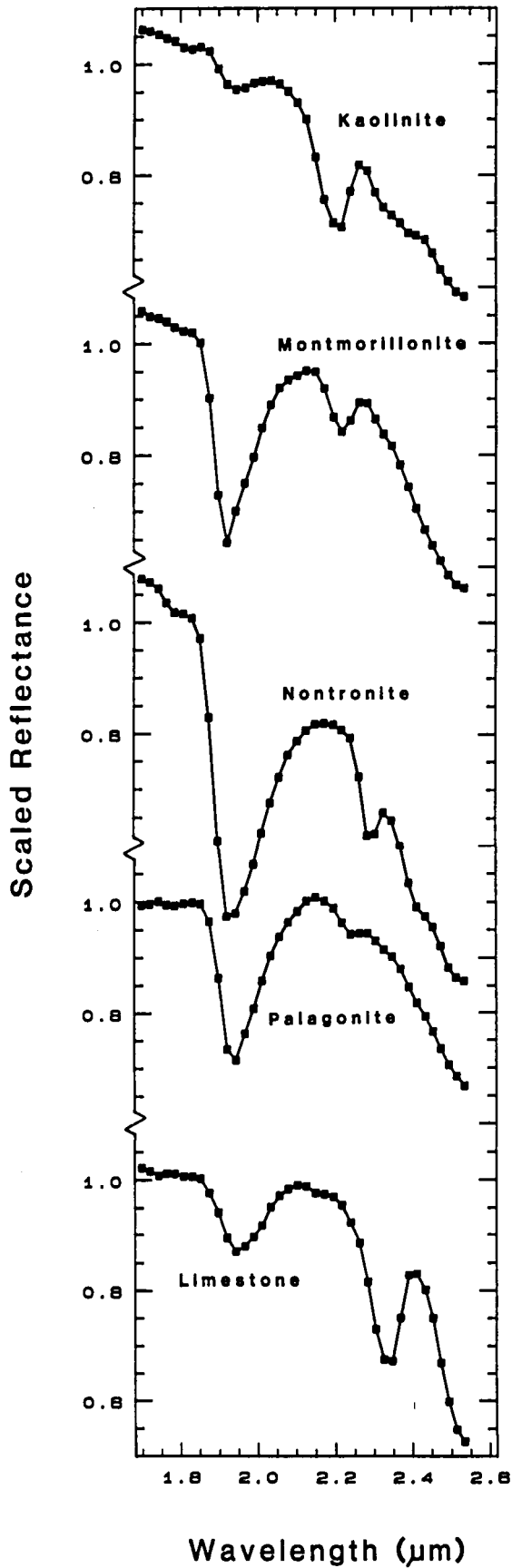
THE DISTRIBUTION OF GROUND ICE FEATURES ON MARS. S.W. Squyres, Space Science Division, NASA Ames Research Center, Moffett Field, CA 94035, and M.H. Carr, U.S. Geological Survey, Menlo Park, CA 94025.

A variety of landforms on Mars show evidence for the former presence of ground ice, including fretted terrain, chaotic terrain, rampart craters, valley systems, outflow channels, and perhaps patterned ground. None of these provide conclusive evidence for the *present* existence of ground ice. However, a variety of other landforms apparently owe their morphology to the presence of ground ice in sufficient quantities to alter the rheology of the surface materials. With large enough amounts of ice present in a matrix of silicate particles, creep deformation of the ice can cause the entire mass of material to undergo quasi-viscous flow. In order to learn more about the present distribution of ground ice on Mars, we have mapped the global distribution of such features using high resolution Viking Orbiter imagery.

Three types of features were mapped: *lobate debris aprons, concentric crater fill,* and *terrain softening.* Lobate debris aprons are thick accumulations of debris at the bases of escarpments. They have distinct convex-upward topographic profiles indicating creep deformation throughout the entire thickness of the material *(1)*. They commonly show surface lineations parallel to flow (probably caused by inhomogeneities in the source region), and compressional ridges where the flow is obstructed. Their morphology is very similar to that of terrestrial rock glaciers. Concentric crater fill is apparently the same material confined within impact craters. Inward flow of the material gives rise to radial compressive stresses that produce crater fill with a pattern of concentric ridges. Terrain softening is a distinctive style of landform degradation apparent only in high resolution orbital images. It is revealed by extreme rounding of features that are elsewhere sharp (*e.g.,* crater rims), and marked convexity of slopes that are elsewhere straight or concave (*e.g.* crater walls, erosional scarps). Lobate debris aprons and concentric crater fill probably require substantial amounts of interstitial ice. Terrain softening, because it preserves the large-scale components of the original topography, probably requires less ice.

Where these deformational landforms are observed, we infer them to indicate recent or present existence of large amounts of ground ice. This inference is based on the following reasoning: (1) Ice must be present in sufficient quantities that its removal would have caused collapse, which is generally not observed (ice contents upwards of $\sim$30% by volume are typically required for creep deformation in rock glaciers on Earth). (2) Removal of the ice would have caused a "stiffening" of the material, so that subsequent mass wasting and impact erosion would not have allowed the rounded morphology to persist. (3) Many of the lobate debris aprons and deposits of concentric crater fill are devoid of impact craters, indicating that flow sufficient to disrupt the surface morphology has taken place recently. Mapping of these features may therefore provide some of the most unambiguous evidence available for the presence of ground ice deep in the martian regolith.

Our mapping technique has been planned to facilitate quantitative statistical analysis of the data. We have examined all of the $\sim$24,000 Viking orbiter images taken within 5000 km of the surface. The resolution of the images used varies from $\sim$125 to 10 m per pixel. Lower resolution images were also used where applicable (for detection of lobate debris aprons and concentric crater fill only). The surface of the planet was divided into a grid of $1° \times 1°$ latitude-longitude boxes for digitization of the results. For each image observed, the presence or absence of the features under consideration was recorded in the latitude-longitude box given by the center point of the image. Because many images cover an area larger than $1° \times 1°$ in size, the data were subjected to a 3×3 low-pass boxcar filter for smoothing. The smoothed data were then transformed to a Mercator projection and displayed in color with

Squyres, S.W., and Carr, M.H.

each type of feature mapped into one color channel in a standard three-color (red/green/blue) display.

The most striking characteristic of the distribution is the nearly complete absence of all three classes of features from the equatorial latitudes. Virtually no examples of lobate debris aprons, concentric crater fill, or terrain softening are found equatorward of 30° latitude in either hemisphere. In the northern hemisphere, lobate debris aprons are most common in Tempe Fossae, Mareotis Fossae, the Phlegra Montes, and particularly in the fretted terrain between longitudes 280° and 0°. Concentric crater fill is also found in these areas, but is most common in Utopia Planitia. Terrain softening is most common in the portion of the cratered highlands lying between the fretted terrain and 30° north latitude. In the southern hemisphere, lobate debris aprons are common in the massifs surrounding the Argyre and Hellas Basins. Concentric crater fill is observed primarily in the area east of Hellas. Terrain softening was observed in virtually all the high resolution images south of −30° latitude.

It has been argued that the primary source of the ice in lobate debris aprons and concentric crater fill is either deposition from the atmosphere (1), or the highland material from which the debris is mass-wasted (2). One argument against the primary source being in the highlands is that the highland material clearly has a much stiffer rheology than the flows. The latitudinal distribution is consistent with an atmospheric origin. Stronger support comes from the observation of a lobate debris apron at the base of an escarpment on the volcano Hecates Tholus at 32° N, 211° W, where abundant ground ice is unlikely. We therefore conclude that the ice content of the materials from which lobate debris aprons arise is generally insufficient to account for their morphology, and that the ice content of these features is enhanced significantly by condensation from the atmosphere.

We have found that virtually all observed regions of old, heavily cratered terrain lying at latitudes poleward of ±30° have undergone terrain softening. This distribution may mean that the deep regolith equatorward of ±30° has been largely devolatilized, while that at higher latitudes still retains most of its original complement of outgassed H_2O. The scale of topographic deformation observed suggests that this high ice content may extend to depths of 1 km or more. The amount of ice present in this resevoir is difficult to estimate, but it may form the largest present resevoir of H_2O on Mars.

(1) Squyres, S.W. (1978). *Icarus* **34**, 600-613.

(2) Lucchitta, B.K. (1983). *Lunar Planet. Sci. XIV*, 446-447.

VOLATILES ON MARS. H. Wänke and G. Dreibus, Max-Planck-Institut für Chemie, Saarstr.23, D-6500 Mainz, F.R.Germany.

Rare gases represent without any doubt the most volatile group of elements. The Viking data showed that per gram of the planet's mass the Martian atmosphere contains only $1.6 \times 10^{-10} cm^3/g$ ^{36}Ar. The ^{36}Ar concentrations observed in C and E 4-chondrites range between $3 \times 10^{-7} cm^3/g$ and $8 \times 10^{-7} cm^3/g$, even ordinary chondrites contain as much as $2 \times 10^{-8} cm^3/g$ ^{36}Ar. Hence, in the Martian atmosphere we have a factor of 100 less ^{36}Ar than in any class of unfractionated meteorites. A huge gas loss from the primitive atmosphere of Mars seems the almost inevitable conclusion. There is also no doubt that accretion is the most effective degassing stage in the evolution of planets (1,2).

The following estimates on the volatile content of Mars are based on the composition of SNC-meteorites. The SNC-meteorites (4 shergottites, 3 nakhlites and Chassigny) represent a small group of differentiated meteorites distinct from all other meteorites. Within the last five years a number of observations were made which pointed towards Mars as the parent body of SNC-meteorites (Shergotty parent body = SPB), their low crystallization ages being the most striking one.(3,4). The recent discovery of trapped Martian atmosphere with its characteristic $^{40}Ar/^{36}Ar$, $^{40}Ar/^{14}N$, $^{14}N/^{15}N$, $^{129}Xe/^{132}Xe$ ratios in the shergottite EETA 79001 (5,6), proves with almost certainty that Mars is indeed the parent body of the SNC-meteorites, although up till today there is no generally accepted model for the dynamical problems involved (7).

We have previously used the composition of the SNC-meteorites to estimate the bulk composition of Mars (8,9). From its bulk composition we have concluded that like the Earth, also Mars accreted from two compositionally very different components. Component A: Highly reduced and free of elements as volatile and more volatile than Na but containing all other elements in C 1 abundance ratios. Iron and all siderophile elements as metals including W and in part also Cr, Mn, V, and even Si. Component B: Fully oxidized. Closely matching C 1-chondrites. Iron, Ni, Co, and almost all siderophiles as oxides. Moderately and probably also volatile elements in C 1 abundances. Furthermore we concluded that contrary to the Earth (10), Mars accreted homogeneously (9).
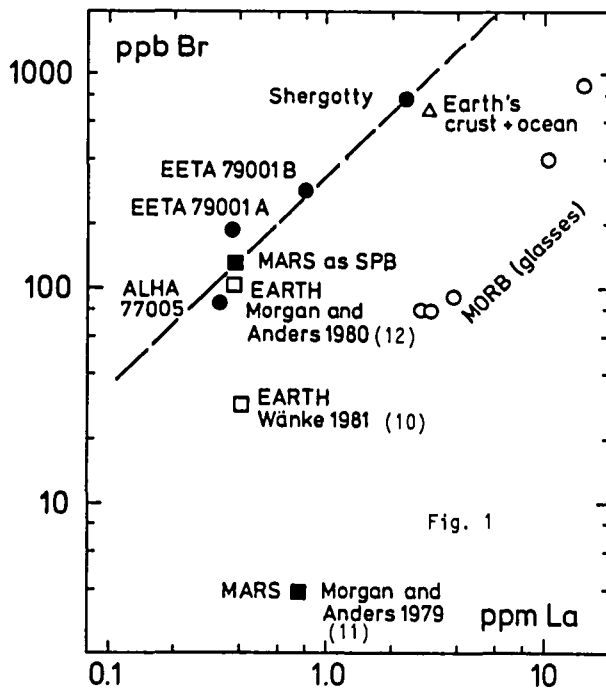
The Br-La correlation observed in shergottites (Fig. 1) couples Br to a refractory element. For Cl and I we assume C 1 ratios to Br. The obtained concentrations of Cl, Br, and I exceed those in the Earth by about a factor of 4. The abundances of Tl and In also given in the Table are based on the Tl/Br and In/Ga ratios (13). As we have previously noted for Cu, Ni, Co, and Zn the abundances of Tl and In in the Martian mantle seem to be lowered because of their segregation as sulfides together with FeS (9).

As illustrated in Fig. 2 normalized to Si and C 1, the composition of the Martian mantle corresponds to a

Fig. 1

Mars as SPB Mantle + crust		
MgO	%	30.2
Al$_2$O$_3$		3.02
SiO$_2$		44.4
CaO		2.45
TiO$_2$		0.14
FeO		17.9
Na$_2$O		0.50
P$_2$O$_5$		0.16
Cr$_2$O$_3$		0.76
MnO		0.46
K	ppm	315
Rb		1.12
Zn		74
Ga		6.6
In	ppb	14
Tl		3.6
Cl	ppm	44
Br	ppb	165
I		37
La		430
Th		56
U		16
Core		
Fe	%	77.8
Ni		7.6
Co		0.36
S		14.24
Core mass		21.7%

mixture of about 65 % component A and 35 % component B. However, an abundance of 35 % for component B as estimated from the mean abundances of Fe, Na, Ga, P, K, F, and Rb is probably somewhat too high. As we shall see later on, part of the FeO comes from the oxidation of metallic iron. The decrease in the abundance of the alkaline elements (Na = 0.38; K = 0.31, Rb = 0.28 and Cs = 0.20) may indicate either a small contribution of component A for the least volatile elements (Na,K) or a slight depletion of the most volatile ones (i.e. Rb and Cs) in component B. In the following we will use the abundance of K (i.e. 0.31) for the abundance of component B. The weight mixing ratio is somewhat difficult to deduce as we do not exactly know the concentration of H_2O in component B. The measured H_2O content in C 1-chondrite Orgueil is close to 20 %, however a considerable part of it is probably terrestrial water as well as H_2O produced from hydrocarbons during combustion while the true C 1 abundance of H_2O is only about 4.5 % (14). To find the composition of component B we devide the C 1 values (15) by 0.85, thus raising the K concentration from 517 to 608 ppm and H_2O from 4.5 to 5.3 %. The value of 315 ppm K (see Table) for the Martian mantle + crust corresponds to 247 ppm K in the whole planet. In this way we find for the weight portion of component B on Mars a value of 247/608 = 0.40 or 40 %.

For the amount of H_2O added to Mars during accretion we find a value of 2.1 % which may seem high but is not at all unreasonable. On reaction with metallic Fe it would produce 8.4 % FeO, while the bulk FeO concentration on Mars is 14.0%. However taking into account the probable presence of some metallic Si (in component A, as in E 4-chondrites), considerably less FeO would be produced as for example 1 % Si in component A would reduce 0.7 % H_2O. The actual conditions are more complicated as the presence of reduced Cr and Mn in component A and of carbon in component B has to be taken into account. In addition to H_2O oxygen is also added in form of SO_4^- and Fe_2O_3. However there can be no doubt that during homogeneous accretion practically all H_2O will be reduced to H_2. A very similar scenario was advocated for the Earth by Ringwood (16), who stated that reduction of H_2O to

Fig. 2
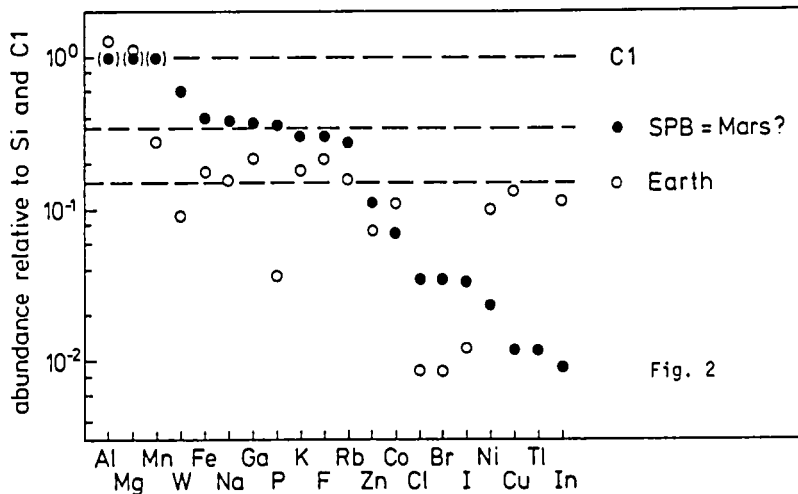
H_2 would mainly occur in the primitive atmosphere during infall of material of component A. The H_2 produced during accretion would continuously have "washed" other volatiles including rare gases and halogens back into space (16). Aside this hydrodynamic escape for mass independent gas loss, removal of the early atmosphere due to large impacts has also to be considered (16).

On Mars, because of the higher abundance of component B, its almost perfect <u>homogeneous</u> accretion and its by a factor of two smaller escape velocity, loss of the early atmosphere is greatly enhanced as compared to the Earth. Furthermore on Earth gases will dissolve in the magma ocean (17,18) and will be effectively carried into the mantle. This effect will be very much smaller on Mars as both the energy of accretion as the energy of core formation is only about 1/4 of that of the Earth.

Mars was meant to become a volatile-rich planet. In respect to halogens and many other volatiles it still is. Of the water originally added all except trace amounts was converted to H_2 which furthered the escape of the rare gases and some other gaseous species. Assuming a C 1 abundance of ^{36}Ar and 100 % release into the atmosphere we find for ^{36}Ar a depletion by factor of 1900. The true depletion factor could be even higher as C 1 chondrites may have also lost a large portion of their original primordial rare gas content.

In order to estimate the amount of water left on Mars after accretion we assume that all H_2O liberated during accretion was reduced by Fe and H_2 was lost. Thus, at the end of accretion the surface H_2O concentration is assumed to be zero. For the whole planet we found a Cl concentration of 34 ppm. Compared with 320 ppm Cl to be expected from component B we find a Cl depletion factor of 0.11. The solubility of HCl in basaltic melts exceeds that of H_2O by about a factor 200 (19), yielding an expected depletion factor for H_2O of 5.5×10^{-4}. With this factor and an amount of 2.1 % H_2O added during accretion we find a total of 11.5 ppm H_2O retained in the interior of the planet corresponding to 14.7 ppm H_2O in the mantle. Making the unrealistic assumption of a 100 % release, 11.5 ppm H_2O correspond to a water layer of 51 m covering the whole planet. Assuming a release factor of H_2O as low as that calculated for ^{40}Ar, i.e.=0.026, we should expect as lower limit a layer of only 1.32 m. Compared with such a small amount the addition of H_2O containing matter (comets and C chondrites), after the actual accretion stage should become dominant.

We do not have definite constraints about the amount of water left on Mars. However, we have good reasons to assume that this water was very salty. As mentioned above the halogen concentration on Mars exceeds that of the Earth by a factor of 4. During accretion Cl and the other halogens are liberated together with H_2O. On today's Earth most of the total water content is in the oceans which have an average NaCl concentration of 3.1 %. Hence, we have to expect that water on Mars was saturated with NaCl since the early days of the planet and had a freezing point of about -20°C. The very important depression of the freezing point of the Martian water was previously pointed out by Anders and Owen (20). In addition to NaCl also $MgSO_4$ and $MgCO_3$ (21) are expected to be present in the Martian water. On its evaporation and freezing huge salt deposits should have formed.

Ref.:(1) Arrhenius, G. et al. (1974) The Sea Vol. 5 (ed. E. Goldberg), Wiley, 839. (2) Lange, M. A. and Ahrens, T.J. (1983) LPS-XV, 419. (3) Wasson, J.T. and Wetherill, G.W. (1979) Asteroids (ed. T. Gehrels) Univ. Arizona, Tucson, 926. (4) Wood, C.A. and Ashwal, L.D. (1981) PLPSC 12B, GCA, Suppl. 16, 1359. (5) Bogard, D.D. and Johnson, P. (1983) Science 221, 651. (6) Becker, R.H. and Pepin, R.O. (1983) Meteoritics 18, 264. (7) Wetherill, G.W. (1984) Meteoritics 19, 1. (8) Burghele, A. et al. (1983) LPS-XIV, 80, (9) Dreibus, G. and Wänke, H. (1984) Proc. 27th Intern. Geol. Con., Vol. 11, 1, VNU Science Press. (10) Wänke, H. (1981) Phil. Trans. R. Soc. Lond. A 303, 287. (11) Morgan, J.W. and Anders, E. (1979) GCA 43, 1601. (12) Morgan, J.W.and Anders, E. (1980) Proc. Natl. Acad. Sci. USA, Vol. 77, No. 12, 6973. (13) Smith, M.R. et al. (1984) PLPSC 14th, JGR. 89, B612. (14) Kaplan, I.R. (1971) Handbook of Elemental Abundances in Meteorites (ed. B. Mason), 21, Gordon. (15) Palme, H. et al. (1981) Landoldt-Börnstein Vol. 2 Astron. and Astrophys. (eds. K. Schaifers, H.H. Voigt), 257, Springer. (16) Ringwood, A.E. (1979) Origin of the Earth and Moon, Springer. (17) Kaula, W.M. (1979) JGR. 84, 999. (18) Matsui, T. and Abe,Y. (1982) LPS-XV, 517. (19) Anderson, A.T. (1975) Rev. Geophys. Space Phys. 13, 37. (20) Anders, E. and Owen, T. (1977) Science 198, 453. (21) Baird A.K. et al. (1976) Science 194, 1288.

LOSS OF VOLATILES FROM MARS AS THE RESULT OF ENERGETIC IMPACTS; Hampton Watkins and John S. Lewis, Department of Planetary Sciences, University of Arizona, Tucson, Arizona 85721

The loss of volatiles from Mars as the result of numerous energetic cometary and asteroidal impacts has been studied. The loss of water by such a mechanism may, in part, account for the observed paucity of water on the present surface of Mars.

Two model Martian atmospheres have been employed, the present atmosphere and a massive, ancient atmosphere. Two simple impact models were developed. The first model assumed that a portion of the impact momentum was simply reflected back from the impact point. The second model assumed that a fraction of the energy of the impact was retained in the vaporized impactor and surrounding material and that this gas was allowed to expand (nearly) freely into the surrounding atmosphere at supersonic velocities. Though these crude treatments of impacts require significant refinement (and such work is currently underway), they yield results of atmospheric blowoff that generally agree within a factor of 3.

As a result of the vaporization of material at the impact site, and the subsequent rapid expansion of this vaporized material, a portion of the impactor and the surrounding planetary material will be driven away from the impact site at high velocity. This mass, if substantially undecelerated by the drag of the surrounding atmosphere, will be ejected and lost from the planet. Of course, only a portion of the mass ejected from the site of impact (of even the most energetic impacts) will be lost from the planet; the remainder of the mass will be retained.

The masses of atmosphere employed in the models of the Martian atmosphere are displayed in Table I. The most important factor to note is the relatively small mass (roughly 1% of the atmospheric mass above the planetary tangent plane at the point of impact) found in the $60°$ zenith-centered cone. This consitiutes the mass most strongly entrained in, and most highly accelerated by, the outrushing fireball.

TABLE I

Model	Atmospheric Mass (gm)	Mass Above Tangent Plane (gm)	Mass Within $60°$ Cone (gm)
Present Mars	2.4×10^{19}	3.51×10^{16}	2.84×10^{14}
Primitive Mars	3.9×10^{21}	9.10×10^{18}	1.22×10^{17}

We have employed a mass/impact velocity distribution in our model that has been derived from the works of Dohnanyi (1),
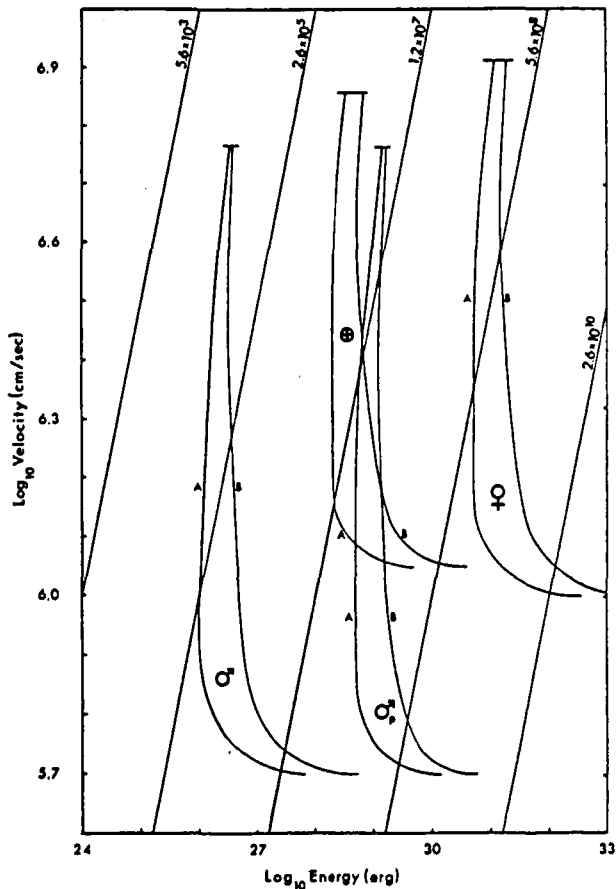
Watkins, H. and Lewis, J.S.

94

Weismann (2), Öpik (3,4), and Hughes and Daniels (5). The
actual mass flux, and its velocity distribution, experienced by
Mars throughout its history is unknown. In order to estimate
the importance of the result of numerous impacts over the course
of planetary history, it was necessary to remove the absolute
flux dependence from the model, and state the results as
atmospheric mass ejected per unit time at the assumed flux
mass/velocity distribution.

In the case of the present Martian atmosphere, it has been
found that at the present flux rate an erosive impact takes
place at a rate of greater than one per 400,000 years. This
impact removes more mass from the atmosphere than it adds in
retained impactor mass. For comparison, such an impact occurs
on Earth ten times less frequently. The results of our model,
applied to both model Martian atmospheres, as well as to Earth
and Venus, are presented in Figure 1. The curves labelled A
indicate the initiation of atmospheric erosion and those
labelled B indicate the mass balance (mass in = mass out). The
areas to the right of the curves labelled B indicate areas of
net erosion. The diagonal lines represent average impact
isochrons. The numbers found on these lines are the mean times
between impacts (at the present terrestrial flux) in years.
These are also lines of constant mass.

FIGURE 1

The fact that one energetic impact is capable of removing atmosphere tells little about the net effect of many impacts of widely varying energy. To obtain an estimate of the long term effects of impacts on the history of the atmosphere of Mars, we convolved the individual impact model with the model of the flux distribution. When this combined model were applied to Mars, it became apparent that the fraction of the atmosphere that could be ejected from Mars was significant. Our results are displayed in Table II. In this Table we present the fraction of atmosphere ejected per 10 million years at the present flux. If the flux was greater than the current flux, as was certainly the case in the early solar system, then the mass removed per unit time would have been considerably greater. In both the case of the primitive Martian model and the present model atmosphere, a significant fraction on the atmosphere can be removed in geologic time.

TABLE II

Model	Fraction of Atmosphere Ejected	Net Mass Gain Ratio
Present Mars	4.9×10^{-2}	1.3
Primitive Mars	5.0×10^{-4}	1.3

From our studies to date, we conclude that through the course of time a portion of the atmosphere of Mars has been removed by energetic impacts. The full extent of this removal has yet to be determined, but with further study it may be determined that such removal has played a major role in the evolution of the atmosphere of Mars.

Dohnanyi, J.S. (1972) Interplanetary Objects in Review: Statistics of Their Masses and Dynamics, Icarus, 17, p. 1-48.
Weismann, P.R. (1980) Physical Loss of Long-Period Comets, Astron. Astrophys., 85, p. 191-196.
Öpik, E.J. (1963) The stray bodies of the solar system Part I. Survival of cometary nuclei and the asteroids, Adv. Astron. Astrophys., 2, p. 219-262.
Öpik, E.J. (1966) The stray bodies of the solar system Part II. The cometary origin of meteorites, Adv. Astron. Astrophys., 4, p. 301-336.
Hughes, D.W. and Daniels, P.A. (1980) The magnitude of Comets, Mon. Not. R. astr. Soc. 191, p. 511-520.

MARS TOPOGRAPHIC MAPS
Sherman S. C. Wu, U. S. Geological Survey, Flagstaff, AZ 86001

Topographic maps of Mars are compiled from imaging and non-imaging data. Imaging data are derived mainly from Viking Mars missions, whereas non-imaging data, including ultraviolet spectrometer data [1], S-band radio occultation measurements [2, 3], and celestial mechanics [4], were derived from experiments on Mariner 9 and Viking Mars missions and from Earth-based radar observations [5]. For compilation using such unconventional spacecraft imagery, newly developed, on-line, special photogrammetric techniques are employed [6, 7]. Topographic maps are compiled at various scales ranging from that of the original global map, 1:25,000,000, to scales as large as 1:500,000 on specialized maps of small areas. The new global map, updated and revised with Viking data, has been compiled at a scale of 1:15,000,000. All contour maps are referred to the Mars topographic datum, which is a gravity surface described in terms of spherical harmonics [8], and are tied to the Mars planetwide control net [9, 10].

Based on Viking Orbiter stereopictures, 17 topographic quadrangle maps of Mars have been compiled at a scale of 1:2,000,000 [11]. The contour interval is 1 km. Each quadrangle covers an area of 15° latitude and 22.5° longitude. Upon completion of the existing Mars planetwide control network and the new control-network extension [12], the entire Martian surface (140 quadrangles) will be mapped at this scale and the existing 30 quadrangles compiled from Mariner 9 data at 1:5,000,000-scale will be revised. Digital elevation data of the Martian surface will also be collected from these maps.

Where high-resolution stereocoverage of Viking Orbiter pictures is available, we are compiling contour maps at large scale (1:500,000) [13] for geologic studies and for studies of possible Mars landing sites; the contour interval for these maps is 200 m. We have already completed these large-scale maps for the areas of Olympus Mons, Arsia Mons, Tithonium Chasma, and Candor Chasma. With digital elevation data collected from stereomodels, some stereoscopic perspective views of the volcanoes and canyons in these areas have been generated by image-processing techniques using Viking Orbiter pictures [14]. The relative elevation accuracy of these large-scale maps is about 60 m. However, the precision of the planetwide control network limits the absolute positioning accuracy to about 4 minutes, or about 4 km on the ground in the equatorial region.

Mars topographic maps have provided information on geologic processes that have formed the surface of the planet. Because elevations on topographic maps are referred to the gravity surface, they also help to interpret directions of lava flows and channel slopes.

References:
[1] Hord, C. W., Barth, C. A., Stewart, A. I., and Lane, A. L. (1972) Mariner 9 ultraviolet spectrometer experiment: photommetry and topography of Mars. Icarus, 17, 2, p. 443-456.
[2] Kliore, A. J., Fjeldbo, G., Seidel, B. L., Sykes, M. J., and Woiceshyn, P. M. (1973) S-band radio occultation measurements of the atmosphere and topography of Mars with Mariner 9. Jour. Geophys. Res., 78, p. 4331-4351.

[3] Lindal, G. F., Hotz, H. B., Sweetnam, D. N., Shippony, Z., Brenkle, J. P., Hartsell, G. V., and Speer, R. T. (1979) Viking radio occultation measurements of the atmosphere and topography of Mars. Jour. Geophys. Res. 84, B14, p. 8443-8456.

[4] Lorell, J. and Shapiro, I. I. (1973) The Mariner 9 celestial mechanics experiment. Jour. Geophys. Res. 78, 20, p. 4327-4329.

[5] Downs, G. S., Reichley, P. E., and Green, R. R. (1975) Radar measurements of Martian topography and surface properties. Icarus, 26, p. 273-312.

[6] Wu, S. S. C., Elassal, A. A., Jordan, Raymond, and Schafer, F. J. (1982) Photogrammetric application of Viking Orbiter photography. Planet. Space Sci. 20, 1, p. 45-55.

[7] Wu, S. S. C. (1984) Analytical systems for data reduction with images of extraterrestrial bodies. Intl. Archives of Photogram. and Remote Sensing, XXV, A2, 549-557.

[8] Wu, S. S. C. (1981) A method of defining topographic datums of planetary bodies. Annales de Géophysique, AGEPA7, Tome 37, fasc. 1, p. 147-160.

[9] Davies, M. E., Katayama, F. Y., and Roth, J. A. (1978) Control net of Mars. The Rand Corp., R-2039-NASA, 91 p.

[10] Wu, S. S. C. and Schafer, F. J. (1984) Mars control network. Tech. Papers of the 50th Annual Meeting, Amer. Soc. of Photogram. and Remote Sensing, 2, p. 456-463.

[11] Wu, S. S. C., Jordan, Raymond, and Schafer, F. J. (1984) Compilation of Mars 1:2,000,000-scale topographic map series. NASA Tech. Memo. (in press).

[12] Wu, S. S. C., Schafer, F. J., and Garcia, P. A. (1984) Mars control-network extension. NASA Tech. Memo. (in press).

[13] Wu, S. S. C., Garcia, P. A., Jordan, Raymond, and Schafer, F. J. (1984) Special large-scale topographic maps of Mars. NASA Tech. Memo. (in press).

[14] Wu, S. S. C., Garcia, P. A., Jordan, Raymond, Schafer, F. J., and Skiff, B. A. (1984) Topography of the shield volcano Olympus Mons on Mars. Nature, 309, 5967, p. 432-435.

MARS: EFFECT OF WATER VAPOR ABUNDANCE ON ATMOSPHERIC
OXIDATION STATE.   J.H. YATTEAU AND M.B. MCELROY

Atmospheric composition is calculated from the surface to the exobase
for a range of tropospheric water vapor abundances. Escape flux of hydrogen
is calculated and used to constrain atmospheric oxidation state.
Implications for past water vapor abundances and photochemical stability
of CO_2 are explored.

SHORT TERM WATER CYCLES WITHIN THE MARS REGOLITH.

A. P. Zent, F. P. Fanale, J. R. Salvail, Planetary Geosciences Division, Hawaii Institute of Geophysics, University of Hawaii, Honolulu, Hawaii 96822

Numerical models have recently been constructed with which Fanale et al., (1984) estimate the long-term rates of reversible and non-reversible withdrawal of water from the martian regolith. As a parallel project, the same basic set of equations is employed to study the seasonal migration and phase partitioning of water within the near surface martian regolith. The primary goal of this work was to map locations as a function of latitude and depth where seasonal thermal forcing of phase transitions may be responsible for changing in the concentration of crystalline ice. In addition, a rigorous search was conducted for regions where seasonal freezing and thawing of favorable brines could occur. Total regolith column abundance of water between the surface and the permafrost table was also tracked. Regions where phase changes occur are likely to shift with obliquity and axial orientation. The shifting of these regions is tracked as a function of orbital parameters.

These calculations have never been done rigorously before on the grounds that the probably high adsorptive capacity of the near surface regolith would effectively buffer the seasonal vapor wave, and that therefore little of interest could occur on timescales as short as a season. However, this overlooks the possibility that the relatively high thermal diffusivity of the regolith may permit seasonal thermal waves to drive water, effectively trapped within the regolith, from one phase to another.

Models which attempt to simulate the behavior of volatiles within a porous adsorbing medium such as a planetary regolith must account for the thermal, diffusive and adsorptive properties of that solid. The current model employs thermal data for the near surface regolith reported in Kieffer et al., (1977). Diffusion of water through the regolith is accounted for via solution of the equation presented in Barrer (1967) for diffusion through a porous, adsorbing medium. Adsorption isotherms are taken from Fanale and Cannon (1971) for basalt, and from Mooney et al. (1952) for montmorillonite. Anderson et al. (1978) extended isothem measurements to relavent pressures and temperatures. Insolation is computed from astronomical parameters and balanced against re-radiation, conduction into the ground and latent heat of CO_2 cap condensation. Surface water vapor densities are calculated by assuming atmospheric mixing times which are proportional to atmospheric pressure.

The model tracks the partial pressure of water vapor within the regolith, along with the masses of adsorbed water and ice, at ten equally spaced points between the surface and the permafrost table. The model is allowed to run for twenty Mars years in order to remove the effects of arbitrary initial conditions.

Seasonal Mars Water Cycles
Zent,A.P., Fanale,F.P. Salvail, J.R.

100

A few results may be presented summarily. No brine formation was found to occur at any point within the martian regolith. Nor could brine formation be induced at any point within the regolith by altering the obliquity and axial orientation of the planet. Seasonal occurence of ice is found at all obliquities greater than that at which the permanent CO_2 cap disappears. Stablization of seasonal ice occurrs in midwinter when absorption fails to keep pace with the falling equilibrium vapor pressure.

At low obliquities, where a permanent CO_2 cap exists, the cap forms an efficient cold trap. If the regolith is in adsorptive equilibrium with the atmosphere, insufficient water exists within the regolith to stablize ice. At medium to high obliquities, pore pressures within the regolith seasonally cross the equilibrium vapor pressure curve of ice, and crystallization occurs. This effect is limited to very high latitudes at medium obliquities, but may extend to 40-50 degrees latitude at highest obliquities.

High latitudes stablize ice in preference to lower latitudes because the two factors which promote ice stablization, high water content and cold temperatures, are preferentially found nearest the poles. Furthermore, the higher the latitude, the longer ice is stable and the greater the mass of water which is able to make the transition to ice. At high latitudes ice may stabilize from the surface to the permafrost table.

The mineralogy of the regolith is of very great importance in determining the seasonal behavior of water ice, because water which transforms to ice is otherwise present in the adsorbed phase. Therefore the mineralogy determines how much water will crystallize to ice, as well as determining the timing for the onset of crystallization. In general a basalt regolith is more favorable than montmorillonite for ice stablization, however the mass of water which is available for phase change in a montmorillonite regolith is many times larger than for basalt. A full characterization of the importance of these three parameters, obliquity, latitude and mineralogy, for the seasonal regolith water cycle will be given. The possible implications of this process for geomorphological interpretation will also be discussed.

References.

Anderson, D.M., M.J. Schwarz, A.R. Tice, Water vapor absorption by sodium montmorillonite at $-5^{\circ}C$, Icarus, Vol. 34 pp. 638-644 (1978).

Barrer, R.M., Surface and volume flow in porous media. In "The solid-gas interface 2"., E.A. Flood, Ed. pp.557-609., Dekker, New York, 1967.

Fanale,F.P. and Cannon,W.A., Adsorption on the martian regolith, Nature, Vol. 230, pp.502-504., 1971.

Seasonal Mars Water Cycles
Zent, A.P., Fanale,F.P. Salvail, J.R.

101

Fanale, F.P., J.R. Salvail, A.P. Zent, S.E. Postawko, Mars: long term changes in the state and distribuiton of H_2O. This volume, 1984.

Kieffer, H.H., T.Z. Martin, A.R. Peterfreund, B.M. Jakosky, E.D. Miner F.D. Palluconi, Thermal and albedo mapping of Mars during the Viking primary mission. J. Geophys. Res. Vol. 82, pp.4249-4295, 1977.

Mooney, R.W., A.G. Keenan, L.A. Wood, Adsorption of water vapor by montmorillonite. I. Heat of desorption and BET theory. J. Amer. Chem. Soc., Vol. 74, pp.1367-1371. 1952.

This Page Intentionally Left Blank

Registered Attendees

Vincent J. Abreu
University of Michigan

Arden L. Albee
California Institute of Technology

David Andersen
San Jose State University

Duwayne M. Anderson
Texas A & M University

Victor R. Baker
University of Arizona

Jeffrey R. Barnes
Oregon State University

J. Kelly Beatty
Sky & Telescope

Bruce Bills
Lunar & Planetary Institute

Joseph Boyce
NASA/Headquarters

Kevin Burke
Lunar and Planetary Institute

Michael H. Carr
United States Geological Survey

Bill Carswell
Space Calendar

Patrick Cassen
NASA/Ames Research Center

Sherwood Chang
NASA/Ames Research Center

Philip Christensen
Arizona State University

Todd Clancy
University of Colorado

Stephen Clifford
Lunar and Planetary Institute

Gary D. Clow
United States Geological Survey

David Colburn
NASA/Ames Research Center

Lelia Coyne
San Jose State University

Henry C. Dones, Jr.
University of California, Berkeley

Richard Durham
Rice University

Jonathan Eberhart
Science News

Larry W. Esposito
University of Colorado

Fraser P. Fanale
University of Hawaii

Stuart Gaffin
New York University

James L. Gooding
NASA/Johnson Space Center

Ronald Greeley
Arizona State University

Edward Guinness
Washington University

Robert M. Haberle
NASA/Ames Research Center

Robert B. Hargraves
Princeton University

Helen M. Hart
University of Colorado

Kenneth Herkenhoff
California Institute of Technology

Martin I. Hoffert
New York Universiy

Jeffrey Hollingsworth
Oregon State University

Robert L. Huguenin
University of Massachusetts

Bruce Jakosky
University of Colorado

Philip James
University of Missouri, St. Louis

Ralph Kahn
Washington University

James Kasting
NASA/Ames Research Center

Steven W. Lee
Arizona State University

Conway Leovy
University of Washington

Sanjay S. Limaye
University Wisconsin, Madison

Hal G. Marshall
University of Michigan

Leonard J. Martin
Lowell Observatory

Harold Masursky
United States Geological Survey

Albert Metzger
Jet Propulsion Laboratory

Henry J. Moore
United States Geological Survey

Jeffrey M. Moore
Arizona State University

Duane O. Muhleman
California Institute of Technology

David A. Paige
California Institute of Technology

Frank Don Palluconi
Jet Propulsion Laboratory

Tim Parker
Jet Propulsion Laboratory

Robert O. Pepin
University of Minnesota

James Pollack
NASA/Ames Research Center

Susan Postawko
University of Hawaii

L. E. Roth
Jet Propulsion Laboratory

M. Rutherford
Brown University

Steve Saunders
Jet Propulsion Laboratory

Thomas W. Scattergood
NASA/Ames Research Center

Peter Schloerb
University of Massachusetts

Peter H. Schultz
Brown University

David Scott
United States Geological Survey

Robert B. Singer
University of Hawaii

Steven Squyres
NASA/Ames Research Center

Carol Stoker
National Center for Atmospheric Research

Hans Suess
University of California, San Diego

James Tillman
University of Washington

Brian Toon
NASA/Ames Research Center

Jose R. Valentin
NASA/Ames Research Center

Tyler Volk
New York University

Heinrich Wänke
Max-Planck-Institüt für Chemie

Hampton Watkins
University of Arizona

Robert West
Jet Propulsion Laboratory

Donald Wilhelms
United States Geological Survey

Sherman S. C. Wu
United States Geological Survey

John Yatteau
CETT/DAS
Harvard University

Aaron Zent
University of Hawaii

Richard W. Zurek
Jet Propulsion Laboratory

End of Document